UTS UNIVERSITY OF TECHNOLOGY SYDNEY

FORWARD OSMOSIS FOR WASTEWATER RECLAMATION: TRACE ORGANIC CONTAMINANTS REMOVAL AND COOLING FOR POST-COMBUSTION CO_2 CAPTURE

By Lei Zheng

Thesis submitted in fulfilment of the requirements for the degree of

Doctor of Philosophy

under the supervision of Long D. Nghiem, Qilin Wang and William E. Price

University of Technology Sydney
Faculty of Engineering and Information Technology

June 2020

This thesis is dedicated to my parents

Liying Liu *and* ***Xiaohong Zheng***

For their endless love, support and encouragement

Certificate of Original Authorship

I, **Lei Zheng** declare that this thesis, is submitted in fulfilment of the requirements of the award of **Doctor of Philosophy**, in the School of Civil and Environmental Engineering at the University of Technology Sydney.

I also certify that the work in this thesis has not previously been submitted for a degree nor it has been submitted as part of requirements for a degree except as fully acknowledged within the text.

This thesis is wholly my own work unless otherwise reference or acknowledged. Any help that I have received in my research and preparation of the thesis has been acknowledged. In addition, I certify that all information sources and literature used are indicated in the thesis. This research is supported by the Australian Government Research Training Program.

Production Note:
Signature removed
prior to publication.

Signature of Student: Lei Zheng

Date: June 17th, 2020

Acknowledgements

First and foremost, I would like to express my sincere gratitude and appreciation to my Principal Supervisor Professor Long Nghiem for his guidance and support of my PhD study. His enthusiasm for research and life has inspired me to achieve the great goals during last four years. In addition, his patience, encouragement and immense knowledge boost my confidence to conquer the challenges in all the time of my research and thesis writing. Furthermore, his detail-oriented attitude teaches me how to be a qualified scientist in future. I am so fortunate to be one of his students and share this amazing journey with him.

Besides, I would like to thank my Co-Supervisor Dr Qilin Wang, External Supervisor Professor William Price, co-authors, reviewers and teachers for their invaluable comments and encouragement in my research work, which greatly incented me to gain thorough insights and widen my knowledge for membrane technology.

My appreciation also extends to my colleagues, whose support and encouragement have helped me overcome the dilemma in the past. They are Ashley, Richard, Minh, Bilal, Allie, Luong, Wenhai, Hung, Sherry, Aileen, Lewa, Jameshed, Hop, Sultan, Tabea, Sihuang, and Biplob. I will never forget the moment when we raised Uniclub Cup Championship Trophy from our great teamwork. Special thanks to the technician staffs: Linda, Johir, and Nirenkumar for their kind assistances in my experimental work.

I sincerely cherish the visiting opportunity offered by Kangkang in CSIRO Energy Centre, Newcastle. His expertise in CO_2 capture technology motivated me to combine membrane process with CO_2 capture.

I would like to thank Samantha for her tremendous guidance in presentation skills and support in entrepreneurship. She is a warm-hearted person who always encourages me towards the vision of bright future.

Apart from PhD study, I volunteered to be an international student mentor that offered me a great chance to assist other international students to grow independence abroad and impart my professional knowledge in the cross-cultural communication. I greatly appreciate the opportunity provided by Ms Liju Dong.

Studying abroad is not always easy since you have to constantly adapt to a new environment. I feel extremely lucky to meet a group of the amazing people, who have greatly helped me overcome obstacles and enjoyed the happiness together during this period. They are Luisa, Joana, Azita, Douglas, Lin, Chunyang, Long, Guanyu, Le, Jiantao, Lan, Qiang, Shiyu, Emily, Jiawei, Minwei, Zhijie, Hanjie, Huan, Chen, Xiaoqing, Dongle, Bing, Bentuo, Zehao, Phong, and Haoding. I thank them for bringing lots of beautiful memories in my life.

Family is the greatest source for me to provide the consistent inspiration. I would like to thank my families, their love and affection assist me to pursue my dream. Special thanks to my parents and grandma for always showing their positive attitude towards challenges in life. My sincere appreciation goes to Weilin and her family for their support and caring in the past 6 years. The generous caring from my landlords Milka and Frank make me feel never alone in this country. Frank passed away due to ill health during my study. I wish him could see my achievement today and may his soul rest in peace.

Last but not least, I greatly acknowledge the scholarship support from Chinese Scholarship Council, University of Technology Sydney, and University of Wollongong.

Research Outcome Summary

Refereed Journal Papers

1) **L. Zheng**, W.E. Price, T. He, and L.D. Nghiem, Simultaneous cooling and provision of make-up water by forward osmosis for post-combustion CO_2 capture. Desalination, 476 (2020), 1-7.
2) **L. Zheng**, W.E. Price, J. McDonald, S.J. Khan, T. Fujioka, and L.D. Nghiem, New insights into the relationship between draw solution chemistry and trace organic rejection by forward osmosis. Journal of Membrane Science, 587 (2019), 1-10.
3) **L. Zheng**, W.E. Price, and L.D. Nghiem, Effects of fouling on separation by forward osmosis: the role of specific organic foulants. Environmental Science and Pollution Research, 26 (2018), 33758-33769.

Submitted and In-preparation Journal Papers

1) **L. Zheng**, K.K. Li, Q.L. Wang, G. Naidu, W.E. Price, X.W. Zhang, and L.D. Nghiem, Low-temperature stripping of CO_2 from aqueous amine-based solvents via integrated direct contact membrane distillation-forward osmosis, Journal of Membrane Science, Submitted.
2) M. Krajewska, **L. Zheng**, M. Szczygielda, L.D. Nghiem, and K. Prochaska, Bio-carboxylic acid recovery from fermentation broth by integrated forward osmosis -reverse osmosis system, Journal of Membrane Science, in preparation.

Conference Presentation

1) **L. Zheng** and L.D. Nghiem, Regeneration of amine-based solvent via integrated direct contact membrane distillation - forward osmosis (DCMD-FO) for post-combustion CO_2 capture. Oral presentation at the *10th International Membrane Science & Technology Conference*, Sydney, 2nd - 6th February 2020.
2) **L. Zheng** and L.D. Nghiem, New insights into the relationship between draw solution chemistry and trace organic rejection by forward osmosis. Oral presentation at the *2nd Green Technologies for Sustainable Water*, Ho Chi Minh City, 1st - 5th December 2019.

3) **L. Zheng** and L.D. Nghiem, Simultaneous cooling and provision of make-up water by forward osmosis for post-combustion CO_2 capture. Oral presentation at the *2nd International Conference on Energy-Efficient Separation*, Melbourne, 27th - 30th December 2019.
4) **L. Zheng** and L.D. Nghiem, Effects of fouling on separation by forward osmosis: the role of specific organic foulants. Oral presentation at the *6th Membrane of Australasia Early Career Researcher Membrane Symposium*, Melbourne, 30th - 1st February 2019.
5) **L. Zheng** and L.D. Nghiem, Effects of fouling and chemical cleaning on the rejection of trace organic contaminants by forward osmosis. Oral presentation at the *9th International Conference in Challenges in Environmental Science & Engineering*, Kaohsiung, 6th - 10th November 2016.

Awards and Prizes

1) First Prize in Three Minutes Short Talk – Best Overall Award at the *2nd International Conference on Energy-Efficient Separation*, 2019, Melbourne.
2) People's Choice Award for Oral Presentation at the *Civil and Environmental Engineering School Research Showcase*, 2019, University of Technology Sydney.
3) People's Choice Award for Oral Presentation at the *Three Minutes Thesis Competition in Faculty of Engineering and Information Technology*, 2019, University of Technology Sydney.
4) Winner of Travel Award, one of 15 student representatives for the research exchange program in Poznan University of Technology, 2019, Poznan.
5) Winner of Travel Award, *6th Membrane Society of Australasia Early Career Researcher Symposium*, 2019, Melbourne.
6) A Prize for Excellence at the *12th Chunhui Chinese Students Innovations and Entrepreneurship Competition*, 2017, Guangzhou.
7) A Prize for Excellence at the *3rd Western China Overseas Hi-tech and High Talents Entrepreneurship Competition (Oceania Division)*, 2017, Sydney.

Table of Contents

List of Figures

List of Tables

List of Abbreviations

Abbreviation	Meaning
AL-DS	Active Layer Facing Draw Solution
AL-FS	Active Layer Facing Feed Solution
BEOP	Biofilm-Enhanced Osmotic Pressure
CA	Cellulose Acetate
CEOP	Cake-Enhanced Osmotic Pressure
COD	Chemical Oxygen Demand
CTA	Cellulose Triacetate
DCMD	Direct Contact Membrane Distillation
DF	Dilution Factor
DI water	Deionized Water
DOC	Dissolved Organic Carbon
DS	Draw Solution
ECP	External Concentration Polarisation
EDX	Energy Dispersive X-ray Spectroscopy
FO	Forward Osmosis
FS	Feed Solution
FTIR	Fourier Transform Infrared Spectroscopy
HA	Humic Acid
HOAc	Acetic acid
ICP	Internal Concentration Polarisation
LC-OCD	Liquid Chromatography with Organic Carbon Detection
LiCl	Lithium Chloride
LMW	Low Molecular Weight
MD	Membrane Distillation
MEA	Monoethanolamine
MPA	Minimum Projection Area
MW	Municipal Wastewater
NaH_2PO_4	Sodium Dihydrogen Phosphate
NaOAc	Sodium Acetate
NF	Nanofiltration
RO	Reverse Osmosis
RSF	Reverse Salt Flux
RSFS	Reverse Salt Flux Selectivity
SA	Sodium Alginate
SG	Sodium Glycinate
SRSF	Specific Reverse Salt Flux
TFC	Thin Film Composite
TOC	Total Organic Carbon
TrOCs	Trace Organic Contaminants
TSS	Total Suspended Solids

Abstract

Water scarcity and global warming are two vexing and intertwined problems with significant impacts on human society and eco-system. Forward osmosis (FO) can potentially be used as an effective tool for wastewater reclamation and alleviating global warming. This study aimed to explore new approaches to deploy FO toward these objectives. This study elucidated the rejection mechanisms of 43 trace organic contaminants (TrOCs) by FO through a systematic investigation of several influencing factors including draw solution chemistry, contaminants species and membrane fouling. This study also demonstrated the viability of FO as an alternative trim cooler in post-combustion CO_2 capture and repetitive CO_2 capture via direct contact membrane distillation - forward osmosis (DCMD-FO) system.

Results from this study revealed that membrane fouling could induce considerable effects on TrOCs rejection via investigations of three specific organic foulants. Municipal wastewater resulted in a more compact fouling cake layer than that caused by humic acid and sodium alginate, which was likely due to large constituents of low molecular weight neutrals and acids. In addition, fouling altered the membrane less negatively charged and less hydrophilic. Steric hindrance caused by the additional filtration cake layer therefore became the dominant rejection mechanism for sulfamethoxazole. However, lower rejection of carbamazepine was likely due to the cake-enhanced concentration polarization.

Through a systemic investigation, results from this study heightened the inherent complexity in TrOCs rejection by FO. Due to the intrinsic bidirectional transport phenomenon, the reverse flux of proton (or hydroxyl radical) could alter the feed solution pH, which governed the separation of ionizable TrOCs. In addition, variation in hydrated radius of draw solution resulted in the sharp contrast in terms of reverse salt flux (NaCl: 33 g/m^2h; LiCl: 2 g/m^2h) and therefore different ionic strength of feed, thus the corresponding electrostatic interaction. Charged compounds generally exhibited higher rejections than neutral ones by the clean membrane, which indicated that electrostatic interaction rather than steric hindrance was the dominant rejection mechanism.

Intrinsic osmotic driving force also enlightened this study to apply FO as an alternative to a trim cooler in post-combustion CO_2 capture. Regenerated amine-based solvents, such as glycine, sodium glycinate, and monoethanolamine (MEA) were successfully used as the draw solution to extract water from treated effluent or seawater, which could provide the make-up water for CO_2 capture. Glycine showed a higher water flux, a lower reverse salt flux and specific reverse salt flux than sodium glycinate and MEA in both membrane orientations, thus was selected for further investigations.

A higher water flux but with considerable flux decline were observed when active layer faced draw solution. Temperature increase in draw solution could alter thermodynamics properties of glycine, thus, resulting in an increase of reverse salt flux. It enhanced water flux due to the diminishing concentrative internal concentration polarisation. On the other hand, changes in water flux were insignificant when active layer faced feed solution even as temperature increased. It appears that temperature increase was likely to aggravate the severity of dilutive internal concentration polarisation and offset the growth of osmotic pressure. Despite of the lower water transportation from seawater than treated effluent due to the less osmotic gradient, seawater could also be as an alternative cooling source and desalinated simultaneously.

This study also demonstrated 85 and 89% of re-absorption capacities for MEA and sodium glycinate in a hybrid DCMD-FO system respectively via the low regeneration temperature. The DCMD achieved respective 33.6 and 33.2% of desorption efficiency for MEA and sodium glycinate at 80 °C. Unlike negligible change caused by sodium glycinate, MEA resulted in either increase or decrease of hydrophobicity for each MD membrane, thus a partial wetting as well. Water production declines were observed for both solvents due to the membrane wetting. However, the high solvent rejection indicated that DCMD resulted in the negligible amine loss.

Regenerated MEA and sodium glycinate resulted in the contrast water flux when deionised water was used as the feed (MEA: 27 L/m^2h, Sodium glycinate: 14 L/m^2h). They both whereas showed a similar water flux (15 L/m^2h) when treated effluent was used as the feed. In addition, sodium glycinate presented a smaller reverse salt flux than that of MEA for both deionised water and treated effluent. A particular membrane structure may lead to the disparity in water flux. More research work is required for the cost-effective CO_2 capture based on membrane system.

Chapter 1 Introduction

1.1 Background

Water scarcity is an increasingly pervasive problem worldwide and has been further exacerbated by population growth, energy shortage and global warming [1]. Based on the current water exploitation rate, water consumption (6900 billion m^3 per year) is expected to exceed over total accessible water source (4200 billion m^3 annually) by 2030 [2]. Wastewater reclamation is arguably the most significant approach to alleviate such tremendous freshwater demand from different economic sectors, such as energy production, industry and agriculture.

Wastewater treatment plant is an integrated part of the water recycling infrastructure as it provides treated effluent to existing water cycle via conventional physical, chemical, and biological process. However, conventional wastewater treatment plant is not specifically designed for the removal of trace organic contaminants (TrOCs). These TrOCs include hormones, pharmaceutically active compounds, industrial chemicals, and pesticides can be detected in the secondary treated effluent. Thus, the removal efficiency of these TrOCs by these wastewater treatment plants are highly variable and low. The potential impacts by TrOCs on human health and the environment have received significant attention from the scientific community [3]. Recent data suggest that these TrOCs may induce chronic biological effects on non-target organisms (including humans) even at low concentrations [4, 5].

Several advanced membrane-based processes, such as nanofiltration (NF), reverse osmosis (RO), and membrane bioreactor have been implemented to effectively remove TrOCs during water and wastewater treatment [6-9]. However, high energy consumption, high fouling propensity and issues associated with brine discharge have all been identified as major drawbacks of these membrane based technologies [10-12]. Therefore, the innovative membrane process containing following features: less energy consumption, low fouling tendency, and high TrOCs removal is desirable to be implemented.

CO_2 emission by anthropogenic activities has significantly accelerated global warming, which also exacerbated water scarcity in recent years. The combustion of fossil fuel accounts for 45% of the total CO_2 emissions or 37.15 Gt CO_2 [13]. A pragmatic approach

for mitigating CO_2 emission is the carbon capture and storage, where CO_2 is removed from flue gas and pumped into deep geologic reservoirs for storage. Thus, three main approaches (pre-combustion, post-combustion and oxyfuel combustion) associated with different combustion processes have been deployed to separate CO_2 from the flue gas [14].

A proven technology to mitigate CO_2 emission from post-combustion CO_2 capture is amine scrubbing [15-17]. In the amine scrubbing process, amine chemically reacts with CO_2 in the low concentration from a flue gas, thus forming CO_2 rich-loaded amine at ambient temperature. CO_2 rich-loaded amine is further regenerated at high temperature (i.e. 100 - 120 °C) to release pure CO_2 for geologic storage. After regeneration, CO_2 rich-loaded amine becomes CO_2 lean-loaded amine for repetitive CO_2 capture. A large volume of make-up water is required for the current post-combustion CO_2 capture process (i.e. CO_2 absorption and desorption column, CO_2 product compression) [18-20]. Amine-based absorption significantly increases the cooling requirement in the trim cooler. Most trim coolers are performed by using the surface water other than the air due to the lower energy cost [21]. Thus, the availability of water resources near the power plant (for instance, in arid regions) will limit the deployment of CO_2 capture. Either improving the efficiency of trim coolers or looking for the alternative cooling process provides a possible method to mitigate large amount of freshwater consumption.

Forward osmosis (FO) may be that solution in response to above problems. FO is an emerging membrane process, which utilizes the osmotic pressure as the driving force for transportation of clean water from feed solution (low concentration) to draw solution (high concentration). In this context, wastewater can be used as the feed solution since its osmotic pressure is far lower than that of selected draw solution. In addition, low energy consumption and fouling tendency are several outstanding advantages of FO. Furthermore, FO can be directly integrated with other membrane process to further enhance TrOCs removal and water production in post-combustion CO_2 capture towards wastewater reclamation.

1.2 Objectives

The overall objective of this study was to investigate the potential application of FO in different scenario for wastewater reclamation, and to provide fundamental insights for practical application of FO.

Specific aims in pursuit of overall objective were to:

1) Describe the systematic effect of feed/draw solution chemistry on FO performance including water flux, reverse salt flux and TrOCs rejection;
2) Elucidate key TrOCs rejection mechanism and how they could be influenced by membrane fouling in FO;
3) Provide a proof-of-concept of the feasibility of FO for simultaneously providing of make-up water from wastewater and cooling as the trim cooler replacement for post-combustion CO_2 capture.
4) Demonstrate a hybrid DCMD-FO system for the repetitive CO_2 capture.

1.3 Research Questions

Along with these specific aims, this thesis was able to answer several key research questions as below:

1) How did organic foulant composition influence the membrane surface properties and therefore membrane fouling?
2) Whether membrane fouling would enhance or exacerbate the TrOCs rejection?
3) How did membrane orientation and temperature gradient affect the cooling performance of FO?
4) Was there any significant membrane wetting during the CO_2 desorption? How were their impact on the water production in DCMD?

1.4 Organization

This thesis contains seven chapters and include two major research topics (Figure 1-1). Chapter 2 offers a critical literature review of current studies related to fouling impact on FO performance, particularly TrOCs rejection. The first research topic aims to elucidate the draw/feed solution chemistry on FO performance (i.e. Chapter 3 - 4). Chapter 3 characterizes three specific organic foulants' influences on FO performance to better understand the importance of feed chemistry. Based on findings in Chapter 3, Chapter 4

systematically investigates the interplay between feed and draw solution chemistry on FO performance. Associated impact on TrOCs rejection mechanism is highlighted in Chapter 4. The target of second research topic is to demonstrate the proof-of-concept of the feasibility of FO as the trim cooler replacement for post-combustion CO_2 capture (i.e. Chapter 5 - 6). Chapter 5 firstly illuminate an innovative FO application to meet dual purposes including desalination and cooling. Furthermore, Chapter 6 proposes a hybrid FO-based process for sustainable CO_2 capture via wastewater and waste heat. The conclusion and recommendations for future work are presented in Chapter 7.

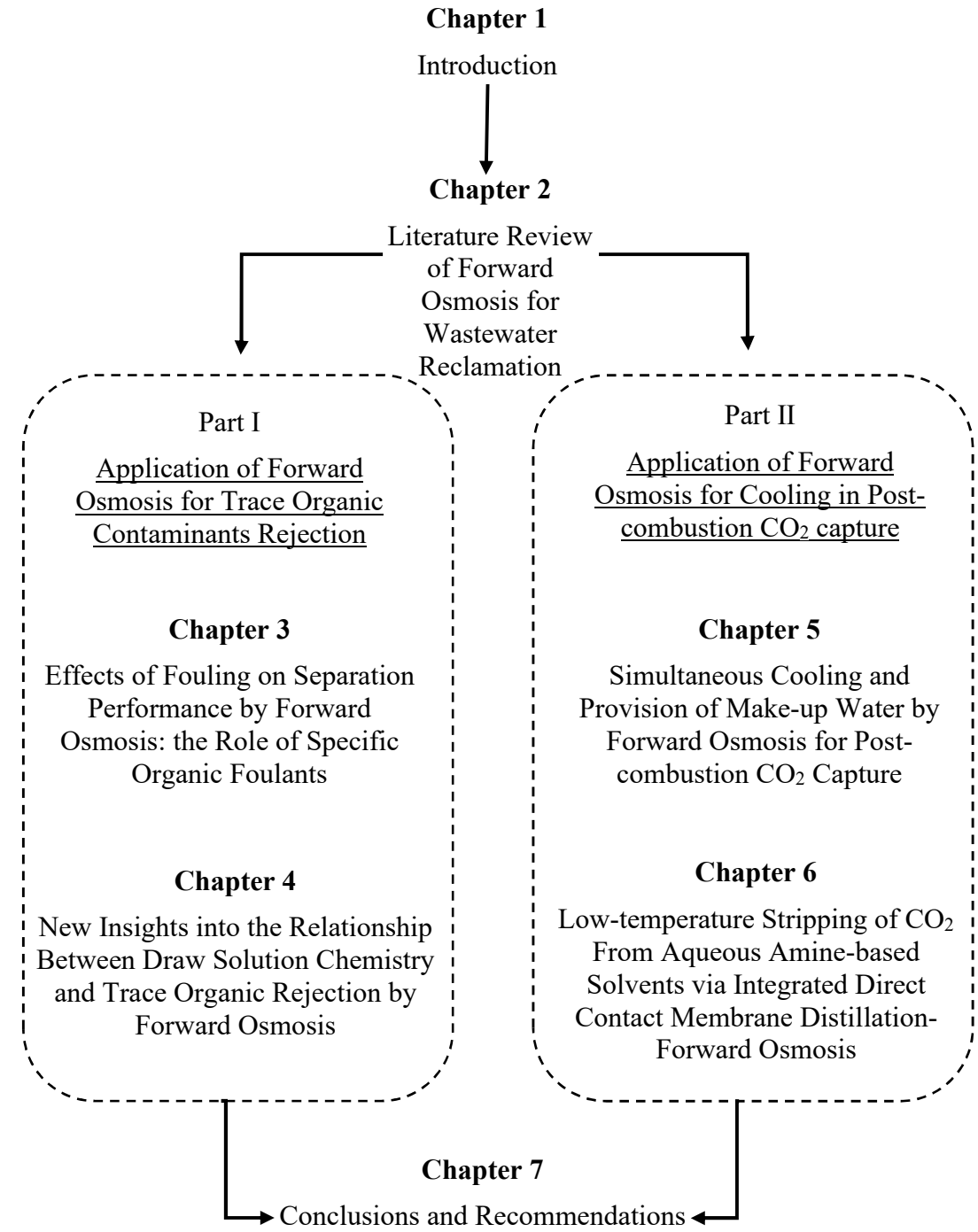

Figure 1-1. Thesis outline

Chapter 2 Literature Review

2.1 Introduction

Using osmotic pressure as the driving force for water transportation across the semi-permeable membrane, FO has the potential for several new separation applications. Compared to hydraulic pressure-driven membrane processes, FO is less susceptible to fouling and requires significantly less energy, particularly when draw solution regeneration is not required [22, 23]. As a novel membrane process, FO has been investigated for the treatment of challenging wastewater [24] and a range of innovative applications including resource recovery [25, 26] , hypersaline desalination [27, 28], and sludge thickening [29, 30].

The ubiquitous occurrence of TrOCs in municipal wastewater has been a topic of major scientific and public concern in the past decade [3]. These TrOCs negatively affect human health and the ecosystem even at a very low concentration. Some of them are specifically designed to be persistent in the environment [31]. Membrane processes, such as NF [32], RO [33], membrane distillation [34], membrane bioreactor [35] and FO [36-39] have been widely explored for removing TrOCs from wastewater.

Given the similarity in membrane structure between FO and NF/RO, recent research has shown that TrOCs rejection by FO may also be governed by the steric hindrance, hydrophobic adsorption and electrostatic interaction [40]. Thus, physiochemical properties of TrOCs, membrane properties and membrane fouling have been reported to play significant roles in governing TrOCs rejection by FO [41, 42].

Wastewater reclamation presents another opportunity for post-combustion CO_2 capture in the context of the carbon-wastewater nexus. Interestingly, FO can also potentially act as a trim cooler in post-combustion CO_2 capture. Due to its high osmotic pressure, amine solvent can be used as the draw solution to extract clean water from wastewater, which can meet the simultaneous cooling and make-up water provision targets. However, this proof-of-concept still remains a challenge to optimize its process for sustainable CO_2 capture.

This chapter critically reviews current applications of FO for TrOCs rejection and cooling in post-combustion CO_2 capture. After briefly introducing the water and solute

transporting phenomena in FO, the review provides the current state of knowledge on formation of different fouling as well as their associated effect on TrOCs rejection. In addition, current studies about effect of draw solution chemistry on FO performance are also discussed. On the other hand, the review also discusses the potential opportunities and challenge for FO as the alternative cooler replacement in post-combustion CO_2 capture. In the end, several concluding remarks are given to strengthen FO practical application for wastewater reclamation.

2.2 Transport phenomena in FO

2.2.1 Water permeation and solute transport

Water permeation is driven by osmotic pressure ($\Delta\pi$) in FO. In contrast, hydraulic pressure provides the driving force in RO. Water permeation in FO and RO is generally described as below:

$$J_w = A(\sigma\Delta\pi - \Delta P) \qquad (2\text{-}1)$$

where J_w represents the water flux, A denotes the pure water permeability of the membrane, σ is the reflection coefficient, and ΔP represents the applied pressure [43]. ΔP is larger than $\Delta\pi$ in RO, whereas no applied pressure is applied in FO. The diagram of water permeation in FO and RO is illustrated in Figure 2-1. The water flux magnitude is illustrated in Figure 2-2 [44].

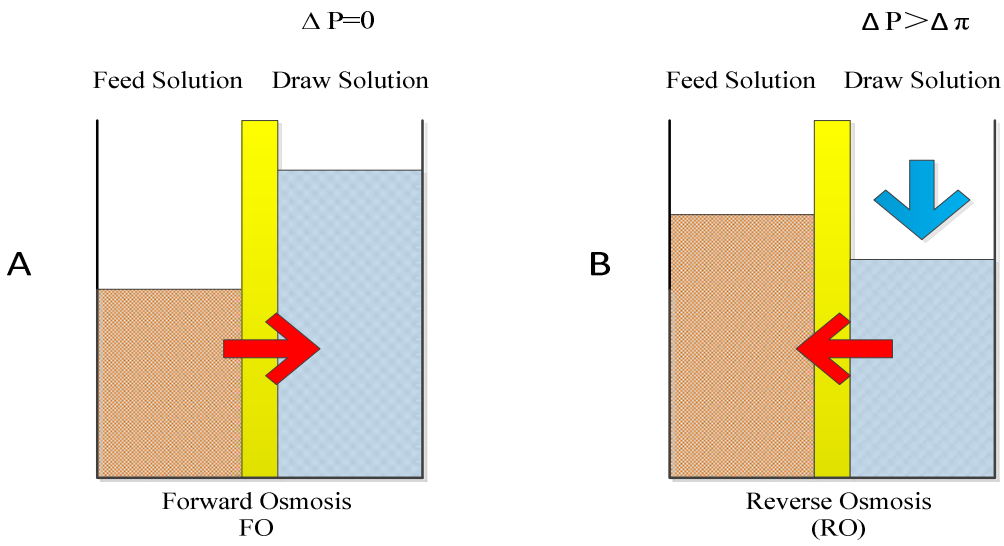

Figure 2-1: A diagram of water permeation in (a) FO and (b) RO

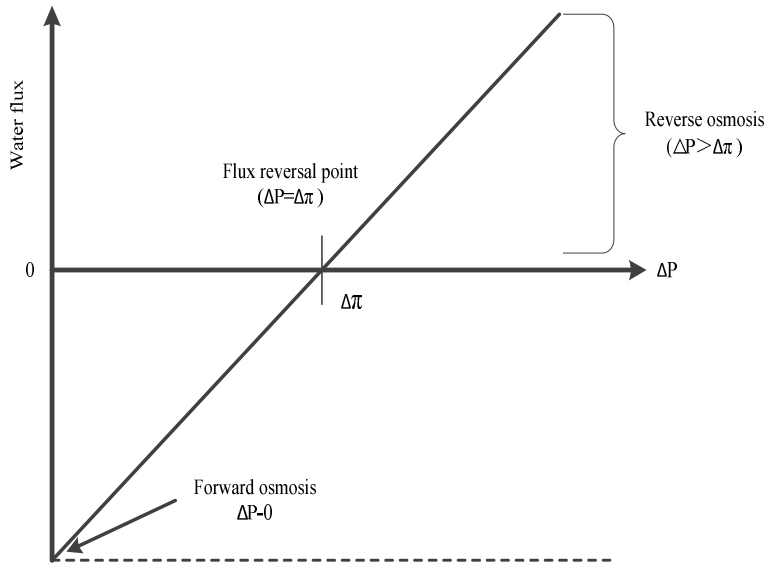

Figure 2-2: Direction and magnitude of water flux as a function of applied pressure in FO and RO (from [44]).

The reverse solute flux (J_s) through membranes is generally described by using Fick's law

$$J_s = B\Delta c \tag{2-2}$$

where B denotes solute permeability coefficient of the membrane and Δc is concentration gap among the two sides of membrane [45]. However, the bidirectional diffusion between feed and draw solution is intrinsic in FO. Besides equation 2-2, we can use specific reverse solute flux (J_s/J_w) to describe reverse solute diffusion [46, 47]. By combining equation 2-1 and 2-2 and relating Δπ to Δc with van't Hoff equation, J_s/J_w can be calculated by the following equation 2-3:

$$\frac{J_s}{J_w} = \frac{B}{A\beta R_g T} \times (1 + \frac{A\Delta P}{J_w}) \tag{2-3}$$

where β is the van't Hoff coefficient, A is the water permeability constant of the membrane, R_g is the gas constant and T is recorded from the absolute temperature.

2.2.2 External concentration polarisation

External concentration polarisation (ECP) exists close to the membrane surface. They can be divided into another two sub-categories: dilutive and concentrative. On the feed side, solutes are concentrated at the membrane surface, which refer to as the concentrative ECP.

On the contrary, draw solutes are diluted at the surface, which refer to as the dilutive ECP [47]. Figure 2-3 presents concentration polarisation types in both membrane orientations. The impact of both concentrative ECP and dilutive ECP can be constrained by flow optimization and spacer placement.

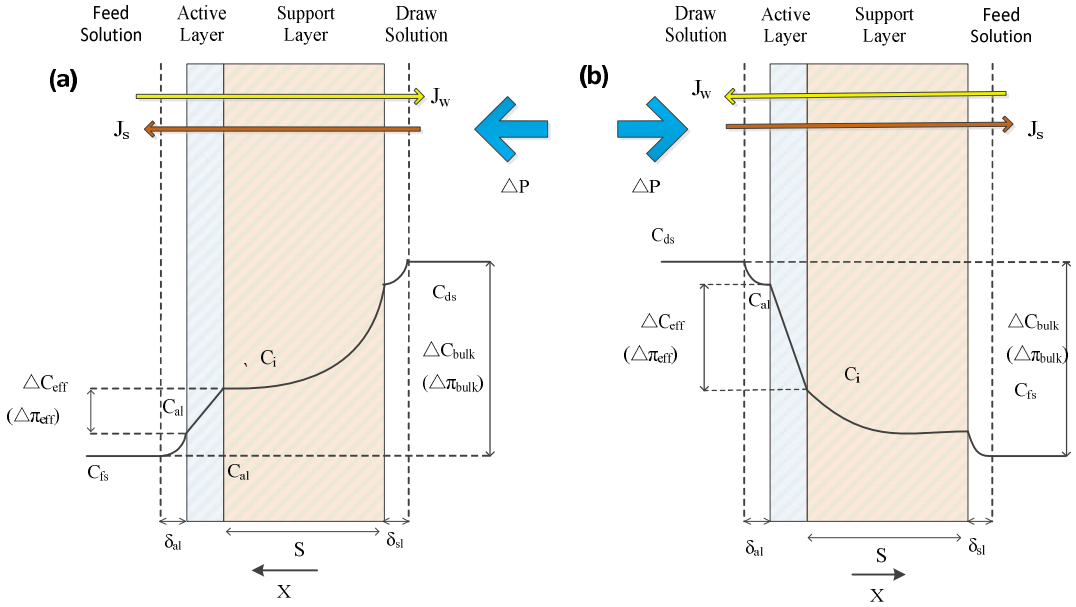

AL - FS Orientation AL - DS Orientation

Figure 2-3: Concentration profile across the membrane because of ICP and ECP in (a) AL-FS orientation and (b) AL-DS orientation (adapted from [47]).

2.2.3 Internal concentration polarisation

Internal concentration polarisation (ICP) generally occurs in the porous support layer of membrane. In the active layer facing feed solution (AL-FS) orientation, the draw solutes are diluted inside the support layer as water permeating through porous support layer, which refer to as the dilutive ICP. Concentrative ECP takes place on the dense separation layer at the same time [48]. In the active layer facing draw solution (AL-DS) orientation, solutes are concentrated inside the support layer, which refer to the concentrative ICP. Both ICP and membrane fouling attribute to hinder water transportation in FO [48].

2.3 Types of membrane fouling in FO

Water permeation in FO is greatly influenced by different membrane fouling, which is similar to other membrane processes. Fouling in FO can be categorized into four major groups namely organic fouling, colloidal fouling, scaling, and biofouling (Figure 2-4)

[49]. The characteristics of each membrane fouling were summarized in the Table 2-1. Complex membrane fouling formation in FO is determined by a combination of several factors, such as hydrodynamics of operating condition, membrane and foulant characteristics, feed/draw solution chemistry, and membrane orientation [10, 50-52].

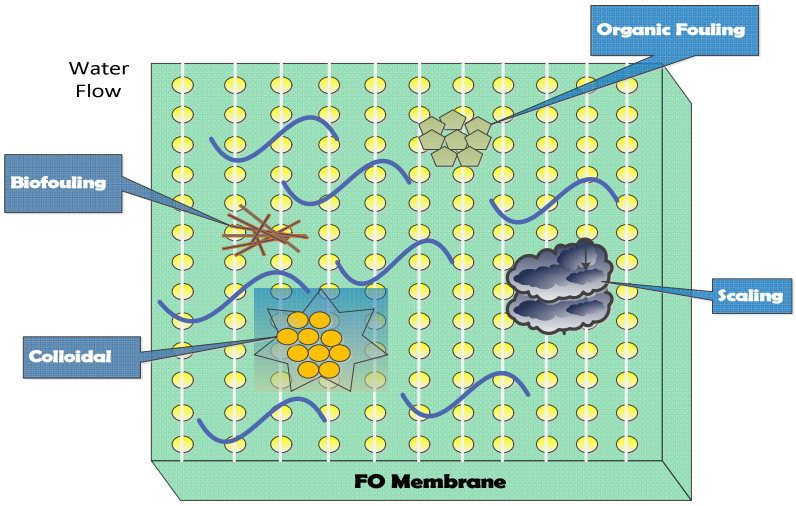

Figure 2-4: Four types of fouling during the membrane treatment (adapted from [53]).

Table 2-1 Characteristics of each membrane fouling

Types of fouling	Foulant	Composition	Size and shape	Reference
Organic fouling	Humic acid	Humic substance	A few kDa to a few hundred kDa	Tang et al., [54]
	Alginate	Polysaccharides	12-80 KDa	Lee et a l., [10]
Colloids fouling	Silica	Inorganic colloids	Round	Boo et al., [52]
Scaling	Calcium carbonate	Inorganic scales	Rhombohedral or spherical	Antony et al., [55]
	Calcium phosphate	Inorganic scales	Amorphous	Antony et al., [55]
Biofouling	E.coli,	Bacteria	Rod-shaped	Liu et al., [56]
	Pseudomonas aeruginosa	Fungi	Brush-like and flask-shaped	Yoon et al., [57]

2.3.1 Organic fouling

Natural macromolecular organic matters, such as alginate and protein normally result in the organic fouling (Figure 2-5) [49, 58]. The compactness and the thickness of the fouling layer are detrimental for the flux behavior during treatment [10]. Both of the physical (i.e. membrane orientation, membrane property, temperature) and chemical (i.e. Ca^{2+}) conditions affect the formation of the organic fouling [59].

First of all, severity of organic fouling is determined by the membrane orientation. Zhao *et al.,* [60] showed that organic fouling caused by bovine serum albumin was more severe in the AL-DS orientation than that in the AL-FS orientation. It was estimated that accumulation and deposition of organic foulant in porous layer caused more severe water flux decline. Similarly, Tang *et al.,* [54] also observed that fouling caused by humic acid in AL-DS orientation was more severe than that in AL-FS orientation. In AL-DS orientation, precipitated humic substances resulted in an internal clogging of support layer, thus for severe flux decline. On the other hand, Jin *et al.,* [61] illustrated that organic fouling formation in different orientation due to different mechanism. In AL-FS orientation, the organic fouling was related to the cake layer formation. However, the organic fouling was attributed to the pore clogging in AL-DS orientation. Of a particular note, AL-FS orientation presented a stronger fouling resistance than that in AL-DS orientation.

Furthermore, organic fouling could lead to the cake-enhanced osmotic pressure (CEOP) in FO [10, 58]. Lee *et al.,* [10] observed that the formation of CEOP in FO contributed to the severe flux decline. It was estimated that CEOP resulted in an increase of osmotic pressure near the feed side, therefore flux decline. In addition, the presence of Ca^{2+} enhanced CEOP via bridging Ca^{2+} with organic foulant.

Membrane surface also influences organic fouling formation. Mi and Elimelech [51] demonstrated that thin film composite (TFC) membrane could potentially attract excessive alginate molecules than cellulose acetate (CA) membrane due to a more rough or heterogeneous surface. TFC membrane had more adhesive sites than CA membrane, which led to easier long-range attraction like the formation of calcium-bridged alginate molecules. Another study of Mi and Elimelech [50] also indicated that membrane surface morphology resulted in different calcium binding and hydrodynamic shear force, which therefore influenced the fouling layer formation on the membrane surface.

It was revealed that Ca^{2+} in feed solution could boost organic fouling formation. Parida and Ng [58] noted that Ca^{2+} addition significantly impeded the water permeation in AL-DS orientation because of the binding effects between Ca^{2+} and foulants in the porous layer. On the contrary, the inclusion of Ca^{2+} had a negligible impact on the water permeation in AL-FS orientation. Mosta *et al.,* [62] confirmed that the size of aggregate increased as the concentration of Ca^{2+} increased, which resulted in the severe flux decline in AL-DS configuration. Besides, Kim *et al.,* [63] also concluded that the extent of organic fouling was as a function of Ca^{2+} concentration. It was likely due to the abundant Ca^{2+} prone to cross link with alginate molecules and precipitate on the membrane surface [50, 51].

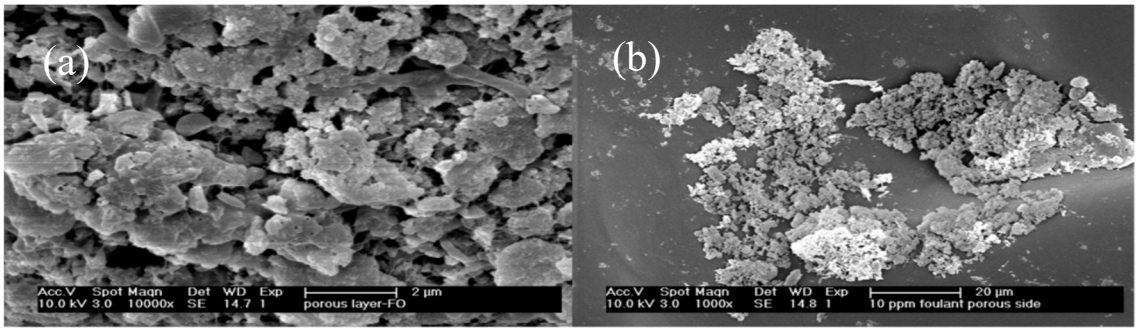

Figure 2-5: Scanning Electron Microscope (SEM) images of organic fouling on FO membrane (a-b) (adapted from [58]).

2.3.2 Colloidal fouling

Due to its infinitesimal size and wide existence in wastewater, colloids have caused severe fouling in pressure-driven membrane process [64]. Sharing the similar membrane structure, FO can be also influenced by colloidal fouling (Figure 2-6). Lee *et al.,* [10] demonstrated that colloidal fouling layer formation was strongly decided by colloidal particle size. Compared to the larger particle, small one was prone to diffuse than precipitate, which formed a thinner fouling layer. The impact of CEOP was negligible in this condition. Large particles formed a thick fouling layer that easily impeded water permeation [65]. Boo *et al.,* [52] confirmed that big size particles were hard to transport through membrane, thus resulting in a thick fouling layer. They also highlighted that the increment of CEOP caused by the colloidal fouling other than fouling layer resistance was the main reason for flux decline in FO.

The presence of organic fouling may exacerbate colloidal fouling, interfering FO performance. Kim *et al.,* [63] observed that the impact of co-existence of two foulants on flux decline was larger than their individual presence. Their results demonstrated that the applied pressure boosted to form a compact fouling layer. Furthermore, presence of Ca^{2+} significantly deteriorated both organic and colloidal fouling [64, 66, 67]. On the contrary, the findings of Motsa *et al.,* [68] revealed that the flux decline caused by either combined foulant or individual foulant was similar. Membrane orientation compromised the synergistic impact from two foulants. On the other hand, in the aspect of surface free energy, alginate other than colloidal silica played a dominant role in fouling formation due to a stronger adhesion.

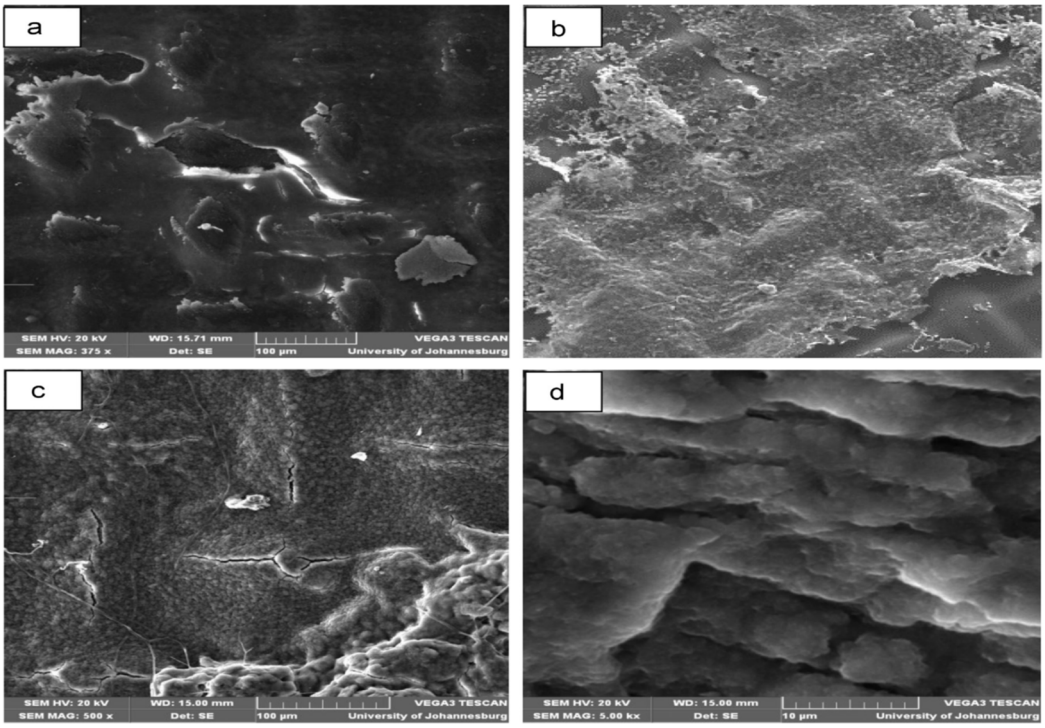

Figure 2-6: SEM images of FO membrane surface fouled with: (a) ST-ZL colloidal silica, (b) alginate and their mixture (c, d) (adapted from [68]).

2.3.3 Scaling

Scaling normally consists of oversaturated solutes, such as barium sulfate, calcium sulfate and calcium carbonates [69]. These oversaturated solutes precipitate onto membrane surface, resulting in a severe membrane flux decline. Scaling in FO membrane are shown in the Figure 2-7.

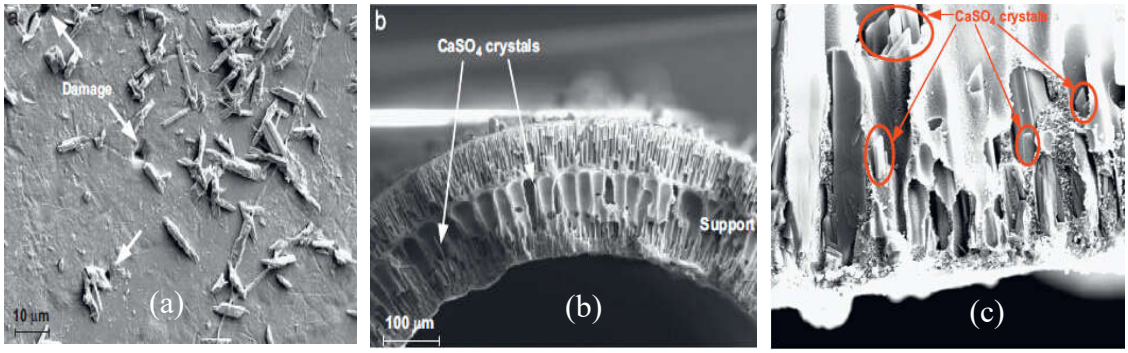

Figure 2-7: SEM images of scaling on different location of FO membrane: (a) surface of support layer, (b) cross-section of membrane and (c) enlarged cross-sectional membrane (adapted from [70]).

Scaling formation is decided by several factors (i.e. membrane property and membrane orientation). The results of Mi and Elimelech [69] indicated that membrane surface had a significant impact on the formation of scaling. Gypsum scaling was likely to precipitate on TFC membrane because of the negatively charged surface caused by carboxyl functional groups [71]. These functional groups were prone to form complexes with Ca^{2+} on the membrane surface. In contrast, gypsum scaling was more likely to get crystallization in the solution other than membrane surface because of the neutral hydroxyls surface of CA membrane. As a result, the structure of scaling on CA membrane was much looser than that on TFC membrane due to the less calcium precipitation.

Two types of mechanisms are further illustrated in Figure 2-8. Mi and Elimelech [67] identified that silica scaling formation on CA and TFC membranes were different from the gypsum scaling. Silica scaling on the membrane surface was closely related to foulant-foulant reaction rather than membrane-foulant reaction. It was anticipated that reactive silica firstly reacted with hydroxyl groups on CA membrane or $–COO^-$/$-NH_3^+$ functional groups on TFC membrane. Silica deposition on the membrane surface was formed after first foulant-membrane reaction. Foulant-membrane reaction was then connected by Si-O-C bonds, which was less stronger than foulant-foulant reaction connected by Si-O-Si bonds [72]. Silica scaling layer on TFC membrane was much strongly bonded than that on CA membrane, which was in accord with the gypsum scaling on these two membranes.

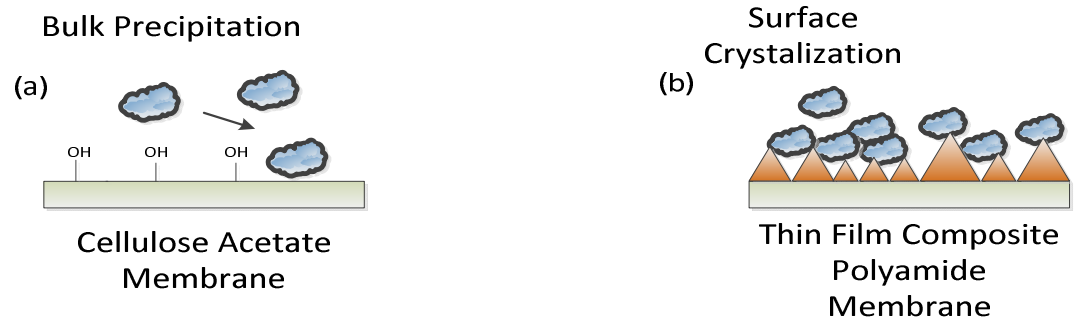

Figure 2-8. Schematic description of the proposed mechanisms controlling gypsum scaling on different membranes (adapted from [69]).

The effect of membrane surface on gypsum scaling was further investigated by Wang *et al.,* [73]. Compared to the cellulose triacetate (CTA) membrane, scaling and membrane damage were prone to occur on TFC membrane. The reason of membrane damage could be attributed to the surface chemistry and structural stability of TFC membrane.

The mechanism of scaling formation in FO might be different depends on the membrane orientation. Arkhangelsky *et al.,* [70] suggested that the scaling was prone to occur in the AL-DS membrane orientation. Either precipitation of crystals or penetration of crystals inside membrane supporting layer resulted in the pore blocking. In addition, the super-saturation index, ionic strength and anti-scaling addition affected the extent of gypsum scaling in FO. Zhang *et al.,* [74] observed that greater surface coverage by large size of gypsum crystals occurred on the FO membrane with higher super-saturation index value of feed solution. In the AL-DS orientation, the unfavorable scaling precursors inside the support layer of FO membrane resulted in the internal scaling, which led to a more severe flux decline than that in AL-FS orientation.

2.3.4 Biofouling

Besides above three fouling types, biofouling is another common fouling type in the engineering application. Biofouling causes an irreversible decrease in the permeate flux and salt rejection because of the accumulation of microorganism on the membrane surface. Yoon *et al.,* [57] compared the biofouling characteristics in FO and RO in a lab-scale system. Flux decline in FO process was less severe than that in RO process, which was consistent with results from other fouling [75]. The biofouling layer in RO was much thicker than that in FO due to the applied hydraulic pressure. In addition, the presence of

organic matter with bacteria led to a more flux decline compared to that without bacteria. The characteristics of the biofouling formation appeared to have a mature biofilm, which was hard to be removed.

It has been demonstrated that a biofouling formation is related to the concentration of phosphate. Kim *et al.,* [76] suggested the extent of biofouling in FO process was related to phosphate limitation in feed solution. They observed that the phosphate concentration determined the growth of biofilm formation by feeding live cells. Furthermore, limitation of phosphate concentration reduced the biofouling regardless of water permeation through the membrane. Since the combined effects of CEOP and biofilm-enhanced osmotic pressure (BEOP) could greatly deteriorate membrane performance, the removal of phosphate in feed water could significantly reduce the biofouling and alleviate BEOP [77].

In addition, spacer thickness can affect the formation of biofouling in FO. Valladres Linares *et al.,* [78] observed that a thicker spacer performed better than a thin spacer in terms of biofouling control. Flux decline can be reduced when they used a thicker spacer. Spacer thickness had the negligible impact on the accumulated bacteria and organic fouling. But the biofilm was prone to occur under the thick spacer in same crossflow velocity. Their results seemed to be consistent with other research which demonstrated that the dominant factor of biofouling interfering flux decline was the resistance of bacterial cells whereas the resistance because of exopolymeric substances, mainly composed of biopolymers and protein-like substances [57].

Ca^{2+} plays an important role in both organic fouling and biofouling. Xie *et al.,* [79] have illustrated the role of reverse Ca^{2+} diffusion in FO. Reverse Ca^{2+} diffusion indicated a higher biofouling incidence compared to the reverse Mg^{2+} diffusion. Ca^{2+} in solution preferred to connect carboxyl groups of polysaccharides to form a highly inter-connected network, resulting in a more stable and cohesive biofilm structure. These results were in good agreement with those reported by Lee and Elimelech [80], which demonstrated that considerable difference in terms of adhesion forces to the specific interaction between Ca^{2+} with the carboxylic groups of alginate and a cross-linked gel network. In addition, the ion complexation and bridging of extracellular polymeric substances also resulted in a thicker biofilm in comparison with Mg^{2+}.

2.4 Removal of TrOCs by FO

2.4.1 Threats from TrOCs

TrOCs refers to the expanding array of organic chemicals (pharmaceuticals, pesticides, industrial chemicals and endocrine disrupting compounds) existing in the environment at the trace levels (in the ng/L to μg/L range). These chemicals are generated from different point and are diffused into aquatic environment via the different path. Although these chemicals are at the low concentration, they may trigger non-traditional toxicological effects on the complex ecosystem. For example, the toxic potential of endocrine disrupting compounds was testified by using the contaminated fish [81]. These fishes showed abnormal hormone activities such as physiological and anatomical aberrations that were attributed to the endocrine disrupting compounds. Moreover, some of these aberrations had negative impacts on reproductive success. In addition to the adverse effects of continuous discharge of TrOCs on ecosystem, the quality of raw water for human consumption may be affected as well. Therefore, to date, the public awareness of these issues related with hazard of TrOCs keeps increasing, especially when human exposure is possible. Wastewater treatment plant appears to be an important section for removing these TrOCs prior to discharging into ecosystem. However, the increasing chemical consumption associated with rapid urbanization development continuously challenges the TrOCs removal in the conventional wastewater treatment plant. Thus, discharge of treated effluent from wastewater treatment plant presents to be the major source of TrOCs.

Several advanced approaches like ultrafiltration [82], RO [83], and NF [84] have been applied to enhance TrOCs removal in treated effluent. Although the results indicated that these treatments offer efficient removal of TrOCs, new treatment is still required to develop for effective protection for potable water. Since utilizing osmotic pressure as the driving force, FO has demonstrated the low energy consumption and less fouling tendency compared to above hydraulic pressure driven membrane process. In addition to the similar structure of selective layer in RO, FO attracts enormous attention in TrOCs removal [85-87]. Nevertheless, fouling is still an inevitable impede in FO for water permeation via affecting membrane property. Besides, the thickness and compactness of fouling in FO and RO were reported significantly different due to their corresponding driving force [51]. As a result, their filtration behaviors were influenced by the variation

of membrane fouling [88]. It is imperative to study effect of fouling on TrOCs removal in FO.

2.4.2 Impact of membrane fouling on TrOCs removal in FO

Previous studies have proposed three main rejection mechanisms for TrOCs removal in NF and RO [6, 89]. They are steric hindrance (namely TrOCs rejection increase as their molecular size increase), electrostatic interaction (relationship between charged compounds and negatively charged membrane), and adsorption (largely depend on compound hydrophobicity). As previous described, FO shares the similar structure of selective layer with NF and RO, three mechanisms are therefore estimated to be the major TrOCs rejection mechanisms. However, membrane fouling induced the change on membrane property including surface charge and hydrophobicity. It was suggested that rejection of TrOCs correlated well to degree of membrane fouling and change of membrane surface characteristics.

Organic fouling layer consists of carboxylic radicals and hydroxyl functional groups could change membrane surface charge. Valladares Linares *et al.,* [90] observed that organic acids and polysaccharides from effluent of treatment plant mainly contributed to organic fouling on membrane. Fouled membrane surface became more negatively charged. Rejection of negatively charged TrOCs by fouled membrane was therefore higher than clean one due to the increasing electrostatic repulsion. Xie *et al.,* [41] also observed that increasing rejection of negatively charged TrOCs was due to the enhanced electrostatic repulsion caused by interaction between membrane surface and humic acid organic foulants. However, effect of fouling on the rejection for positively charged compounds is still incomplete understood. It is also suggested to conduct the investigation related with rejection mechanism of positively charged TrOCs by fouled membrane.

Organic fouling can not only influence electrostatic interaction but also affect steric hindrance by changing membrane pore size. It was reported that the fouling accumulated on the membrane surface could minimize the pore size of membrane, thus enhancing the effect of steric hindrance on neutral compounds [91]. Xie *et al.,* [41] observed that fouling layer caused by humic acid resulted in the decreasing permeation of neutral TrOCs. The hypothesized organic fouling extended a hydration layer of membrane to shrink the effective membrane pore size, thus, for the neutral compound growing rejection. However, fouling layer in FO is a considerable porous structure, which therefore leads to the cake-

enhanced concentration polarisation and elevated concentration of TrOCs, enhancing TrOCs diffusion consequently [92].

It is also interesting to note that fouling structure is largely determined by the initial permeate flux, resulting in a variation in TrOCs rejection. A porous cake structure caused by the low initial permeate flux improved the steric hindrance through pore blockage. On the contrary, a cohesive dense fouling layer caused by the high initial permeate flux whereas reduced TrOCs rejection due to the cake-enhanced concentration polarization [42]. Similar observations based on the compact fouling in NF showed that cake-enhanced concentration polarisation resulted in a noticeable decline of rejection for ibuprofen, carbamazepine, sulfamethoxazole and bisphenol A [89, 93].

Adsorption is one of three proposed rejection mechanisms as well. The relationship between hydrophobicity of TrOCs and foulants had a significant impact on compound rejection. Valladres Linares *et al.,* [90] observed the hydrophobicity of the fouled membrane decreased, thus hindering the diffusion of hydrophilic neutral TrOCs. For example, the rejection of caffeine increased 15% by fouled membrane due to the formation of hydrophobic fouling layer. These results were consistent with the study that indicated membrane swelling decreased the rejection of the hydrophilic neutral TrOCs [94]. Besides, cake-enhanced concentration polarisation also decreased the rejection of hydrophobic neutral TrOCs [95]. Different TrOCs rejection mechanism hypothesis related with compound hydrophobicity is illustrated in Figure 2-9.

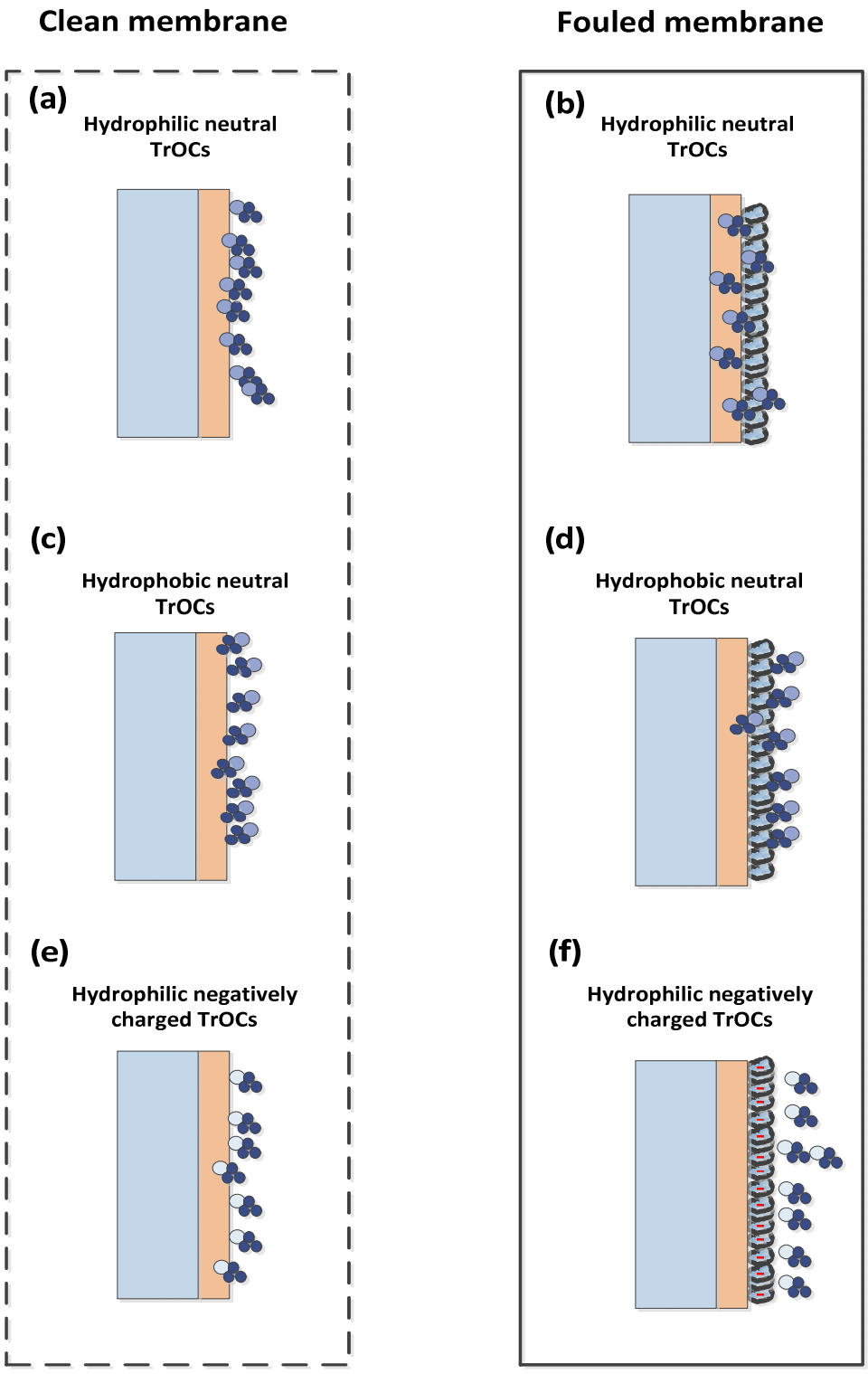

Figure 2-9: Different hypothesis about rejection of TrOCs by cleaned and fouled membrane. (a) and (b) for the hydrophilic neutral TrOCs; (c) and (d) for the hydrophobic neutral TrOCs; (e) and (f) for the hydrophilic negatively charged TrOCs (adapted from [90]).

2.4.3 Impact of draw solution chemistry on TrOCs removal in FO

Table 2-2: Effect of draw solution chemistry on FO performance.

Compounds	Membrane	Draw solution	Investigating parameters	Effects	References
Bisphenol A Triclosan Diclofenac	CTA	NaCl $MgSO_4$ Glucose	Species	Reverse diffusion of Na^+ was larger than that of Mg^{2+} and glucose, which enhanced the TrOCs rejection	Xie *et al.,* [88]
Boron	TFC	NaCl $CaCl_2$ $LaCl_3$	pH and species	pH had a negligible impact on boron transportation; Reverse of Na^+ greatly hindered the boron solute flux than other two ions;	Kim *et al.,* [96]
Atenolol Atrazine Caffeine	CTA	Mono-ammonium phosphate Di-ammonium phosphate KCl	Species and concentration	Di-ammonium phosphate showed the highest TrOCs rejection whereas lowest water flux due to the lowest concentrative ECP; High draw concentration reduced TrOCs rejection due to the enhanced concentrative ECP;	Kim *et al.,* [97]
Boron	TFC	NaCl Na_2CO_3	pH and species	pH increase enhanced boron rejection due to the stronger electrostatic repulsion in AL-FS orientation; Na_2CO_3 showed a better boron rejection than NaCl because of larger back diffusion of OH^-	Wang *et al.,* [98]
9 TrOCs	TFC CTA	NaCl $MgCl_2$	Species and concentration	Mg^{2+} showed a lower negatively charged TrOCs rejection than Na^+ due to the weaker electrostatic interaction;	Sauchelli *et al.,* [37]

				High concentration reduced electrostatic interaction, therefore diminishing negatively charged TrOCs rejection	
30 TrOCs	Aquaporin	NaCl $MgSO_4$ Glucose	Species and concentration	TrOCs rejection increased as a function of concentration; Reverse diffusion of Na^+ was larger than that of Mg^{2+} and glucose, which enhanced the ionic TrOCs rejection	Xie *et al.,* [36]

Previous studies have extensively investigated the feed solution chemistry (i.e. fouling) on TrOCs removal in FO. As discussed in section 2.2.1, unlike the NF/RO process in which solute and solvent transport can only occur in one direction from the feed to the permeate side, solute transport in FO is bidirectional. In the FO process, as water is transported from the feed to the draw solution under an osmotic gradient, due to engineering defects, some substances (e.g. draw solutes, protons or hydroxyl ions) can also be transported in the opposite direction from the draw to the feed solution. This phenomenon is often referred to as 'reverse salt flux'.

Reverse salt flux and draw solution chemistry are important factors governing FO performance (in terms of solute rejection and water flux) but to date they have been largely overlooked in the literature. Indeed, several recent studies have highlighted the significance of draw solution chemistry on solute rejection by FO (Table 2-2). Wang *et al.,* [98] demonstrated a significant increase in boron rejection by FO when using an alkaline draw solution. They ascribed the observed increase in boron rejection to the interaction between their draw and feed solutions whereby there was an increase in hydroxyl ions near the membrane surface on the feed side. This lead to the protonation of boric acid and subsequently increase of boric acid rejection by charge repulsion [98]. Xie *et al.,* [88] observed that the extent of forward diffusion of TrOCs was related to the reverse diffusion of draw solutes. They reported that the highest rejection occurred with highest reverse diffusion of draw solutes [88]. On the contrary, Sauchelli *et al.,* [37] observed that TrOCs permeation was only affected by the reverse salt flux at high draw solution concentration. Considerable back diffusion of draw solute penetrated through the membrane to influence electrostatic interaction between charged compounds and negatively charged membrane surface.

2.5 Innovative FO application in post-combustion CO_2 capture

2.5.1 Water usage in amine-based solvent absorption

Post-combustion CO_2 capture can be readily retrofitted to existing power plants. Thus, this technology has become possibly the most studied technology for CO_2 sequestration [99]. Several types of approaches including chemical absorption [100-102], adsorption [103], membrane separation [104], and cryogenic fractionation [105] have been proposed and investigated. Of a particular note, chemical absorption is considered as the most-

likely dominant technology to be implemented for the commercial-scale CO_2 capture from coal-fired power station before 2030 [17]. In fact, this method has been demonstrated in two commercial scale post-combustion CO_2 capture plants in Boundary Dam [106] and Petra Nova [107].

The amine-based chemical absorption process is briefly described in the Figure 2-10. Exhaust flue gas containing 12-14% CO_2 is fed to the absorption column. Chemical adsorbents such as MEA [108, 109], amino acid (i.e. glycine) [102], ionic liquid-based solvent [110], and ammonia-based solvent [111] in the absorption column can react with 75-90% of CO_2 to purify the exhaust gas at 30-50 °C. The terms CO_2 lean and rich solution are referred to solutions before and after CO_2 absorption, respectively. Due to the thermally reversible reaction between CO_2 and chemicals, CO_2 can be released by heating at a reduced pressure. The CO_2 rich solution is transferred to the desorption column to obtain pure CO_2 product. On the other hand, the heated CO_2 lean solution is cooled down by a trim cooler for re-absorbing CO_2.

Cooling and make-up water provision in amine-based solvent absorption increase water demand of existing power station. There are two types of water cooling system depends on the water circulation loop. The first one is once-through cooling system (open loop), which directly discharge the warm cooling water to nearby lake or river after heat transfer from regenerated CO_2 lean-loaded solution. The second cooling system is wet recirculating system conducted in a cooling tower. Temperature decrease of regenerated CO_2 lean-loaded solution is realised by heat transfer via water evaporation. Water loss after evaporation can be made up by withdrawing water from nearby freshwater bodies (e.g. lake or river). The water consumption in once-through system can be as two orders of magnitude higher than that in recirculating system [112]. On the other hand, it is necessary to reduce flue gas temperature for effective CO_2 capture, which needs the implement of evaporative cooling and suitable water quality.

Specifically, make-up water is greatly required in water wash section at the head of absorption column, where fresh water is required to constrain amine concentration in the washing loop. Due to the impurity in flue gas, the condensed water after regeneration process failed to be reused directly for make-up water without purification process. In Australia, flue gas without desulphurization results in additional cooling water demand to satisfy the requirement of retrofit CO_2 capture [113].

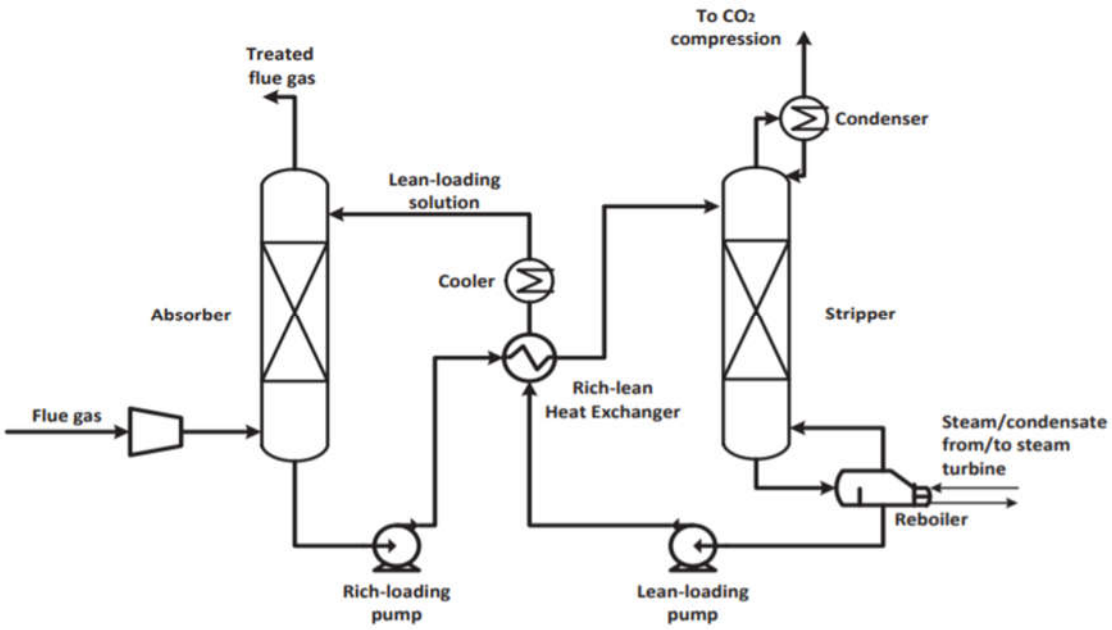

Figure 2-10. A schematic diagram of chemical absorption process in post-combustion CO_2 capture (adapted from Feron *et al.,* [113]).

2.5.2 Make-up water production by FO

FO has been explored for several novel applications including sludge dewatering [30], resource recovery from wastewater [114], food processing [115] and produced water treatment for the oil and gas industry [27]. Feron *et al.,* [113] have recently proposed to replace the trim cooler by FO in post combustion CO_2 capture (Figure 2-11). Due to the osmotic gradient, water transfer was observed from simulated seawater to three CO_2 absorption solvents (glycine, sodium glycinate, and MEA) at 45 °C. Feron *et al.,* [113] demonstrated that sodium glycinate could generate the highest water flux. However, further experiments were needed to validate the replacement by FO based on their current heat transfer simulation results. Gwak *et al.,* [116] have conducted a number of investigations into high saline water or flue gas desulfurization wastewater as the cooling source (feed solution) when 5 M rich MEA was used as draw solution. Potential of replacement by FO was also testified by the observed water fluxes varied from 8-20 L/m^2h as salinity of feed solution decreased. In addition, the fouled membrane could be readily cleaned despite of the high scaling potential. However, little is still known about the feasibility for the replacement of a trim cooler by FO.

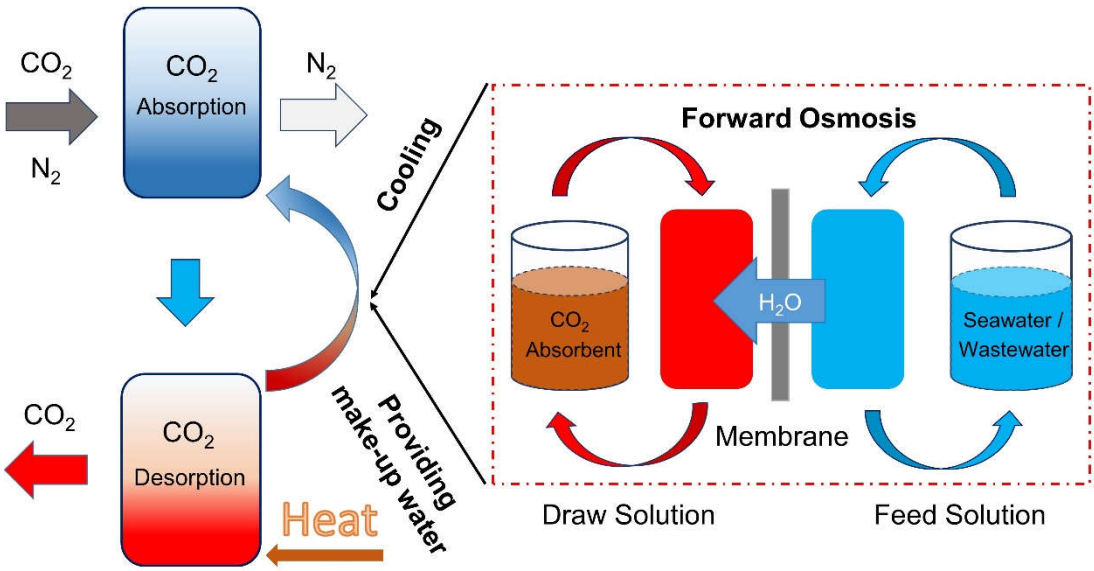

Figure 2-11: Replacement of the trim cooler by forward osmosis in post-combustion CO_2 capture.

2.6 Conclusion

This chapter provides some perspectives of innovative FO application on TrOCs removal and cooling for amine-based solvent absorption in the context of wastewater reclamation. Due to its bidirectional solute transport, chemistry of draw solution may affect feed solution chemistry and therefore FO performance. In accordance with this proposal, investigation of feed chemistry (i.e. membrane fouling) can provide a state-of-the-art understanding on TrOCs rejection in FO. For example, fouling cake layer results in either increasing rejection for neutral compound caused by enhanced steric hindrance or decreasing rejection caused by cake-enhanced concentration polarization. In addition, systematic investigation on draw solution chemistry is recommended for development and deployment of FO-based hybrid system for practical wastewater reclamation.

Furthermore, a proof-of-concept about using FO as an alternative cooler using wastewater in post-combustion CO_2 capture is highlighted in this chapter. Based on the limited findings related to this study, further development of the practical aspects of this concept via FO-based hybrid system is recommended. Techno-economic assessments regarding energy consumption of this concept should be evaluated to address the likely advantages than current technologies. Developments of FO membrane material and draw solution are expected to enhance FO separation performance towards wastewater reclamation.

Chapter 3 Effects of fouling on separation performance by forward osmosis: the role of specific organic foulants

This thesis chapter has been published as the following journal article.

L. Zheng, W.E. Price, and L.D. Nghiem, Effects of fouling on separation by forward osmosis: the role of specific organic foulants. Environmental Science and Pollution Research, 26 (2019), 33758-33769.

3.1 Introduction

Although several researchers have demonstrated that FO has a much lower fouling propensity compared to the pressure driven membrane treatments [10, 88], any fouling layer formed can still potentially affect the rejection behavior of TrOCs. Organic matter including biopolymers, humic substances and other small molecular weight organic compounds are major sources of foulants during the FO process. Biopolymer, such as sodium alginate is made up of repeating manuronic and guluronic acids. Humic substances are a mixture of heterogeneous recalcitrant macro-organic compounds that occur naturally in the environment.

Rejection of target contaminants, water flux and reverse salt flux can all be affected by membrane fouling. However, to date, there have only been a few investigations to elucidate the effect of membrane fouling during FO operation on the performance particularly for TrOCs rejection. The impacts of fouling on TrOCs rejection can be attributed to several mechanisms. Valladares Linares *et al.,* [90] found that membrane fouling caused by natural organic matter in wastewater enhanced the rejection of ionic and neutral TrOCs by altering membrane surface charge and hydrophobicity. Xie *et al.,* [41, 42] have recently investigated the impact of colloidal fouling on the rejection of TrOCs. They hypothesized that the mechanism for the rejection of TrOCs by a humic acid fouled membrane was based on the membrane pore size and steric hindrance. In addition, combined fouling with organic and colloidal particles was the result of membrane pore blockage and thus enhanced steric hindrance effects. D' Haese *et al.,* [92] found that an alginate fouled membrane exhibited lower rejections for some TrOCs than

a clean membrane. This was thought to be possibly due to the cake enhanced concentration polarization arising from the cake layer formed by organic foulants.

This chapter aims to investigate the effect of membrane fouling caused by specific organic foulants (humic substances, sodium alginate and municipal wastewater) on the rejection of two model TrOCs (i.e. sulfamethoxazole and carbamazepine) by a commercially available TFC FO membrane. These chemicals at trace level are persistent in the environment and have been frequently detected in the secondary treated effluents. Key membrane properties and the rejection behaviors of the clean and fouled membranes are assessed to systematically elucidate the mechanism of different foulants on the rejection of TrOCs.

3.2 Materials and Methods

3.2.1 Materials

A flat-sheet TFC FO membrane purchased from Porifera (Hayward, CA, USA) used in this study. Similar to other TFC FO membranes in the market, it consists of an ultra-thin active polyamide skin layer on the top of a microporous polysulfone supporting layer.

Municipal wastewater (primary effluent) was obtained from a wastewater treatment plant in New South Wales, Australia. Humic acid and sodium alginate from Sigma-Aldrich (St. Louis, MO, analytical grade) were selected as model foulants to represent humic substances and polysaccharides, respectively, since they commonly occur in municipal wastewater. Deionized (DI) water was used to prepare stock solutions containing 2 g/L of each model foulant. These stock solutions were stored in sterilized glass bottles at -4 °C.

Analytical grade sulfamethoxazole and carbamazepine from Sigma-Aldrich (St. Louis, MO, analytical grade) were selected as model TrOCs. Their key physicochemical properties are presented in the Table 3-1. A combined stock solution containing 2 g/L of each TrOCs was prepared in pure methanol which was kept at -18 °C in the dark and was used within one month.

Analytical grade erythritol, xylose, and glucose (Sigma-Aldrich, St. Louis, MO) were used as reference organic solutes to estimate the effective pore size of membrane active layer. These organic solutes were individually dissolved in DI water to obtain a concentration of 40 mg/L (as total organic carbon (TOC)).

Table 3-1: Key physicochemical properties of sulfamethoxazole and carbamazepine.

Pharmaceutical	Sulfamethoxazole	Carbamazepine
Structure	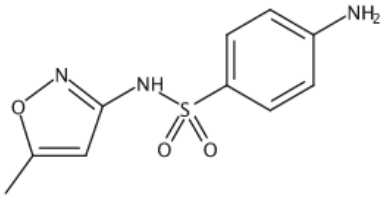	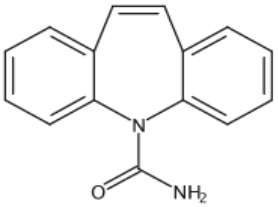
Molecular weight (Da)	253.3	236.3
pK_a[1]	1.7, 5.8	9.73
Log K_{ow}[1]	0.89	2.45
Dipole moment (Debye)[2]	5.4	3.6
Stokes radius (nm)	0.38	0.37
Molecular length (nm)[2]	1.031	0.891
Molecular width (nm)[2]	0.587	0.529
Molecular depth (nm)[2]	0.526	0.507

[1] From the SciFinder Scholar (ACS) database. [2] Molecular dimensions and the dipole moment calculated using Molecular Modeling Pro Version 6.3.3 (Chem SW Inc.)

3.3 Experimental systems

A bench scale FO system was used in this study (Figure 3-1). A membrane cell consists of two acrylic plastic semi-cells with length, width and height of 10, 5, and 0.2 cm, respectively. The membrane was placed between the two semi-cells with an effective area of 44.65 cm^2. Two gear pumps (Micropump, Vancouver, WA) were used to circulate the feed and draw solution simultaneously at a constant cross flow rate of 0.5 L/min (corresponding to a cross-flow velocity 8.9 cm/s) which was monitored by two rotameters. A draw solution reservoir was placed on a digital balance (Mettler-Toledo Inc., Hightstown, NJ) and weight change was recorded every 5 minutes by a data logger. A conductivity probe (Cole-Parmer, Vernon Hills, IL) was used to measure the conductivity of the draw solution. When the draw solution conductivity deviated from the set point by 0.1 mS/cm, a small volume of concentrated draw solution (5 M NaCl) was automatically added into the draw solution reservoir using a peristaltic pump to maintain a constant draw solution concentration. The concentrated draw solution reservoir was also placed on

the same digital balance to avoid any interference caused by liquid transfer between the two reservoirs.

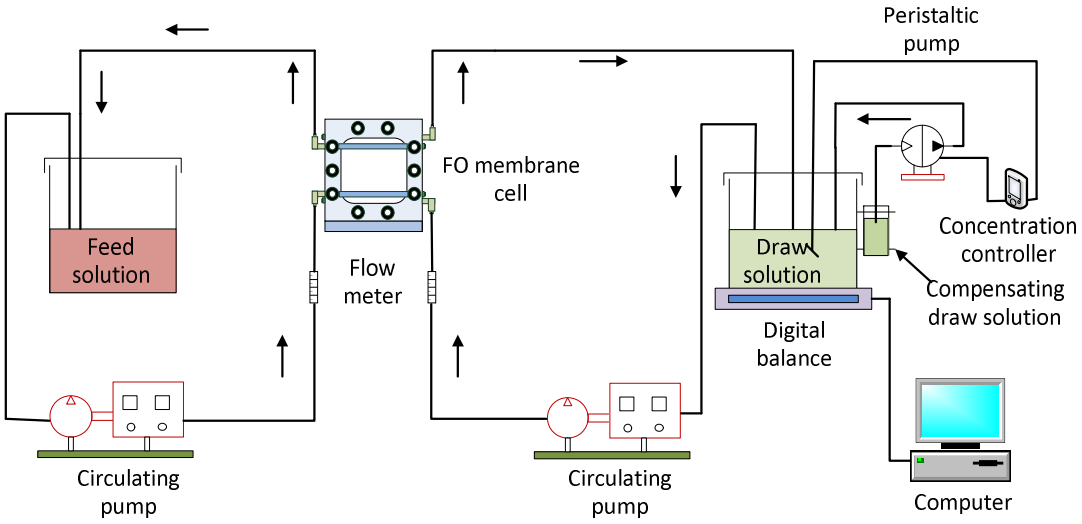

Figure 3-1: The schematic diagram of the forward osmosis system.

Water permeability (A value) and salt (NaCl) permeability (B value) were characterized according to the standard method previous described by Cath *et al.,* [117]. This involves a cross-flow system consisting of a stainless steel cross flow membrane cell, a Hydra-Cell pump (Wanner Engineering, Minneapolis, MN) and chiller (Neslab RTE7, Waltham, MA). The membrane cell had a flow channel with dimensions of length, width and height of 10, 4, and 0.2 cm, respectively. The effective membrane area was 40 cm^2. The feed solution was pressurized into the membrane cell by pump. The cross-flow rate and the hydraulic pressure were controlled by a back-pressure regulator and a bypass valve, respectively. The temperature of feed solution was maintained at 20 ± 1 °C by the chiller equipped with a stainless steel heat exchanger. A digital flow meter (Optiflow, Palo Alto, CA) connected to a computer was used to record the permeate flux.

3.4 Membrane characterisation

3.4.1 Membrane active layer transport properties

The pure water permeability coefficient (A value) and salt (NaCl) permeability coefficient (B value) of the membrane active layer were determined according to the standard protocol developed by Cath *et al.,* [117]. DI water and NaCl solution (2 g/L) were used as feed solutions to determine the membrane A and B values, respectively. The membrane was first compacted for 2 h at the applied hydraulic pressure (ΔP) 10 bar and

cross flow velocity of 25 cm/s to yield a stable water flux. The water flux values of DI water (J_{DI}) and NaCl solution (J_{NaCl}) were then determined. At the end of the filtration experiment, the feed and permeate samples were collected to measure the concentration of NaCl for calculating the observed rejection (R). The A and B values were calculated as follows:

$$A = \frac{J_{DI}}{\Delta P} \tag{3-1}$$

$$B = J_{NaCl} \times (\frac{1-R}{R}) \times \exp(-\frac{J_{NaCl}}{k_f}) \tag{3-2}$$

where k_f represents the mass transfer coefficient of the channel of the cross-flow membrane cell [117]. The mass transfer coefficient k_f was calculated using the Sutzkover *et al.,* [118].

$$k_f = \frac{J_{DI}}{\ln\left\{\frac{\Delta p}{\pi_b - \pi_p} \times \left[1 - \frac{J_{NaCl}}{J_{DI}}\right]\right\}} \tag{3-3}$$

where π_b and π_p are the feed and permeate osmotic pressures, which can be calculated by their corresponding salt concentrations based on van't Hoff equation.

3.4.2 Membrane support layer structural properties

The membrane structure parameter, S, was experimentally obtained in the cross-flow FO setup as described above in FO mode (i.e. active layer facing feed solution). A NaCl draw solution (0.5 M) and DI water feed solution were used. The membrane S value was calculated using following equation [117]:

$$S = \frac{D_s}{J_w} \times \ln\left(\frac{B + A\pi_{D,b}}{B + J_w + A\pi_{F,m}}\right) \tag{3-4}$$

where D_s is the diffusivity of the draw solute, $\pi_{D,b}$ is the bulk osmotic pressure of the draw solution, and $\pi_{F,m}$ is the osmotic pressure at the membrane surface on the feed side.

3.4.3 Determination of the membrane average pore radius

The effective pore radius of membrane active layer was estimated by the three reference organic solutes previously described in section 3.2.1. These solutes are inert, neutral and

do not adsorb onto membrane. The experiments were conducted in the cross-flow RO setup as described in section 3.3. The membrane sample was compacted for 3 h at 10 bar. Subsequent experiments were conducted at 5, 6, 8, 10 and 12 bar with a cross-flow velocity of 25 cm/s. At each pressure value, the RO filtration system was operated for 1 h before taking permeate and feed samples.

In this model, the ratio of solute radius (r_s) to the membrane pore radius (r_p), $\lambda = r_s / r_p$ is related to the distribution coefficient of hard-sphere particles (ϕ) when only steric interactions are considered:

$$\phi = (1-\lambda)^2 \tag{3-5}$$

To obtain the real rejection of the reference organic solutes (R_r) from so-called sieving coefficient, S_a, the calculations below were applied:

$$S_a = \frac{C_L}{C_0} = \frac{\phi K_c}{1-\exp(-Pe)(1-\phi K_c)} \tag{3-6}$$

$$R_r = 1-\frac{C_L}{C_0} = 1-S_a = 1-\frac{\phi K_c}{1-\exp(-Pe)(1-\phi K_c)} \tag{3-7}$$

where C_0 and C_L are the solute concentrations outside the pore entrance (i.e. on the membrane surface in the feed side) and pore exit (i.e. on the membrane surface in the permeate side), respectively; K_c is the hydrodynamic hindrance coefficient for the conviction; and P_e represents the membrane Peclet number, which can be defined as:

$$Pe = \frac{K_c J_r l_a}{K_d D} = \frac{K_c J_v l_a}{K_d D \varepsilon_a} \tag{3-8}$$

where K_d is the hydrodynamic hindrance coefficient diffusion; J_r denotes the radial average fluid velocity in a cylindrical membrane pore, which equals to the membrane volumetric permeate flux (J_v) divided by the effective porosity of the membrane active layer (ε_a); D is the Stokes-Einstein diffusion coefficient, l_a is the theoretical pore length (i.e. the thickness of the membrane active layer). Details on the calculations of P_e, K_c and K_d have been described elsewhere [119, 120].

Using the film theory for concentration polarization, the relation between observed rejection of organic solutes (R_o) and the real rejection (R_r) can be represented via:

$$\ln\frac{1-R_r}{R_r}=\ln\frac{1-R_o}{R_o}-\frac{J_v}{k_f} \qquad (3\text{-}9)$$

where the R_o is calculated based on the different concentrations of TOC between feed and permeate samples.

The real rejection (R_r) of each reference organic solute was calculated from observed rejection (R_o) by considering concentration polarization effects using equation (3-8) and the mass transfer coefficient in equation (3-3). In the pore hindrance transport model, since ϕK_c and P_e/J_v are unlikely related to R_r, thus they can be determined by fitting the reference organic solute rejection data to the model using equation (3-7). The optimization procedures were conducted by the Excel (Solver, Microsoft). Furthermore, the parameters ϕK_c and P_e/J_v can be expressed as a sole function of the variable λ, which is the ratio of solute radius (r_s) to membrane pore radius (r_p). Therefore, the membrane average pore radius can be calculated from the variable λ.

3.4.4 Membrane surface charge and hydrophobicity

The membrane surface charge represented by zeta potential was analyzed by a SurPASS streaming current electrokinetic analyzer (Anton Paar GmbH, Graz, Austria). Based on the Fairbrother-Mastin method [121], the zeta potential was calculated from the measured streaming potential data. Membrane samples were mounted in the cell and to form a capillary flow channel. All streaming potential measurements were performed in a background electrolyte solution containing 10 mM KCl. The same electrolyte solution was used to rinse the cell through the channel thoroughly prior to automatic pH titration within HCl (1 M) or KOH (1 M). All measurements were conducted at room temperature (ca 25 °C).

The membrane surface hydrophobicity was evaluated by contact angle measurement using a Rame-Hart Goniometer (Model 250, Rame-Hart, Netcong, NJ). Standard sessile drop method was used for analyzing contact angle. Membrane samples were air-dried in a desiccator before the analysis. Ten droplets of DI water were applied to each membrane sample and the mean values of contact angles on both sides of the droplet were evaluated.

3.5 Forward osmosis experiments

NaCl solution (0.5 M) was used as the draw solution. The synthetic wastewater was prepared by adding either sodium alginate or humic acid to an electrolyte solution of 1 mM $CaCl_2$ to obtain 200 mg/L of each of these model organic foulant. The initial volumes of the feed and draw solution were 3 L and 0.25 L, respectively. All experiments were conducted in FO mode for 20 h. The synthetic feed solutions were adjusted to the same pH of municipal wastewater (pH 5.5) by adding a small volume of either 1 M HCl or NaOH. TrOCs were introduced into the feed solution to obtain 2 mg/L of each compound. It is noted that this concentration and the typical concentration of TrOCs in wastewater are too small to contribute to membrane fouling. Approximate 3 mL of feed and draw solution samples were collected at specific time intervals for analysis. The experiment was conducted in a temperature controlled room (25 ± 1 °C).

Since the concentration of TrOCs in permeate during the experiment is diluted by the draw solution, a dilution factor is introduced to determine the permeate concentration:

$$J_N = \frac{J_t}{J_0} \tag{3-10}$$

$$DF = \frac{V_{draw,t}}{\Delta V_{feed,t}} \tag{3-11}$$

$$\Delta V_{feed,t} = \frac{M_{draw,t} - M_{draw,0}}{\rho_{water}} \tag{3-12}$$

$$V_{draw,t} = V_{draw,0} + \Delta V_{feed,t} \tag{3-13}$$

where J_N is the normalized flux; J_t is the water flux at time t; J_0 is the initial water flux; DF is the dilution factor; $\Delta V_{feed,t}$ is the volume of permeated feed solution during t hour; $M_{draw,t}$ is the weight of draw solution at time t; and $M_{draw,0}$ is the weight of draw solution at initial time. $V_{draw,t}$ is the volume of draw solution at time t; ρ_{water} is the density of water.

Thus, the rejection of TrOCs is calculated by the following equation:

$$R(\%) = \left[1 - \frac{DF \times C_{draw,t}}{C_{feed,t}}\right] \times 100 \tag{3-14}$$

The reverse flux of draw solute J_{salt} is calculated by the mass balance calculation:

$$J_{salt} = \frac{\left(C_t \times V_{feedt} - C_0 \times V_{feed0}\right)}{A \times t} \quad (3\text{-}15)$$

$$V_{feedt} = V_{feed0} - \Delta V_{p,t} \quad (3\text{-}16)$$

where C_0 and C_t are the concentrations of the draw solute in the feed at initial time 0 and time t, respectively. $V_{feed,0}$ and $V_{feed,t}$ are the volumes of the feed at initial time and time t, respectively. A is the effective membrane area.

3.6 Analytical methods

The concentrations of sulfamethoxazole and carbamazepine in the feed and draw solution were analyzed by an High-Performance Liquid Chromatography system (Shimadzu, Kyoto, Japan). The system was equipped with a Supelco Drug Discovery C18 column (with a diameter, length, and pore size of 4.6 mm, 150 mm and 5 μm, respectively) and a UV-Vis detector. The detection wavelength used was 280 nm. The mobile phase composed of acetonitrile and Milli-Q water buffered with 25 mM KH_2PO_4. Eluent A (80% acetonitrile + 20% buffer, V/V) and Eluent B (20% acetonitrile + 80% buffer) were delivered at 0.8 mL/min through the column in time-dependent gradient for 30 mins. The sample injection volume of 50 μL was used. The coefficient of determination (R^2) of the calibration was above 0.99. The limit of quantification for both sulfamethoxazole and carbamazepine under these conditions was 10 μg/L.

Conductivities of the feed and draw solutions were measured using an Orion 4-Star plus conductivity meter (Thermo Fisher Scientific, Waltham, MA). A V_{CSH} TOC analyzer (Shimadzu, Kyoto, Japan) was used for TOC concentration measurement.

Molecular weight distribution of each organic foulant was analyzed by Liquid Chromatography with Organic Carbon Detection (LC-OCD) (Model 8, DOC-Labor, Karlsruhe, Germany). The concentrations of dissolved organic carbon (DOC) of three samples were approximate 1 mg/L, which were analyzed by A VCSH TOC analyzer (Shimadzu, Kyoto, Japan). All samples were filtered through 0.45 μm filter paper prior to analysis. The physical description and method of LC-OCD analysis have been previously published by Huber et al. [122]. The customized software (ChromCALC, DOC-LABOR, Karlsruhe, Germany) was used to acquire data and process data.

3.7 Results and discussion

3.7.1 Membrane transport parameters

The separation performance of the FO process is dependent on the membrane transport parameters, including A, B, and S value. These transport parameters of the TFC FO membrane in this study were characterized and compared to those from commercially available membranes, such as CTA FO membranes (Table 3-2). CTA FO membrane is composed of a cellulose triacetate active layer with an embedded woven support layer. Results in Table 3-2 show that this TFC FO membrane has a significantly higher A value and slightly higher B value than the CTA membranes from Hydration Technology Innovations (HTI, Albany, OR). On the other hand, the TFC FO membrane in this study has lower performance parameters in terms of both A and B values compared to the TFC FO membrane from HTI. In addition, the TFC FO membrane in this study has a lower S value than the other commercial membranes shown in Table 3-2. A low S value is desirable as it results in a less severe internal concentration polarization (ICP) effect [124, 125], thus, a higher flux and solute rejection [91, 123]. Overall, the results in Table 3-2 suggest that the TFC FO membrane used in this study is comparable to other currently available in terms of key performance parameters.

Table 3-2: Comparison of key transport parameters between the TFC FO membrane used in this study and several other FO membranes currently available in the market The experimental conditions were as follows: For A and B value, DI water and NaCl (2g/L) as feed solution in cross flow RO setup, applied hydraulic pressure = 10 bar, cross flow velocity = 25 cm/s. For S value, NaCl (0.5 M) as draw solution and DI water as feed solution in cross flow FO setup (average ± standard deviation from duplicate experiments) ([1] from Xie *et al.,* [123]; [2] from Luo *et al.,* [7]).

Membrane	Literature			This study
	CTA[1]	CTA[2]	TFC[1]	TFC
Pure water permeability, A ($L \cdot m^{-2} \cdot h^{-1} \cdot bar^{-1}$)	0.65 ± 0.03	0.84 ± 0.03	4.70 ± 0.16	3.20 ± 0.22
Salt (NaCl) permeability coefficient, B ($L \cdot m^{-2} \cdot h^{-1}$)	0.25 ± 0.07	0.32 ± 0.06	0.16 ± 0.03	0.41 ± 0.01
Membrane structural parameter, S (mm)	0.67 ± 0.13	0.57 ± 0.02	0.52 ± 0.11	0.46 ± 0.05

3.7.2 Membrane average pore radius

Steric hindrance is expected to be the key rejection mechanism of TrOCs. Thus, it is imperative to determine the membrane pore radius. The TFC FO membrane used in this study has an estimated pore radius of 0.37 nm (Table 3-3), which is similar to that of the CTA membranes from HTI (Table 3-4). Nevertheless, the TFC FO membrane used in this study shows a higher water permeability (A value) as can be seen in Table 3-2. On the other hand, the pore radius of the TFC membrane in this study is smaller than that of the TFC polyamide FO from HTI (Table 3-4). In agreement with this pore size observation, the membrane investigated here also shows lower water permeability (A value) compared to the TFC FO membrane from HTI.

Table 3-3: Estimated average membrane pore radii of the clean FO membrane. The experimental conditions were as follows: The membranes were compact for 3 h at the 10 bar. The concentration of each organic solute in DI water is 40 mg/L. Subsequent experiments were conducted at 5, 6, 8, 10 and 12 bar with a cross-flow velocity of 25 cm/s.

Test	Organic solute	Solute size r_s (nm)	$\lambda = r_s/r_m$	Pore radius r_m (nm)
1	Glucose	0.32	0.790	0.41
2		0.32	0.769	0.42
1	Xylose	0.29	0.824	0.35
2		0.29	0.758	0.38
1	Erythitol	0.26	0.830	0.31
2		0.26	0.768	0.34
		Average		0.37 ± 0.04

Table 3-4 Calculated average membrane pore radii of the CTA and TFC FO membrane active layers ([1] from Xie *et al.,* [123]; [2] from Luo *et al.,* [7]).

	Literature			This study
Pore radius r_p (nm)	CTA[1]	CTA[2]	TFC[1]	TFC
	0.37	0.34	0.42	0.37

3.7.3 Organic characterization of model organic foulants by LC-OCD

The molecular weight distributions of the organic matter in wastewater and model foulant solutions were determined by size exclusion chromatography using LC-OCD (Figure 3-2). The organic matter was eluted successively based on the molecular size, namely fraction A: biopolymers (≥20,000 Da including proteins, protein-like material, polysaccharides, polysaccharide-like material, amino sugars), fraction B: humic

substances (1000 – 20,000 Da), fraction C: building blocks (breakdown products of humic substances, 350 – 500 Da), fraction D low molecular weight (LMW) acids (< 350 Da, which are anions at the neutral pH of the buffer), fraction E: LMW neutrals (< 350 Da, which are hydrophilic in nature) [122].

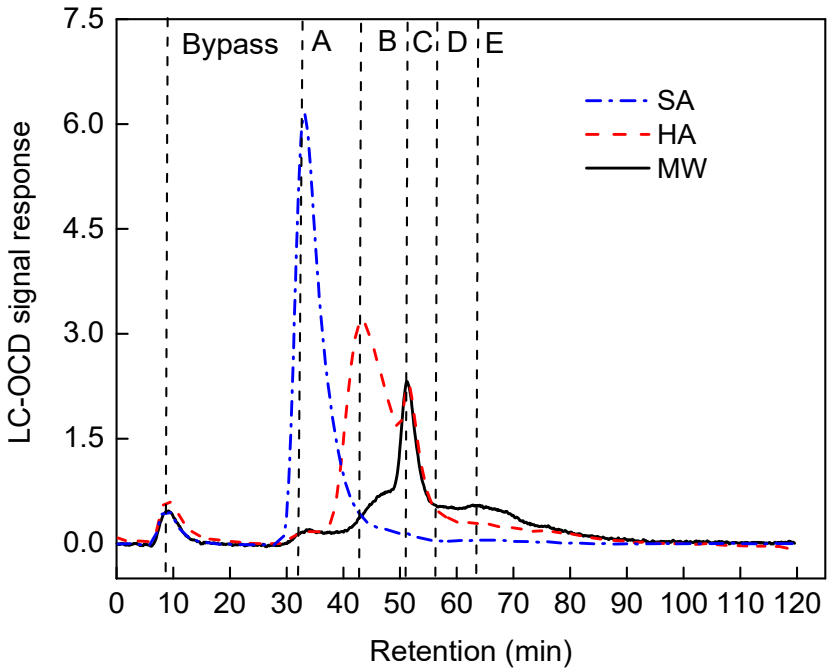

Figure 3-2: LC-OCD chromatograms of sodium alginate (SA) and humic acid (HA) solutions and municipal wastewater (MW). Fraction A: biopolymer, Fraction B: humic substances, Fraction C: building blocks, Fraction D: low molecular weight acids, Fraction E: low molecular weight neutrals.

Building blocks and LMW matter (both acids and neutrals) are the two most prevalent organic fractions in municipal wastewater (Figure 3-2). The estimated contents of these fractions in municipal wastewater are biopolymer (3.6%), building blocks (21.6%), LMW neutrals (29.1%), LMW acids (11.6%). Municipal wastewater contains more LMW matter than the other two model foulant solutions, thus a more compact fouling layer and more severe flux decline can be observed. This is discussed in more detail in section 3.7.5.

Biopolymers contribute 68.1% of the total DOC in sodium alginate. The other fractions found were building blocks (26.1%), LMW neutrals (2.1%) and LMW acids (0.1%). Sodium alginate consists of mostly polysaccharides, which is a good representative of extracellular polymeric substances [126]. This suggests that alginate solution can also induce a considerable fouling due to the interaction between polysaccharides and calcium.

For humic acid, the peaks of humic substances and building blocks peaks are more obvious than biopolymer and LMW neutrals. The estimated contents of these contents are humic substances (45.2%), building blocks (25.1%), LMW neutrals (12.5%) and biopolymer (1.7%). Compared to LMW neutrals, humic substances is expected to form a less compact fouling layer, thus less severe the flux decline.

3.7.4 Impact of fouling on membrane surface charge and hydrophobicity

Membrane fouling leads to significant changes in the membrane surface charge (Figure 3-3). In all cases, the fouled membranes became less negative than the clean membrane. Municipal wastewater shows the most significant impact on zeta potential, followed by sodium alginate and the humic acid foulant solutions. A possible explanation for this is the abundance of Mg^{2+} and Ca^{2+} in wastewater neutralizes the negatively charged adsorption of organic molecules to the membrane surface [90].

It has been established that organic foulants particularly sodium alginate can form a cation-stabilized gel, dubbed the "egg-box" shaped gel [127]. Thus, cations such as Mg^{2+} and Ca^{2+} in wastewater can adsorb into an organic fouling layer rendering the membrane surface less negative as can be seen in Figure 3-3. Results of this study also illustrate that the impact of fouling on the surface charge is dependent on the membrane materials. Indeed, Xie *et al.,* [41] examined the impact of organic fouling on the surface charge using a CTA FO membrane. Unlike the polyamide material which is abundant in uncross-linked carboxylic functional groups (and thus is highly negatively charged), the CTA FO membrane used by them was neutral under a clean condition. They also observed that humic acid fouling rendered the membrane surface more negatively charged.

The effect of different foulants on the membrane surface can also be examined by changes in contact angle of the membrane surface. In general, the presence of the fouling layer makes the membrane surface more hydrophobic (Table 3-5). Increasing membrane hydrophobicity resulted in a higher fouling propensity because of the increase in hydrophobic interaction between the foulant and the membrane surface. As can be seen in Table 3-5, municipal wastewater significantly increased the membrane surface hydrophobicity. The presence of polysaccharides and humic substance in municipal wastewater promoted surface hydrophobicity through adsorbed organic molecules on the active layer [127]. Sodium alginate also increases the hydrophobicity of the active layer significantly. This would suggest that the increasing hydrophobicity is due to the

interaction between high carboxylate functionality of sodium alginate and Ca^{2+} [127]. However, changes in the active layer hydrophobicity caused by humic acid fouling are insignificant.

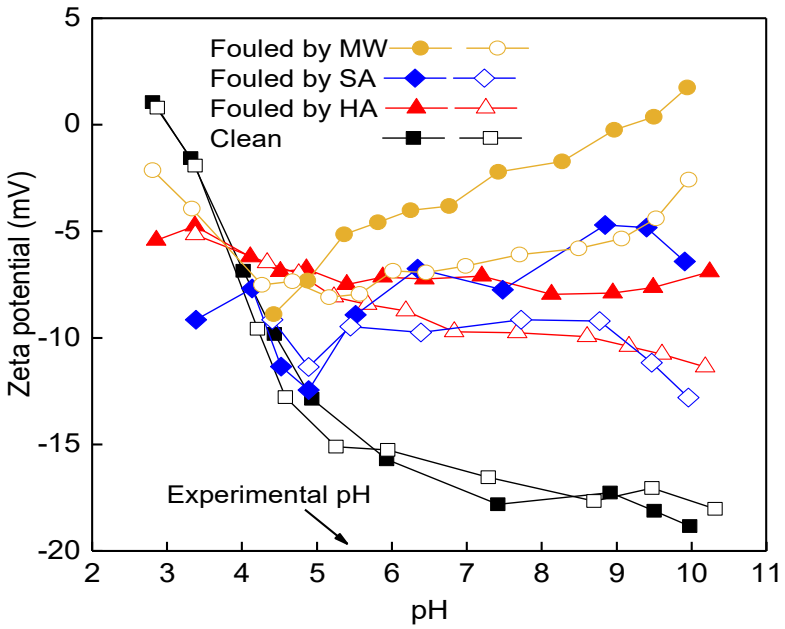

Figure 3-3: Zeta potential of the active layer of membrane samples. FO experimental conditions were as follows: For feed solution, the concentration of each model organic solutes is 200 mg/L except municipal wastewater. Background electrolyte contained 1mM $CaCl_2$. NaCl (0.5 M) as draw solution, initial feed solution pH = 5.5, operation time = 20 h (HA: 200 mg/L humic acid + 1 mM $CaCl_2$; SA: 200 mg/L sodium alginate + 1 mM $CaCl_2$; MW: municipal wastewater. Each membrane sample was analyzed in replicate).

There was a notable decrease of the hydrophobicity of the support layer after sodium alginate fouling (Table 3-5). These results are rather unexpected since the supporting layer is not in contact with the feed solution. It may imply that some components from the fouling layer migrate to the support layer, thus interfering the hydrophobicity of support layer. However, other fouling tests showed both humic acid and municipal wastewater resulted in the discernible changes of hydrophobicity in support layer. Further work is required to explain these phenomena.

Table 3-5 Comparison of the contact angle of membrane layers in the different feed conditions. The experimental conditions are described in Figure 3-3 (average ± standard deviation from duplicate experiments).

Feed condition	Contact angle (°)	
	Active layer	Support layer
DI water	49.5 ± 3.4	56.2 ± 0.1
Humic acid + 0.1 mM $CaCl_2$	47.0 ± 3.6	66.8 ± 1.5
Sodium alginate + 0.1 mM $CaCl_2$	73.2 ± 4.8	39.7 ± 2.1
Municipal wastewater	82.0 ± 2.2	60.7 ± 3.5

3.7.5 Impact of fouling on water and reverse salt flux

The effect of fouling on the membrane performance can be assessed in terms of water flux and reverse salt flux. The flux decline is attributed to the coupled concentration polarization and fouling layer. Indeed, 20% flux decline was observed when DI water was used as the feed (Figure 3-4a). During all FO experiments, the draw solution concentration was constant, however, the feed osmotic pressure increased gradually due to the reverse salt flux. On the other hand, the water flux through the membrane dilutes the concentration of the draw solution inside the membrane support layer. Thus, the small decrease in water flux can be explained by the loss of effective osmotic driving force [54, 128].

In contrast to the small flux decline observed with a clean feed solution, significant membrane fouling could be seen with all fouling solutions. The severity of the flux decline was in decreasing order of municipal wastewater, alginate solution, and humic acid solution (Figure 3-4b-d). This is consistent with the molecular weight distribution of organic matter within these solutions as discussed in section 3.7.3. When municipal wastewater was used as the feed, a 70% flux decline was observed at the end of the experiment (Figure 3-4d). The flux decline profile when the membrane was fouled with municipal wastewater also differs markedly from the much more gradual flux decrease when DI water was used as the clean feed solution. With municipal wastewater, a sharp flux decline was observed in the first 4 h of the experiment followed by a more gradual flux decline. On the other hand, flux decline caused by the increase in feed osmotic pressure when a clean feed solution was used was linear throughout the experiment (Figure 3-4a). The municipal wastewater consists of large amounts of building blocks and

LMW neutrals (section 3.7.3). Thus, these foulants form a more compact and dense fouling layer during the FO process [129]. The large flux decline is attributed to the increasing hydraulic resistance of the fouling layer (with the assumption that fouling layer reduces the water permeability but it does not change the salt permeability) [54].

Notable membrane fouling could also be observed when 200 mg/L of either alginate or humic acid was used as the feed solution (Figure 3-4b-c). Alginate forms a gel layer on the FO membrane surface. This may be due to calcium ions in the feed solution making a strong bond between alginate molecules through the formation of cross-linking between calcium ions and carboxyl groups on the surface of alginate. The normalized flux decline caused by sodium alginate (Figure 3-4b) is less severe than that caused by municipal wastewater in this study. Compared to the municipal wastewater, sodium alginate contains more biopolymers and less LMW neutral fractions (section 3.7.3). Thus, sodium alginate may form a less compact fouling layer than municipal wastewater. On the other hand, humic acid naturally has more humic substances and less LMW neutral fractions than municipal wastewater (section 3.7.3). Despite the deposition from interaction between carboxylate or phenolic hydroxyl group and Ca^{2+} on the membrane surface, humic acid forms a relatively less compact fouling layer than municipal wastewater as well. However, a notable flux decline was also observed during the fouling test (Figure 3-4c). A plausible explanation for this is because of the smaller ICP effect in this configuration [54].

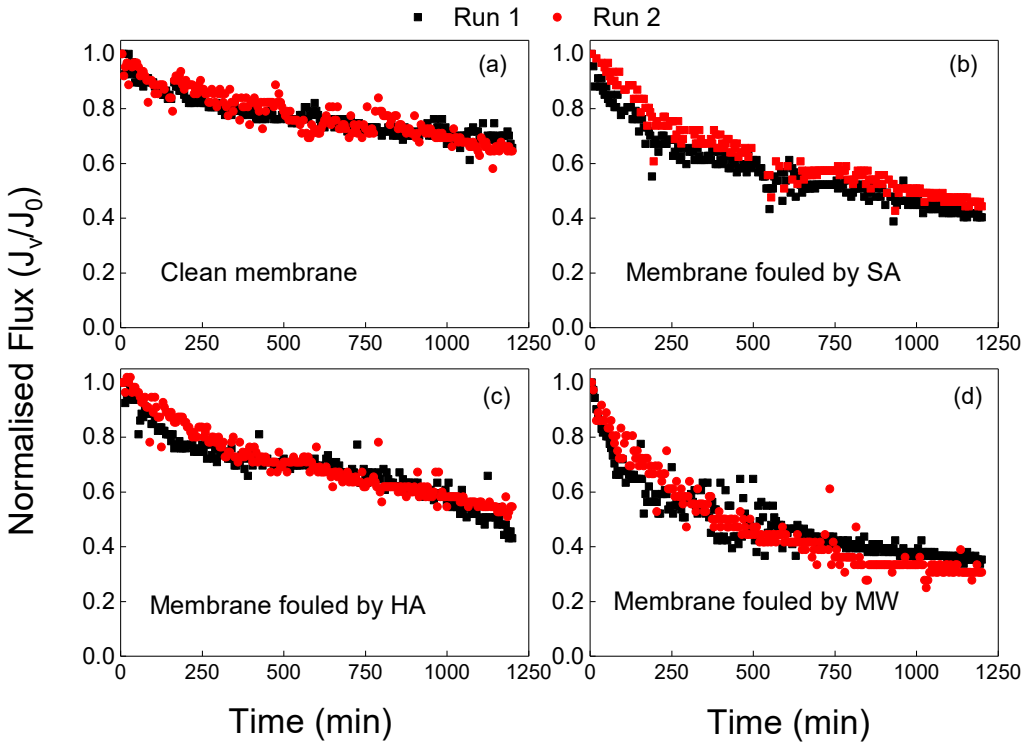

Figure 3-4: Water flux of the membrane at the presence of different foulant as a function of time. The experimental conditions are described in Figure 3-3.

Bidirectional diffusion, namely forward diffusion (from feed to draw) and reverse diffusion (from draw to feed), is intrinsic in the FO process. The reverse diffusion of draw solute is related to several aspects, including the species of draw and feed solutes, their concentrations and cross-flow velocities. The difference between reverse salt fluxes in Figure 3-5 is associated with feed solutes since it is the only variable here.

The observed reverse salt fluxes in all the membranes decrease as a function of water flux and time. The highest reverse salt flux is observed with municipal wastewater at the beginning of the experiment after which there is a notable decline as a function of time (Figure 3-5). This observation is consistent with the rapid water flux decline observed in Figure 3-4. The coupling effect of membrane fouling and ICP reduces the effective osmotic pressure, leading to a decreasing water flux as well as reverse salt flux simultaneously [130]. Corresponding to the gradual decline in water flux, a small but discernible decline in reverse salt flux as a function of time was also observed with humic acid and sodium alginate fouled membranes. Hancock and Cath [45] suggested that the reverse diffusing draw solutes were concentrated at the CTA membrane surface facing

feed solution. In addition, the concentration boundary layer on the draw solution side of the membrane was not well mixed and remained diluted at lower and equal flow velocities. Thus, these two phenomena resulted in diminishing chemical potential gradient between draw and feed solutions and reduce both water and reverse salt fluxes. Sharing the similar membrane structure with CTA, TFC membrane also showed that reducing effective osmotic pressure resulted in reverse salt flux decline.

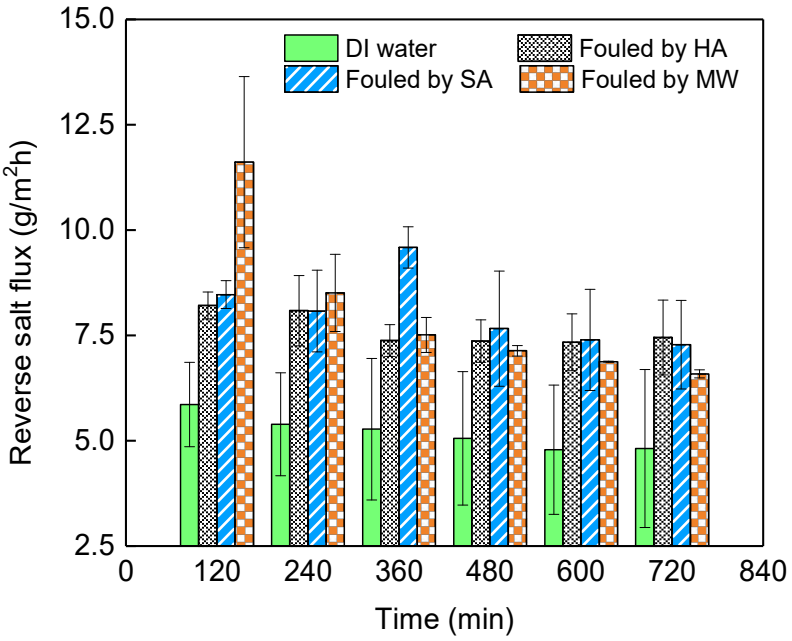

Figure 3-5: The reverse salt flux of the membrane at the presence of different foulant as a function of time in feed solution. The experimental conditions are described in Figure 3-3.

It is interesting that the reverse salt flux of the fouled membranes (either by a model foulant or municipal wastewater) was considerably higher than that under a clean (non-fouling) condition. This can be attributed to the cake enhance concentration polarization within the thin cake layer on the feed side. The fouling cake layer on the membrane can be considered as part of the supporting layer. As a result, the effective structure parameter (S) of the membrane increases because of the fouling, which leads to an increase in reverse salt flux [7].

3.7.6 Impact of fouling on the removal of TrOCs

In general, the removal of an organic molecule by FO is controlled by the steric hindrance (i.e. steric hindrance), the charge exclusion (i.e. electrostatic repulsion), and the sorption-

diffusion mechanism within the membrane polymeric matrix [95]. In this study, the pH of all feed solution was adjusted to pH 5.5 which is the pH of the municipal wastewater. At pH 5.5, carbamazepine and over 90% of sulfamethoxazole exist as neutral species. As a result, separation of sulfamethoxazole and carbamazepine are primarily governed by the steric hindrance. Since the molecular dimensions of sulfamethoxazole and carbamazepine are considerably larger than the estimated membrane pore size (Table 3-3), as expected, high rejection of both sulfamethoxazole and carbamazepine was observed under all experimental conditions in this study. Nevertheless, the results do show a clear effect of membrane fouling on the rejection of these two TrOCs.

The role of steric hindrance in the rejection of sulfamethoxazole can be observed in Figure 3-6. All fouled membranes show the higher rejection of sulfamethoxazole than the clean membrane. Decreased pore size caused by introduced Ca^{2+} with each model organic foulant hinders the transport of sulfamethoxazole [41, 131]. It is also notable that rejection of fouled membrane caused by municipal wastewater is lower than that observed with the humic acid and alginate fouled membranes. As a possible explanation for this, the hydrophobic organic fouling layer can interfere with the separation of sulfamethoxazole and thus disrupts the diffusion of this compound through membrane.

The separation behaviors of carbamazepine by clean and fouled membranes differ markedly from one another (Figure 3-7). Fouling has a negative impact on the rejection of carbamazepine. Compared to the rejection of sulfamethoxazole by fouled FO membranes, this result is likely due to the cake enhanced concentration polarization which results in an elevated concentration of the solutes within the fouling layer [132].

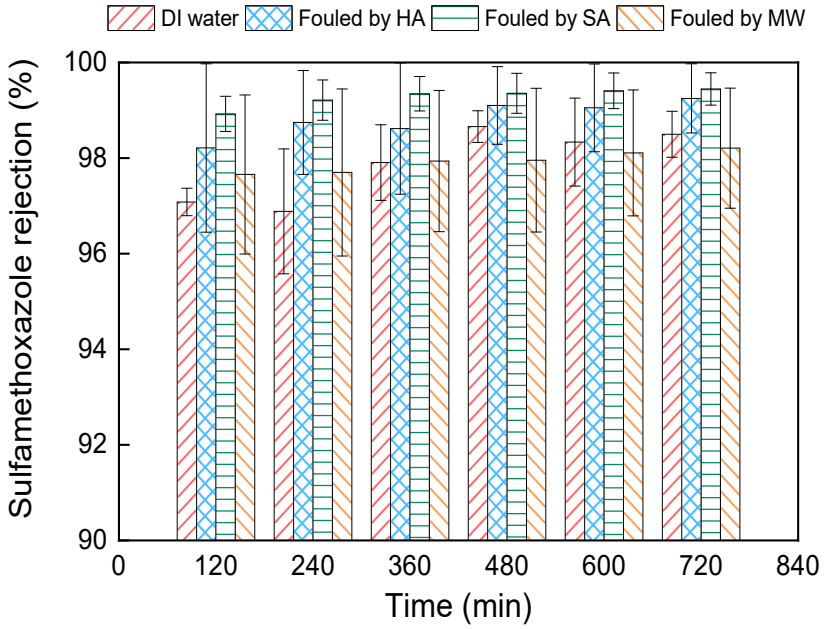

Figure 3-6: Sulfamethoxazole rejection by the clean and fouled membrane as a function of time. The FO experimental conditions are described in Figure 3-3.

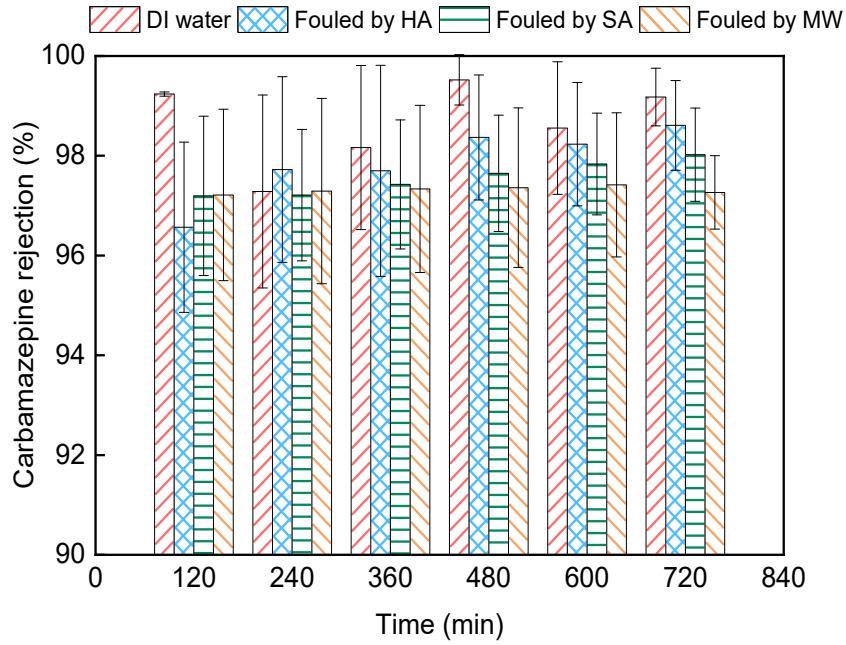

Figure 3-7: Carbamazepine rejection by the clean and fouled membrane as a function of time. The FO experimental conditions are described in Figure 3-3.

3.8 Conclusion

Results reported here indicate that membrane fouling results in notable changes in the membrane properties in terms of the membrane surface charge and hydrophobicity. LC-

OCD analysis shows that membrane fouling behavior is governed by the composition of the feed solution. Water flux and reverse salt flux are affected by the fouling layer and the internal concentration polarization. Furthermore, membrane fouling can exert a considerable effect on the separation process of carbamazepine and sulfamethoxazole. Fouled membranes caused by different organic fractions exhibit quite different rejection behavior for sulfamethoxazole and carbamazepine which were selected as model TrOCs in this study. Both TrOCs were well rejected by clean and fouled FO membranes. Membrane fouling results in an increase in sulfamethoxazole rejection, whilst carbamazepine rejection decreases due to membrane fouling. Since only TFC membrane was used in this study, these findings may not necessarily applicable to other membrane materials such as cellulose triacetate. Further research to investigate the impact of draw solution chemistry on the removal of TrOCs by FO is also recommended.

Chapter 4 New insights into the relationship between draw solution chemistry and trace organic rejection by forward osmosis

This thesis chapter has been published as the following journal article.

L. Zheng, W.E. Price, J. McDonald, S.J. Khan, T. Fujioka, and L.D. Nghiem, New insights into the relationship between draw solution chemistry and trace organic rejection by forward osmosis. Journal of Membrane Science, 587 (2019), 1-10.

4.1 Introduction

As discussed in the Chapter 3, feed solution chemistry induced a noticeable impact on membrane properties and therefore FO performance. Feed solution chemistry can also influence both ionization state of TrOCs, and therefore TrOCs rejection by FO has been extensively investigated in the literature. Xie *et al.,* [133] compared the rejection of two pharmaceuticals (carbamazepine and sulfamethoxazole) by the CTA FO membrane as a function of feed pH. Electrostatic repulsion and steric hindrance both exhibited effects on rejection in relation to the speciation of compounds. In agreement with previous findings by Xie *et al.,* [133], Zhu *et al.,* [134] observed that the electrostatic repulsion was the dominating mechanism for the rejection of negatively charged compounds (cyclohexane carboxylic acid, 1-adamantaneacetic acid) since the CTA membrane became more negatively charged when pH was increased.

Of the equal importance, draw solution chemistry may influence feed chemistry due to the reverse salt flux. Therefore, previous studies have focused on effect of draw solution species and concentration on TrOCs rejection [37, 98]. Despite these recent and dedicated studies, to date, little is known about the role of draw solution chemistry especially pH on the rejection of TrOCs by FO. Thus, it is essential to conduct the study related with TrOCs rejection influenced by draw solution chemistry.

This chapter aims to elucidate the impact of draw solution chemistry on the rejection of TrOCs by FO. In addition to the impact of reverse salt flux on TrOCs rejection, which has been investigated in the few previous studies, the current work also focuses on the interplay between draw solution pH and species, membrane fouling, and water flux to generate new insights into the FO performance.

4.2 Material and Methods

4.2.1 Materials and trace organic contaminants

A flat-sheet TFC-FO membrane from Porifera (Hayward, CA, USA) was used in this study. According to the manufacturer, the operational pH range of this membrane is from pH 2 to 13. Both layers of the membrane are negatively charged above pH 4 and become more negative as pH is increased.

To better contrast the draw solute hydrated size (thus the reverse salt flux) on FO performance, in addition to NaCl, which has been the most widely used draw solute in the literature, lithium chloride (LiCl) was also used in this study. LiCl and NaCl were provided from Chem-Supply (SA, Australia). Sodium acetate (NaOAc), acetic acid (HOAc), sodium dihydrogen phosphate (NaH_2PO_4), and disodium hydrogen phosphate (Na_2HPO_4) from VWR (QLD, Australia) were used in buffer solutions. DI water was used to prepare the solution for this study. All chemicals were analytical grade. Municipal sewage was collected after primary sedimentation from a wastewater treatment plant in New South Wales, Australia. Key parameters of this sewage are summarized in Table 4-1.

Table 4-1: Characteristics of primary treated municipal sewage.

Parameter	Value
pH	7.2-7.3
COD	692.6 mg/L
TOC	114.9 mg/L
TSS	166.3 mg/L
Conductivity	3525 μS/cm

As the representatives of widespread TrOCs from four categories (pesticides, pharmaceuticals, personal care products and industrial chemicals) in raw sewage, 43 TrOCs were selected in this study (Supplementary Data Table S4-1). A stock solution of

all TrOCs was prepared in pure methanol at a concentration of 20 mg/L each on a monthly basis and stored at -18 ℃.

4.2.2 Experimental system and protocol

All experiments were performed using a bench scale FO system (Figure 4-1). The membrane cell has two identical and symmetrical plastic flow chambers with length 10 cm, width 5 cm and height 0.2 cm. The effective area of membrane is approximately 44.6 cm^2.

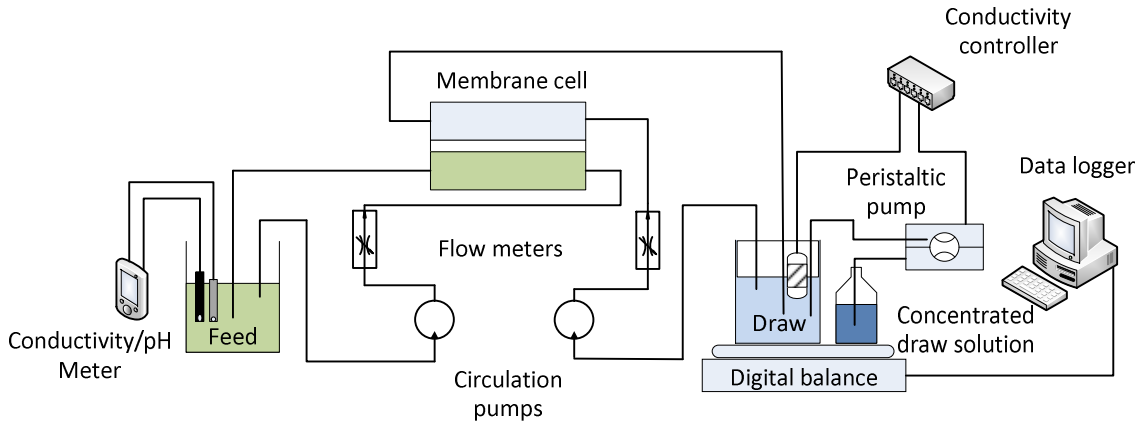

Figure 4-1: Schematic diagram of the bench-scale forward osmosis system.

Unless otherwise stated, the draw solutions were buffered at pH 4.6 by using NaOAc/HOAc (0.7 M/0.1 M); at pH 6.8 by using NaH_2PO_4/Na_2HPO_4 (0.1 M/0.48 M); at pH 8.0 by using NaH_2PO_4/Na_2HPO_4 (0.1 M/0.76 M). NaCl or LiCl was then added to the buffer solution to obtain a draw solution of 0.5 M. The draw solution volume was 0.5 L. The feed solution (DI water or municipal sewage) volume was 2 L.

The system was operated in the co-current FO configuration (active layer facing feed solution) with a cross-flow rate of 1.0 L/min (corresponding to a cross-flow velocity 19.8 cm/s). The draw solution reservoir was placed on a digital balance (Mettler-Toledo Inc., Hightstown, NJ) and weight change was recorded every 5 minutes by a computer. In order to diminish the weight interference between two reservoirs, the concentrated draw solution reservoir (5 M NaCl or LiCl) was placed on the same digital balance where draw solution was placed. The concentration of draw solution was monitored and maintained by a conductivity probe (Cole-Parmer, Vernon Hills, IL) connected with a peristaltic pump (control accuracy was ± 0.1 mS/cm).

All experiments were conducted until 50% water recovery has been achieved (i.e. 1 L water from the feed had permeated through the membrane to draw solution). The feed solutions were prepared by spiking 43 TrOCs into the DI water or municipal sewage to generate a concentration of 10 μg/L of each TrOCs (ignoring initial amount of TrOCs in municipal sewage). Feed and draw solution samples (500 mL each) were taken at the beginning and end of each experiment for the analysis. Conductivity, pH of feed and draw solutions were monitored by an Orion 4 Star plus conductivity meter (Thermo Fisher Scientific, Waltham, MA) at specific time intervals. All FO experiments were conducted in duplicate. Water flux, J_w, was calculated as:

$$J_w = \frac{M_t - M_{t-5}}{\Delta t \times A \times \rho_{water}} \tag{4-1}$$

where M_t and M_{t-5} are the weights of draw solution at time t min and $t-5$ min, respectively. A is the effective membrane area; ρ_{water} is the density of water; Δt is 5 mins.

The reverse salt flux (RSF), J_s, was calculated by a mass balance calculation as:

$$J_s = \frac{(C_t V_{feed,t} - C_0 V_{feed,0})}{A \times t} \tag{4-2}$$

$$V_{feed,t} = V_{feed,0} - \Delta V_{p,t} \tag{4-3}$$

where C_0 and C_t are the concentration of the draw solute in the feed at the beginning and corresponding time t of the experiment, respectively; $V_{feed,0}$ and $V_{feed,t}$ are the volumes of the feed at the beginning and corresponding time t of the experiment; $\Delta V_{p,t}$ is the volume of permeate at time t.

The reverse salt flux selectivity (*RSFS*) was calculated as:

$$RSFS = \frac{J_w}{J_s} \tag{4-4}$$

Water recovery, R_w, or the water extraction rate of the FO experiment was calculated as:

$$R_w = \frac{A\int_0^T J_w d_t}{V_{feed,0}} \tag{4-5}$$

4.3 Analytical methods

4.3.1 Membrane morphology analysis

Membrane samples were coated by a Quorum-SC7620 Mini Sputter Coater (Quorum Technologies, UK) prior to the surface morphology analysis. Each sample was investigated by a scanning electron microscope (SEM) (Phenom-ProX, Thermo Fisher, USA) in the detector mode for backscattered electrons with an operating voltage of 10 kV and an operating pressure of 1 Pa. Elemental analysis was conducted by an energy dispersive X-ray spectroscopy (EDX).

4.3.2 Municipal sewage characterization

The pH and conductivity of municipal sewage were measured by the pH and conductivity meter. Total suspended solids (TSS) was measured according to the standard method [135]. Chemical oxygen demand (COD) was measured following the US-EPA Method 8000 using high range COD vials (HACH, Colorado, USA). TOC was measured by a VCSH TOC analyzer (Shimadzu, Kyoto, Japan).

Molecular weight distribution of municipal sewage was determined by LC - OCD (Model 8, DOC - Labor, Karlsruhe, Germany). The feed samples were filtered through 0.7 μm pore size glass microfiber filter paper prior to analysis. This method is described elsewhere [122]. Customized software (ChromCALC, DOC - LABOR, Karlsruhe, Germany) was used to acquire and process data.

4.3.3 Trace organic contaminant analysis

The analysis of TrOCs followed the method developed by Tadkaew *et al.,* [136]. In brief this was carried out in three parts: solid phase extraction (SPE), liquid chromatography, and quantitative measurement by tandem mass spectrometry with electrospray ionization. Each sample was spiked with a surrogate (50 ng) of 43 isotopically labelled standards for method recovery and detection level determination. A 1 μm pore size glass microfiber filter paper followed by 0.7 μm one was used to treat municipal sewage feed samples for subsequent SPE. All liquid samples were loaded onto the preconditioned Oasis HLB cartridges (Waters, Millford, MA, USA) for TrOCs extraction. The precondition method followed the order: 5 mL methyl tert-butyl ether, 5 mL methanol, and 2×5 mL Milli-Q water at the flow rate of approximate 15 mL/min. The SPE procedure was conducted

slowly at a rate about 15 - 20 drop/min. The cartridges were rinsed twice with Milli-Q water after SPE and were dried by nitrogen gas.

Two solutions: methanol (5 mL), mixture of methanol and methyl tert-butyl ether (1:9, v/v, 5 mL) were used to extract TrOCs from loaded cartridges. Then, the extracted TrOCs were firstly concentrated to 100 μL followed by diluting to 1 mL with methanol. The diluted extracts were analyzed by a high performance liquid chromatography (Agilent 1200 series, Palo Alto, CA, USA) with a Luna C18 (2) column (Phenomenex, Torrence CA, USA) for TrOCs separation. Selected TrOCs were identified and quantified by an isotope dilution method using a triple quadrupole mass spectrometer (API 4000, Applied Biosystems, Foster City, CA, USA) equipped with a turbo V ion source that was employed in both positive and negative electro - spray modes. This method had a limit of quantification of 20 ng/L for bisphenol A, 10 ng/L for caffeine, triclocarban and diuron, and 5 ng/L for all other TrOCs [137].

TrOC rejection, R, was calculated as:

$$R(\%) = \left(1 - \frac{DF \times C_{TrOC,d}}{C_{TrOC,f}}\right) \times 100 \qquad (4\text{-}6)$$

where $C_{TrOC,d}$ is the concentration of each TrOC in the draw solution, $C_{TrOC,f}$ is the concentration of each TrOC in the feed solution, and DF is the dilution factor and defined as:

$$DF = \frac{V_d}{V_p} \qquad (4\text{-}7)$$

where V_d is the final volume of the draw solution and V_p is the total volume of permeate.

4.4 Results and discussion

4.4.1 Impact of draw solution chemistry on water flux and reverse salt flux

The draw solution pH asserted a small but nevertheless discernible impact on water flux (Figure 4-2). At a draw solution of pH 4.8, the flux decline was most noticeable when DI water was used as the feed solution, corresponding to the longest time to achieve 50% water recovery. This was followed by draw solutions at pH 6.7 and pH 8.0 (Figure 4-2a-c). It is noted that the DI feed water was at pH 6.4. Results in Figure 4-2a-c could be attributed to the difference in pH between the draw and feed solution, leading to the

transfer of proton ions into the feed solution. Since pH is a logarithmic function of proton concentration, the concentration gradient for the proton transfer between solutions at pH 4.8 and pH 6.4 (feed pH) is several orders of magnitude higher than between those at pH 6.7 and pH 6.4. On the other hand, there was also the back diffusion of Na^+ from the draw to the feed solution. The transport of both proton and Na^+ was coupled with the transport of a counter ion, Cl^- in this case, for electro-neutrality. Thus, a high concentration of proton in the draw solution can interfere with the transport of Na^+ at pH 4.8, leading to a smaller overall osmotic gradient across the membrane active layer, and hence, lower water flux when compared to pH 6.7 (Figure 4-2a-b). Indeed, the lowest NaCl reverse salt flux was observed with draw solution at pH 4.8 (Figure 4-3). The interplays among the transport of key solutes at different draw solution pH are schematically presented in Figure 4-3.

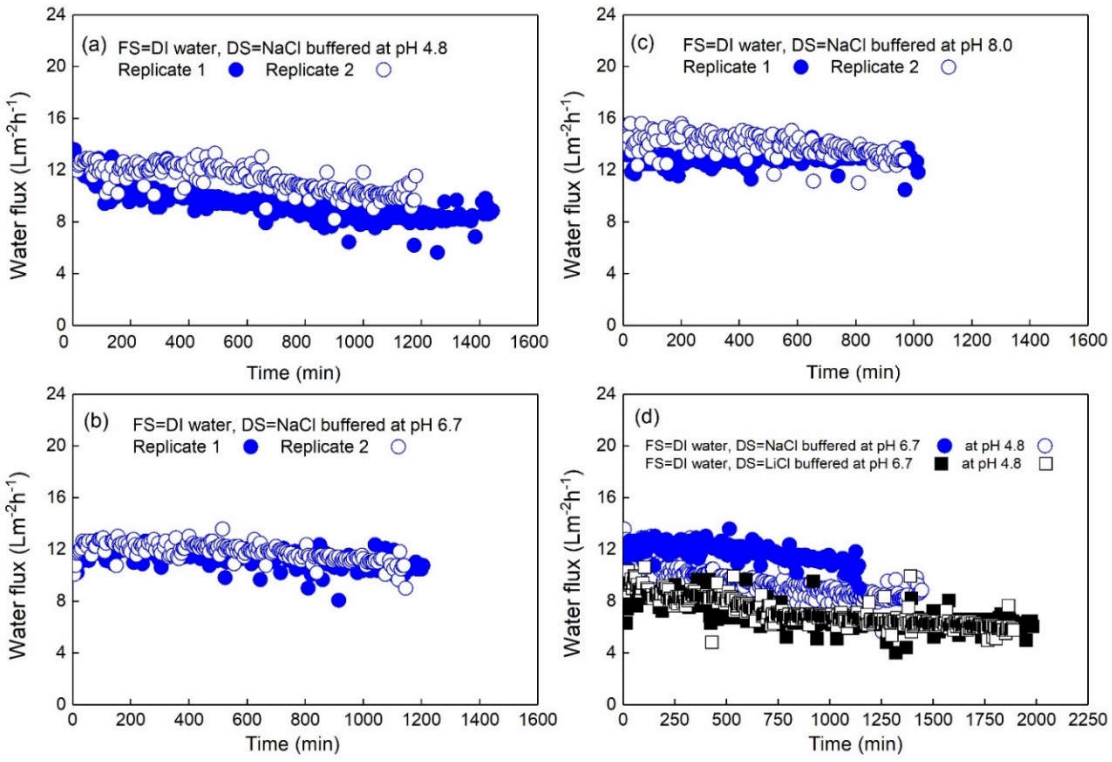

Figure 4-2: Water flux as a function of time. In (a) – (c), DI water was used as the feed solution (FS) and NaCl (0.5 M) at buffered pH 4.8/6.7/8.0 was used as the draw solution (DS), respectively. In (d), comparison of water flux when either NaCl (0.5 M) or LiCl (0.5 M) at buffered pH 4.8/6.7 were used as the draw solutions. DI water was used as the feed solution. The initial pH of feed solution in all experiments was 6.4 ± 0.2 and all experiments were conducted until 50% water recovery.

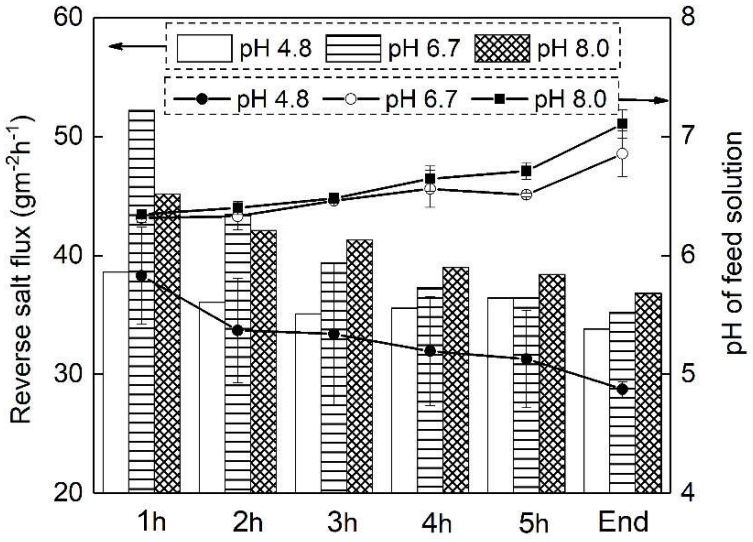

Figure 4-3: Reverse salt flux and pH in the feed solution (The data were recorded in the first 5 h and end of experiment). DI water was used as feed solution and NaCl (0.5 M) at buffered pH 4.8/6.7/8.0 was used as draw solution, respectively. The initial pH of feed solution in all experiments were 6.4 ± 0.2 and all experiments were conducted until 50% water recovery. Error bars represent the difference of two replicate measurements.

NaCl and LiCl as the draw solutes showed different flux performance despite their similar osmotic potentials based on the van't Hoff theory (Figure 4-2d and Supplementary Data Figure S4-1). At the same pH and draw solution molar concentration, LiCl resulted in a lower water flux compared to NaCl corresponding to a longer operation time to achieve 50% water recovery. The effect of external concentration polarisation can be mitigated by maintaining a crossflow (19.8 cm/s) over the membrane surface [138]. Thus, the observed differences in water flux profile at the same draw solution concentration (thus osmotic potential) in Figure 4-5 can be attributed to the difference in hydrated radius between two draw solutes and the ICP effect. In this study, the active layer was against the feed solution. Thus, within the porous supporting layer, the draw solution is diluted by the water flux, which is referred to as the dilutive ICP on the permeate side. With a larger hydrated radius and lower diffusivity, Li^+ potentially leads to a more severe dilutive ICP (Figure 4-5), and thus a lower water flux as observed in Figure 4-2d.

Of a particular note, the impact of draw solution pH on water flux was less significant when LiCl was used as the draw solute (Figure 4-2d). As discussed above, the transfer of

H^+ from the draw solution to the feed at pH 4.8 could be impacted by the diffusion of hydrated Li^+ (in the same way as hydrated Na^+) across the membrane (Figure 4-5c-d). In addition, the diffusion coefficients of alkali metals decrease as their hydrated radii increase [139]. Since Li^+ has a larger hydrated radius than Na^+, the reverse salt flux of LiCl is therefore much smaller than that of NaCl (Figure 4-4). Hence, the impact of draw solution pH on water flux was negligible when LiCl was used as the draw solute (Figure 4-2d).

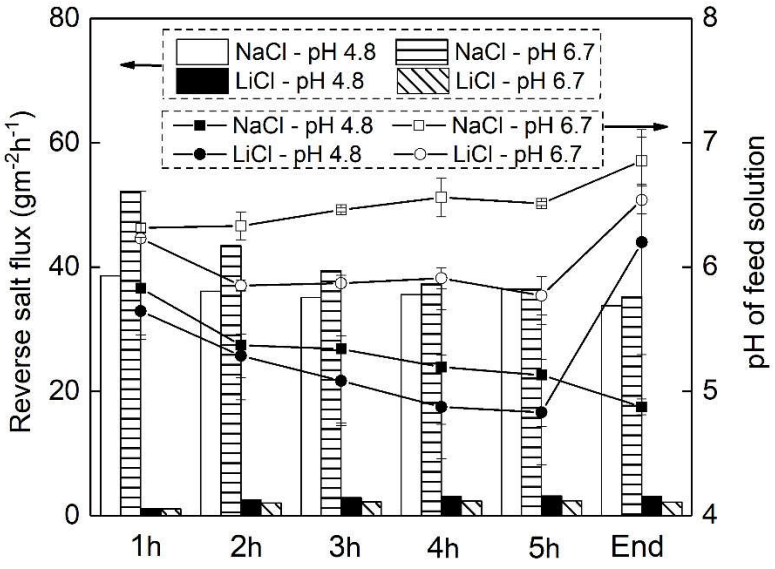

Figure 4-4: Comparison of reverse salt flux resulted from two draw solutes and monitored pH in the feed solution (The data were recorded in the first 5 h and end of experiment). NaCl (0.5 M) or LiCl (0.5 M) at buffered pH 4.8/6.7 was used as draw solution, respectively. DI water was used as feed solution at pH 6.4 ± 0.2. All experiments were conducted until 50% water recovery. Error bars represent the difference of two replicate measurements.

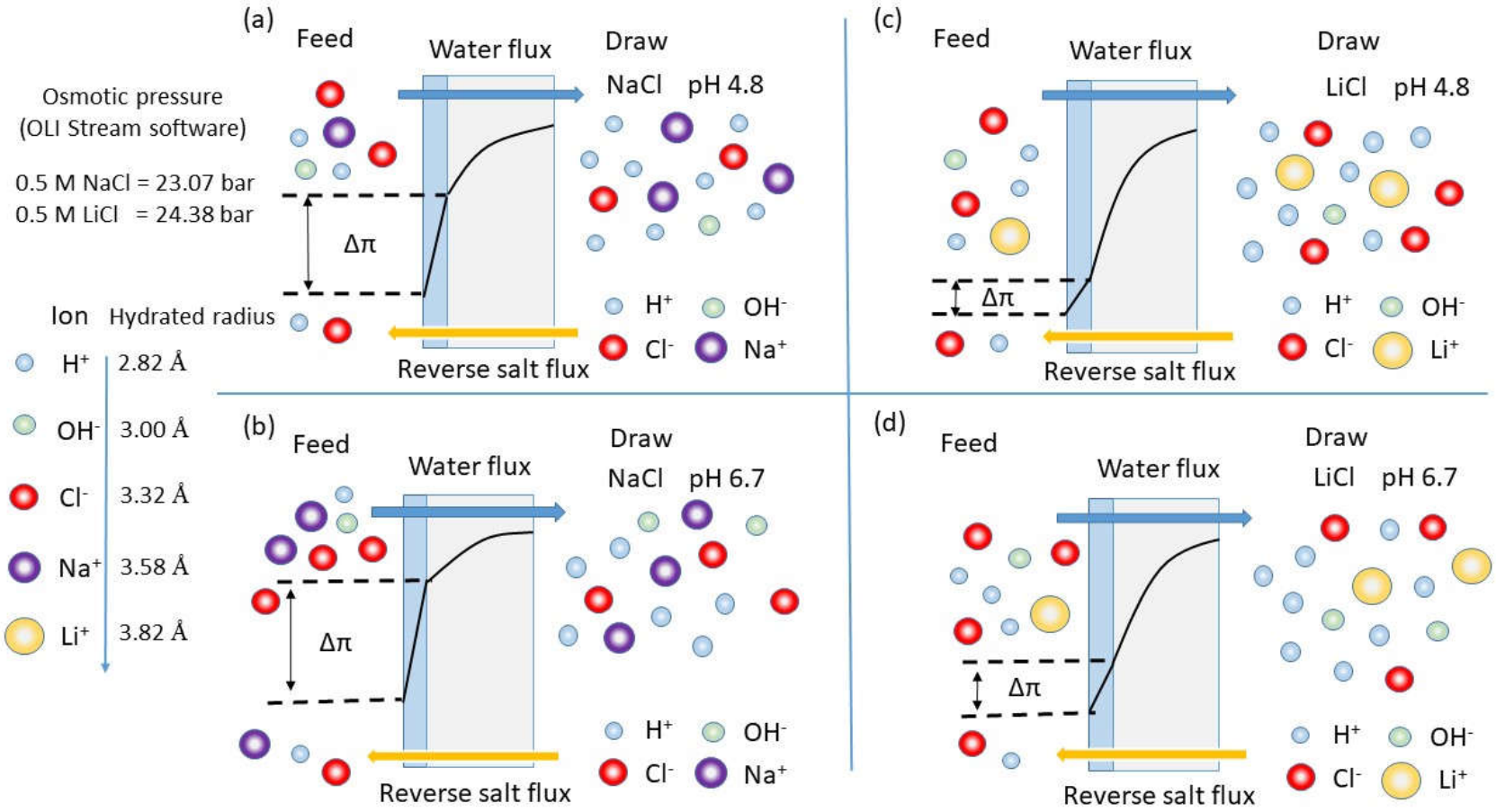

Figure 4-5: A schematic diagram of coupled effects resulting from draw solution pH and species on water flux and reverse salt flux. In (a) - (b), NaCl (0.5 M) at buffered pH 4.8/6.7 was used as the draw solution, respectively. In (c) - (d), LiCl (0.5 M) at buffered pH 4.8/6.7 was used as the draw solutions, respectively. DI water at pH 6.4 ± 0.2 was used as the feed solution in all experiments. Hydrated radii data are from [140]. Δπ is the effective osmotic driving force.

4.4.1 Reverse salt flux selectivity

LiCl had a higher reverse salt flux selectivity than NaCl in this study (Figure 4-4 and Figure 4-6). Despite a slightly lower water flux because of a more severe dilutive ICP, LiCl had a much lower reverse salt flux than that of NaCl. As a result, the higher reverse salt flux selectivity of LiCl was observed in comparison to NaCl. It is interesting to note that when LiCl was used as the draw solute, pH had a more significant impact on reverse salt flux selectivity (Figure 4-6). This observed impact was in contrast to that on water flux as discussed in section 4.4.1. It was likely due to the very small reverse salt flux of LiCl, where even a small change in water flux caused by the variable pH could lead to a noticeable change in reverse salt flux selectivity. On the other hand, the draw solution pH affected both the water and reverse salt flux to a similar magnitude when NaCl was used as the draw solute.

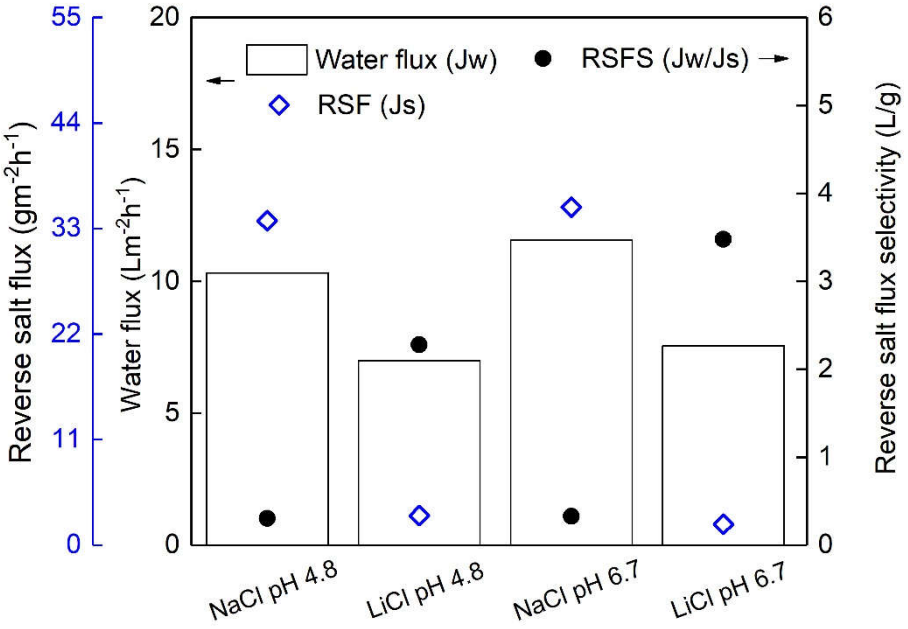

Figure 4-6: Average water flux, RSF and RSFS of two draw solutions at two pH gradients. Experimental conditions: DI water was used as the feed solution; NaCl (0.5 M) or LiCl (0.5 M) at buffered pH 4.8/6.7 was used as the draw solution.

4.4.2 Rejection of TrOCs by FO

4.4.2.1 Role of electrostatic interaction

Results in Figure 4-7 show that average rejection for charged TrOCs by FO (negatively charged compounds: 86.7 ± 8.6 %; positively charged compounds: 86.9 ± 7.6%) were marginally better than that of neutral TrOCs (84.4 ± 6.8%). The difference in rejection between charged and neutral TrOCs was discernible but not as significant as previously reported with NF membranes [40]. When a molecule attained a charge, electrostatic interaction could be a major rejection mechanism. An alternative view is to consider the hydrated size of the molecule which is larger than the neutral state of the compound. Electrostatic interaction or the hydrated size can be expressed by the Debye length which is governed by the solution ionic strength [40]. Unlike a NF system, in which the feed solution usually has a low ionic strength. FO has a high ionic strength in feed because of the back diffusion from draw solution. Therefore, the ionic strength at the membrane surface on the feed side can suppress electrostatic interaction between charged TrOCs and the membrane surface. As a result, the impact of solute charge on rejection by FO was less significant as observed in Figure 4-7 compared to the previous literature on the NF process.

The results showed a little correlation between the rejections of neutral TrOCs by FO and their corresponding molecular sizes in terms of MPA. MPA is the two-dimensional area of the conformer projected with its circular disk. Assuming the passage of compound through FO membrane as a circular shape, MPA is supposed to be most correlated with the rejection of neutral TrOCs. Results in Figure 4-7 are in contrast to the NF process, in which steric hindrance plays a much more significant role in the rejection of neutral TrOCs [141]. Hence, these results suggest that steric hindrance was not a prevalent rejection mechanism in this study and other phenomenon such as adsorption or dipolar interaction likely influenced the transport of TrOCs through FO membrane. For examples, benzophenone (Log D = 3.43) and phenylphenol (Log D = 3.31) are small in sizes but are also hydrophobic (log D > 3). Thus, adsorption was an additional removal mechanism, leading to relatively high observed rejection values, particularly when a limited feed volume was applied in this study. On the other hand, carbamazepine has a large MPA, but was not well rejected by FO. A plausible explanation for this observation was the high dipole moment of carbamazepine (3.6 Debye [142]), which facilitated dipolar

interactions with the membrane surface [143]. In other words, due to the dipolar interaction, carbamazepine orientated toward the membrane pore, resulting in a lower rejection [144].

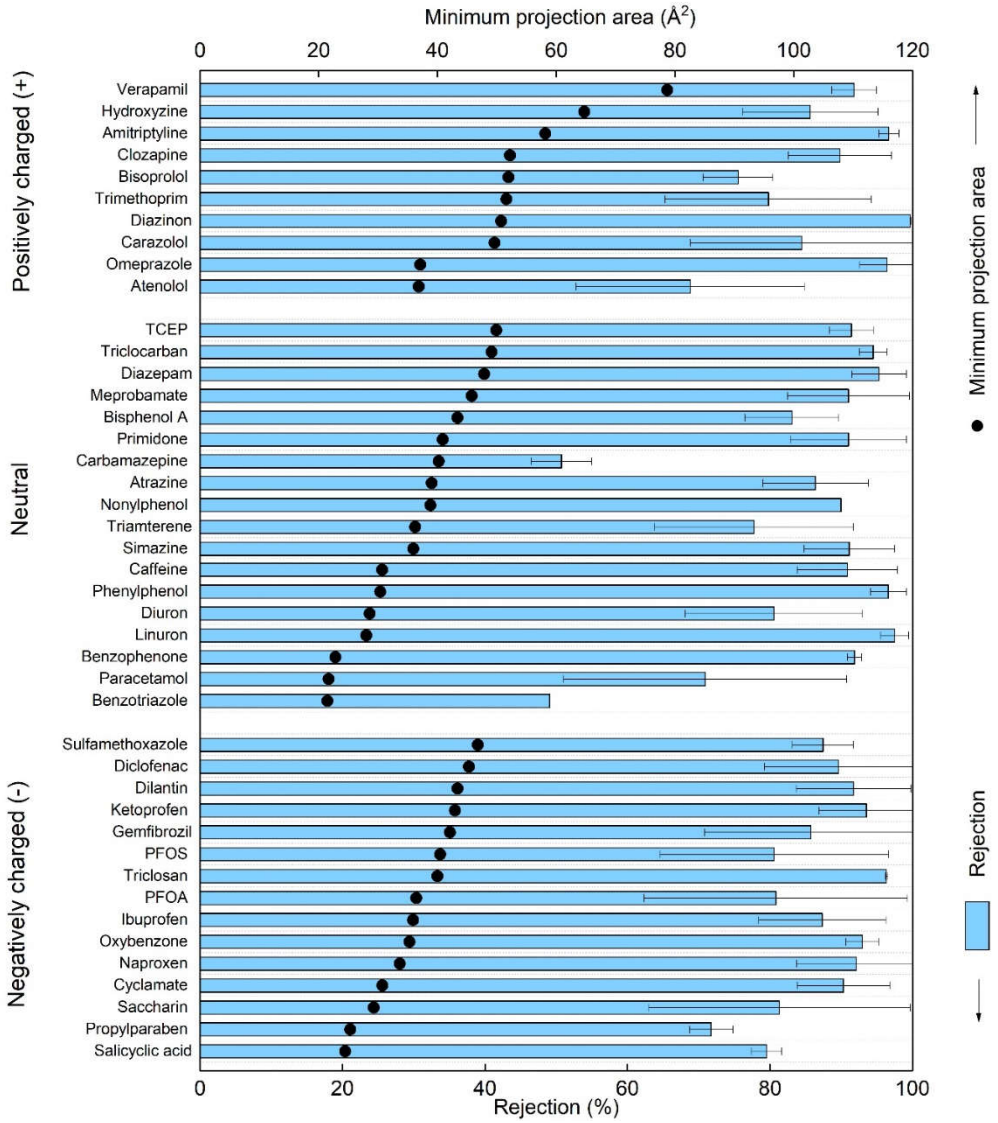

Figure 4-7: TrOC rejection at buffered pH 6.7. Experimental conditions: DI water was used as feed solution and NaCl (0.5 M) at buffered pH 6.7 was used as the draw solution. Minimum projection area (MPA) is calculated based on the Van der Waals radius. The MPA of each compound was obtained from the *Chemicalize* online platform. Error bars represent the difference of two replicate measurements.

4.4.2.2 Role of compound speciation

Due to the bidirectional transport of proton across the membrane, pH in the feed solution (and thus the speciation of ionisable TrOCs) could be influenced by a pH gradient between the feed and draw solution. Hence, higher rejections were observed when TrOCs became either negatively or positively charged compared to their neutral forms because of the electrostatic interaction (Figure 4-8). For example, the rejection of triclosan (pKa = 7.68) increased from 47.8% (neutral) to 96.3 and 96.1% when it became negatively charged in buffered draw solutions at pH 6.7 and 8.0, respectively. On the other hand, the rejection of triamterene (pKa = 6.2) decreased by 8.8% and 6.4% when it transformed from positively charged (pH 4.8) to a neutral form (pH 6.7 and 8.0), respectively. In particular, pH 6.7 showed a lower rejection than pH 8.0 when compounds (propylparaben and dilantin) were both negatively charged at these two pH values. As discussed in section 4.4.1, since the feed solution ionic strength decreased from pH 6.7 to pH 8.0 due to the increasing reverse salt flux (Figure 4-1), electrostatic repulsion at pH 8.0 became a more prevalent rejection mechanism, leading to a higher rejection.

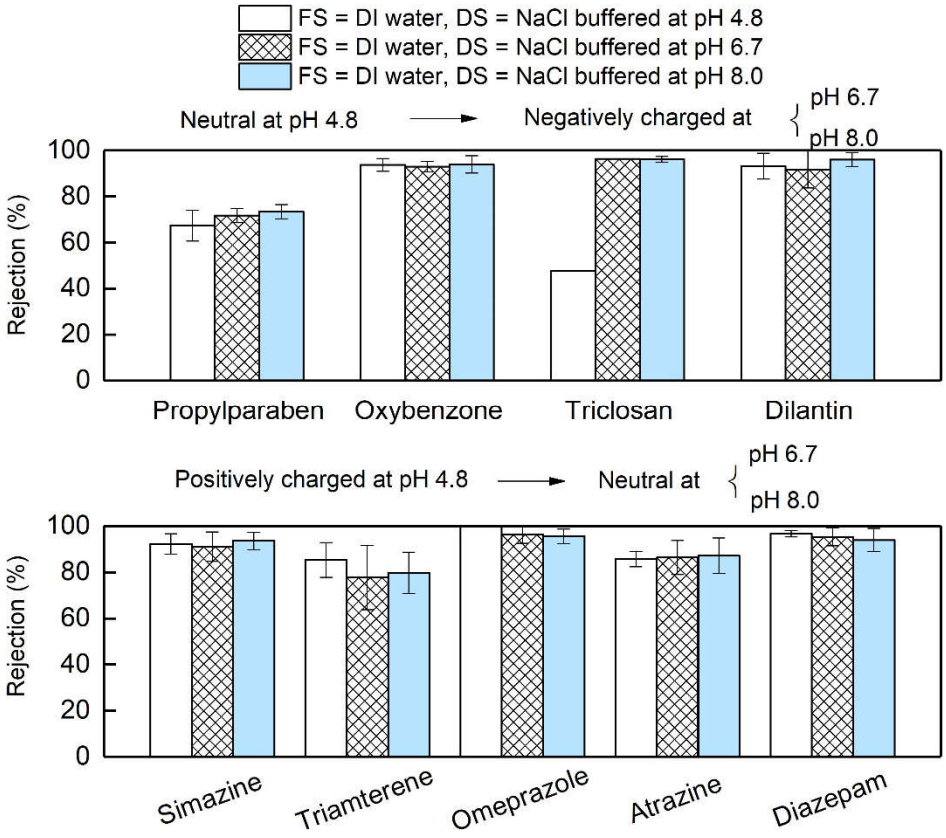

Figure 4-8: Rejection of ionisable TrOCs at different buffered pH. Experimental conditions: DI water was used as the FS and NaCl (0.5 M) at different buffered pH (pH

4.8/6.7/8.0) was used as the DS, respectively. Error bars represent the difference of two replicate measurements.

4.4.2.3 Role of draw solute species

Using LiCl as the draw solute resulted in slightly higher rejections of most TrOCs compared to NaCl (Figure 4-9), which showed the data for 28 TrOCs with the discernible rejection difference between these two draw solutes. As noted in section 4.4.1, the reverse salt flux of LiCl was less than that of NaCl at two pH gradients. Ionic strength of the feed immediately at the membrane was therefore expected to be lower than NaCl. A lower ionic strength could possibly lead to a stronger electrostatic interaction between charged TrOCs and the negatively charged membrane surface, resulting in a higher rejection. On the other hand, ionic strength could also influence the charge layer within the membrane pore or the effective membrane pore size. In other words, at a lower ionic strength, the double layer could extend further, resulting in a smaller effective pore size [37]. As a result, the effect of the lower ionic strength on the feed side was also observed for several neutral TrOCs when LiCl was used as the draw solute (Figure 4-9).

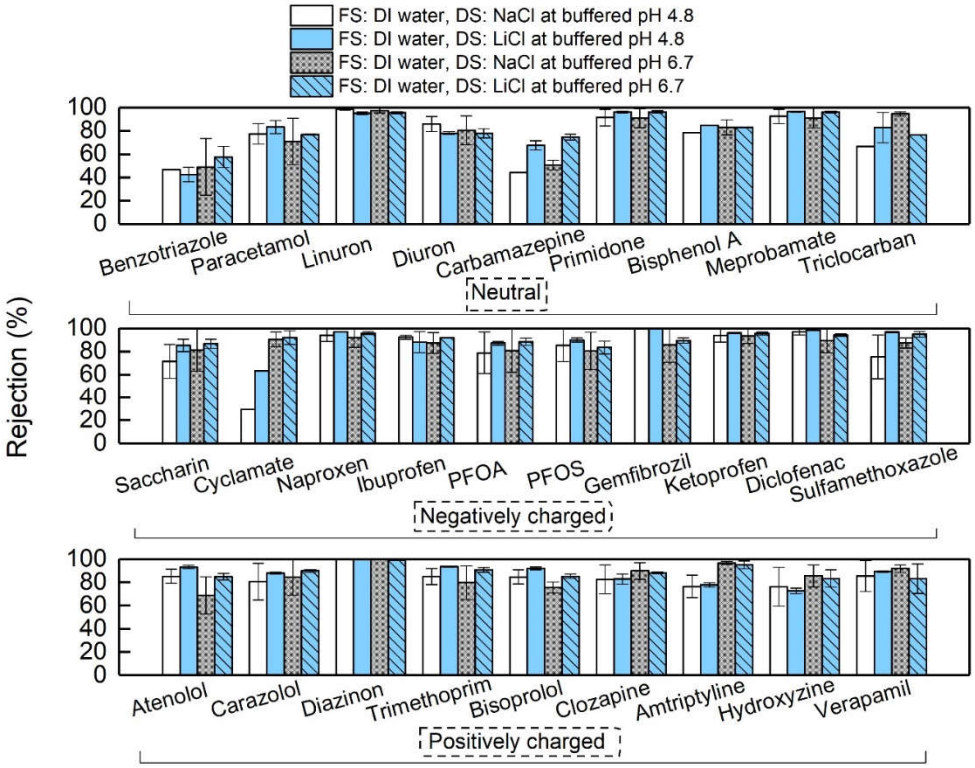

Figure 4-9: Impact of draw solution species on TrOCs rejection. Experimental conditions: DI water was used as the FS and NaCl (0.5 M) or LiCl (0.5 M) at different buffered pH

(pH 4.8/6.7) was used as the DS, respectively. Error bars represent the difference of two replicate measurements.

4.4.1 Rejection of TrOCs with the presence of fouling

4.4.1.1 Impact of membrane fouling on water flux

The presence of foulants in the feed solution was a significant factor in the determination of the permeate flux. The corresponding flux declines were 70% for fouled membrane and 19% for clean membrane at 50% water recovery, respectively (Figure 4-10). The gradual flux decline in DI water was due to the diminishing osmotic gradient caused by the reverse draw solute diffusion. Two instinct fouling stages were observed, possibly related to two different fouling mechanisms. A sharp drop in permeate flux was observed within the first 10 h of each filtration experiment. This initial rapid fouling stage can be likely attributed to the development of a fouling cake layer on the membrane surface. After 10 h of filtration, the rate of flux gradually became stable until the end of the experiment, which was possibly due to the thickening and compaction of the fouling layer. Similar water flux decline profiles were reported in our previous study [145].

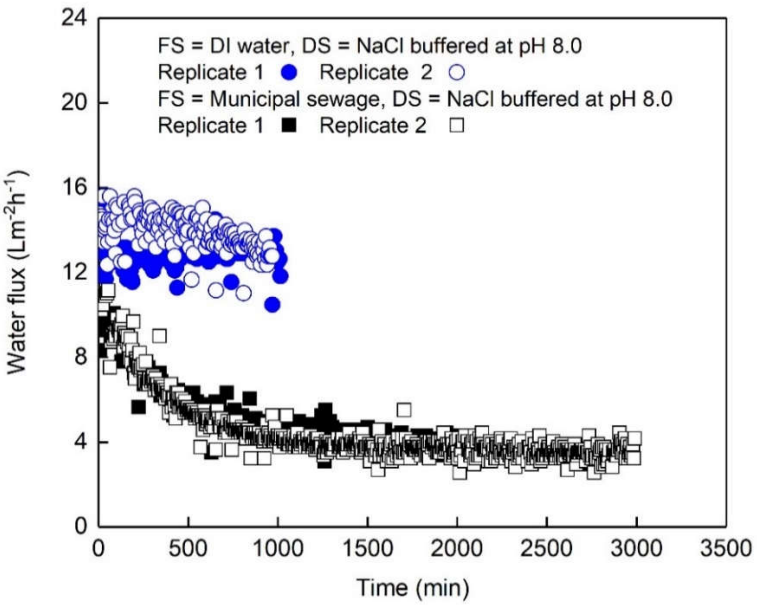

Figure 4-10: Impact of fouling on the water flux: DI water or municipal sewage was used as the FS, respectively. NaCl (0.5 M) at buffered pH 8.0 was used as the DS. The initial pH of feed solution in duplicate experiments was 6.4 ± 0.2 and duplicate experiments were conducted until 50% water recovery.

4.4.1.2 Membrane fouling characterization

Results from LC-OCD analysis indicate that low molecular weight neutrals accounted for most (>70%) of the dissolved organics in municipal sewage (Figure 4-11a). Despite a high fraction of low molecular weight neutrals in municipal sewage, the organic removal by the FO process was 97.2% as indicated by a small peak of low molecular weight neutrals in the FO permeate (Figure 4-11b). Although the water recovery was 50%, the accumulation of other fractions except low molecular weight neutrals were negligible in the FO concentrate. Thus, it is likely that almost all low molecular weight neutrals retained by the FO process had deposited on the membrane surface to form a cake layer, resulting in a considerable flux decline as previously discussed in section 4.4.1. This cake layer on the membrane surface was confirmed by SEM-EDX analysis (Supplementary Data Figure S4-2). In addition, the cake layer had a significant impact on the reverse salt flux demonstrated by the Supplementary Data Figure S4-3.

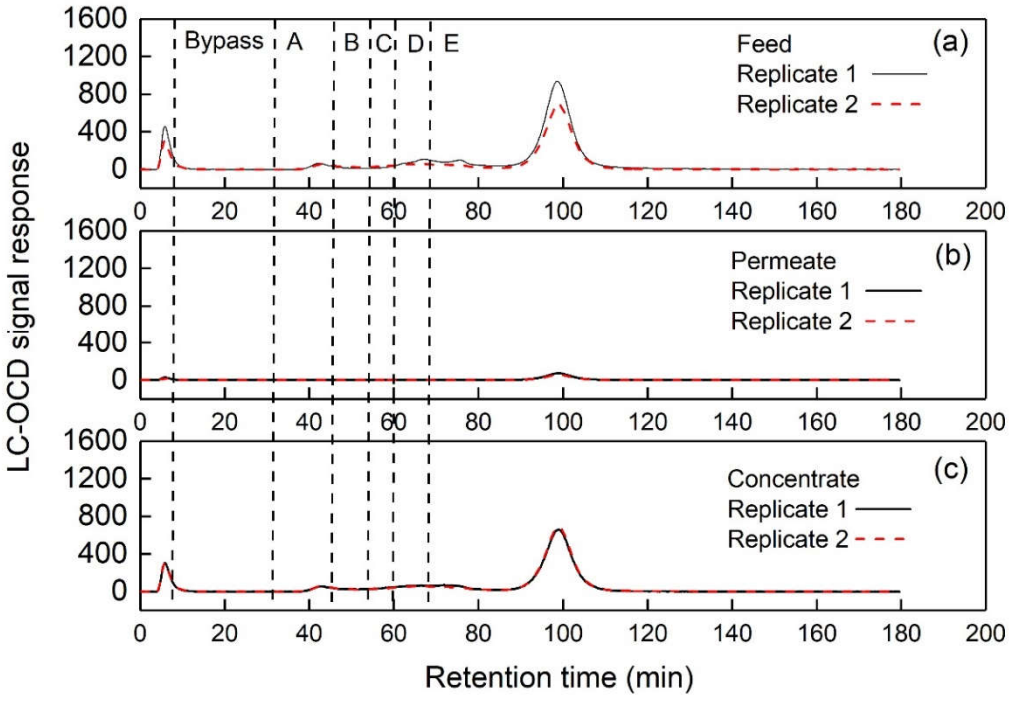

Figure 4-11: LC-OCD chromatograms of (a) feed, (b) permeate, and (c) concentrate of municipal sewage after FO experiment. Fraction A: biopolymer; Fraction B: humic substances; Fraction C: building blocks; Fraction D: low molecular weight acids; Fraction E: low molecular weight neutrals. The experiments were conducted in duplicate.

4.4.1.3 Impact of fouling on TrOCs rejection

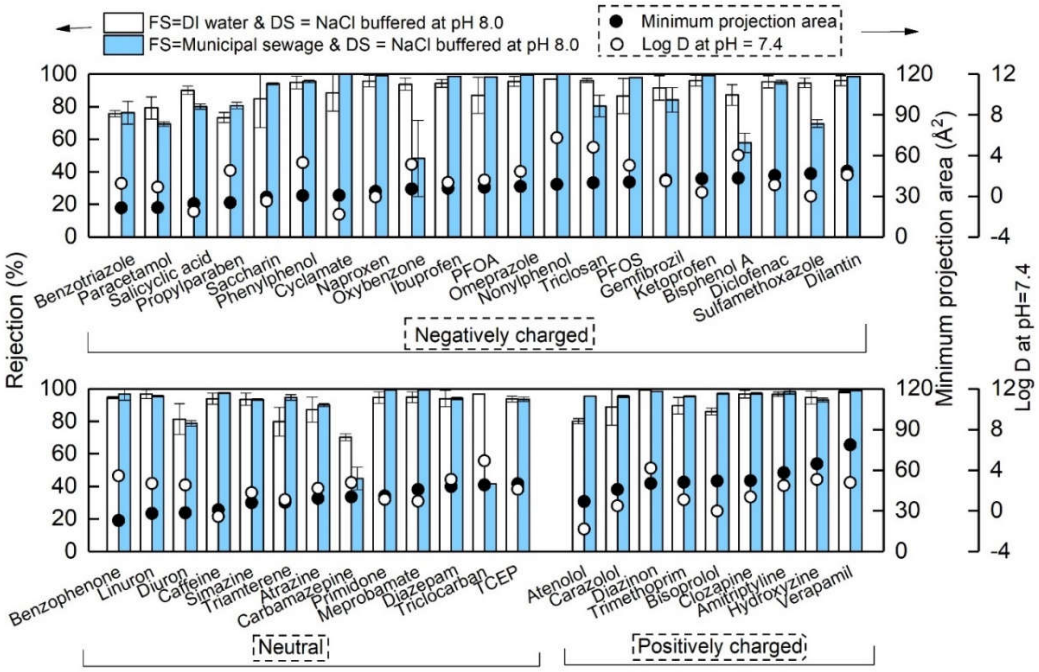

Figure 4-12: TrOCs rejection by clean and fouled membranes. Experimental conditions: DI water or municipal sewage was used as FS, respectively. NaCl (0.5 M) at buffered pH 8.0 was used as the DS. Error bars represent the difference of two replicate measurements.

The cake layer on the membrane surface could result in variable TrOCs rejection. Higher rejections by the fouled FO membrane were observed for 32 out of 43 TrOCs investigated in this study when it was compared to that under clean no-fouling conditions (Figure 4-12). These observations could be attributed to the additional filtration effect by the cake layer and possibly pore blocking. As discussed in section 4.4.1.2, the fouling layer consisted of mostly low molecular weight neutrals (molecular weight of approximate 350 g/mol), thus penetration of TrOCs through the cake layer to the membrane pore were negligible. These findings were consistent with those previously reported by Xie *et al.,* [42] that the rejection was enhanced at a low initial permeate flux associated with a fouled membrane. It is noteworthy that several neutral compounds including carbamazepine and triclocarban exhibited lower rejections at the presence of fouling (Figure 4-12). The lower rejections for neutral compounds were likely attributed to a cake-enhanced concentration polarisation effect as steric hindrance is probably the main rejection mechanism for neutral compounds. On the other hand, similar to the findings in the previous section

4.4.2.1, rejection behaviors exhibited no correlation with molecular size of compound (i.e. MPA) regardless of the presence of a fouling layer.

4.5 Conclusions

Results from this chapter indicate that draw solution chemistry (i.e. pH and draw solute type) could induce discernible impacts on both water flux and TrOC rejection. The impact on TrOC rejection was further interfered by the membrane fouling. Due to the bidirectional transport in the FO process, pH of the draw solution and feed solution were interrelated. As a result, the draw solution pH influenced the speciation of ionizable TrOCs in the feed solution and their rejection mechanisms by FO. Electrostatic interaction other than steric hindrance was identified as the prevalent rejection mechanism for the clean membrane, which could also be explained by a poor correlation between rejections and molecular sizes of the 43 TrOCs. Compared to NaCl, LiCl as the draw solution showed slightly higher rejections for most selected TrOCs. LiCl had a much lower reverse salt flux than NaCl because of a larger hydrated radius of Li^+. Therefore, a lower ionic strength in the feed side and within the membrane pore caused a stronger electrostatic interaction. On the other hand, low molecular weight neutrals in municipal sewage mainly formed a fouling cake layer. This cake layer attributed to an increase in TrOCs rejection because of the severe pore blockage. However, a decrease in the rejection for several neutral TrOCs was also observed and this was likely due to the cake-enhanced concentration polarisation effect.

Chapter 5 Simultaneous cooling and provision of make-up water by forward osmosis for post-combustion CO_2 capture

This thesis chapter has been published as the following journal article.

L. Zheng, W.E. Price, T. He, and L.D. Nghiem, Simultaneous cooling and provision of make-up water by forward osmosis for post-combustion CO_2 capture. Desalination, 476 (2020), 1-7.

5.1 Introduction

Recent technology provides multiple approaches to transform wastewater to a source of energy and water. As discussed in Chapter 3 and 4, FO is one sort of approaches for purifying wastewater via rejecting TrOCs. The investigation about complex interplay between feed/draw solution chemistry and FO performance lays the foundation on variable FO application. As addressed in Chapter 2, an innovative FO application was proposed to meet increasing make-up water demand after installing CO_2 capture facility to an existing power station. By using regenerated amine-based solvent as the draw solution, FO can be used as an alternative to a trim cooler through extracting clean water from wastewater or seawater. Such novel proposal also facilitates FO application towards wastewater reclamation.

In such context, temperature gradient naturally exists between feed solution and draw soluiton. As the diffusion coefficient of the solution increases as temperature increases [146, 147], whereas the viscosity of the solution decreases as temperature increases [148]. This phenomenon reduces solute resistivity and diminishes the effect of ICP, thus enhancing the FO performance. As a result, a temperature gradient is considered as a vital operating parameter regarding water transport in FO. Phuntsho *et al.,* [149] observed a small but discernible increase of draw solution osmotic pressure as temperature increased from 25 to 45 °C. This phenomenon resulted in the corresponding flux increase (4.1-21.4%). With the increasing draw solution temperature, change of solution viscosity and

diffusion coefficient resulted in the decreasing ICP effect and further improving the water flux.

The effect of temperature gradient on water flux can also be interfered by the membrane orientation, which is strongly related with ICP. ICP has been prescribed as the main factor accounting for flux decline apart from membrane fouling [150]. Due to the intrinsic asymmetric structure of FO membranes, the two membrane orientations with (a) the AL-FS and (b) the AL-DS lead to dilutive and concentrative ICP, in addition to the different flux decline [151]. Chowdhury *et al.,* [152] observed a larger increase of water flux in the AL-DS configuration than that in the AL-FS configuration when the draw solution temperature was 20 °C more than the feed solution. However, when draw solution temperature decreased, the flux decline in AL-DS configuration was smaller than that in AL-FS configuration. Since mass transfer was mainly hindered in the support layer, a relatively larger temperature gradient was observed in AL-DS configuration. A lower temperature resulted in a higher solution viscosity and a smaller diffusion coefficient, therefore lessening the extent of ICP.

This chapter therefore aims to evaluate a novel application of FO as an alternative for the trim cooler, which used the non-potable water (i.e. treated effluent and seawater) as the cooling water resource, in addition to supplement for cooling tower or flue gas desulphurization. The current work also focuses on the influencing factors, such as temperature gradient and membrane orientation on the FO performance, which yields a prospect for a practical application of FO in post-combustion CO_2 capture.

5.2 Material and Methods

5.2.1 FO membrane

A commercial TFC polyamide membrane (Porifera, Hayward, USA) was used to benchmark the transport of water from the feed solution to the draw solution. This membrane consisted of a thin active layer and a porous supporting layer. Key properties of this membrane have been reported elsewhere [145]. Briefly, the membrane structural parameter was 0.46 ± 0.05 mm. The average pore radius of this membrane was estimated to be 0.37 ± 0.04 nm. According to the manufacturer, the operational pH range of this membrane is from pH 2 to 13. The active and supporting layers of this membrane are negatively charged above pH 4.

Table 5-1: Key physicochemical properties of draw solutions used in this study (data were obtained from *Chemicalize* online platform).

Chemical Name	Glycine	Sodium glycinate	MEA
Chemical formula	$C_2H_5NO_2$	$C_2H_4NNaO_2$	C_2H_7NO
Chemical structure	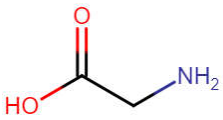	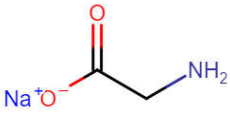	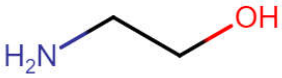
Molar mass (g/mol)	75.07	97.05	61.08
pKa	2.31, 9.24	2.31, 9.24	9.55, 15.61
Charge at pH 6.5	Neutral	Neutral	+ 1.00
Charge at pH 12	- 1.00	- 1.00	Neutral
Water solubility at pH 6.5 (g/L)	345.90	Miscible	Miscible
Water solubility at pH 12 (g/L)	Miscible	Miscible	Miscible
Minimum projection area ($Å^2$)	17.88	17.87	17.12

5.2.2 Feed solution

Secondary treated effluent (pH = 7) was collected from the Shellharbour wastewater treatment plant (NSW, Australia) and stored at 4 °C. The conductivity of the effluent sample was 2.4 mS/cm and TOC was 7.5 mg/L. Seawater (pH = 8) was collected from the Tasman Sea, South Pacific Ocean (34.25° S, 150.54° E). The seawater was allowed to settle for at least 48 h and the sediment was discarded. The conductivity and TOC of the seawater sample was 52.1 mS/cm and 22.1 mg/L.

5.2.3 Draw solution

Analytical grade glycine and MEA were from Chem-Supply (SA, Australia). Sodium glycinate was prepared by mixing glycine and sodium hydroxide (Chem-supply, SA, Australia) at a 1:1 molar ratio. These amine-based CO_2 adsorbents (Table 5-1) were used to prepare draw solution for FO experiments using DI water.

5.2.4 Analysis

The electrical conductivity and pH of the feed solution were measured using an Orion 4 Star plus pH/conductivity meter (Thermo Fisher Scientific, Waltham, MA). TOC analysis was conducted by sparging Non-Purgeable Organic Carbon using a VCSH TOC analyzer (Shimadzu, Kyoto, Japan). Acid (2 M HCl) was added to maintain sample integrity by reducing the microbiological growth rate.

5.2.5 Experiment system

FO experiments were conducted using a bench scale system consisting of a cross-flow membrane cell (with length of 10 cm, width of 5 cm, height of 0.2 cm, and effective membrane surface area of 44.6 cm^2), draw and feed gear pumps, rotameters, and temperature regulating units (Figure 5-1). A draw solution reservoir was placed on a digital balance (Mettler-Toledo Inc., Hightstown, NJ), and weight change was monitored every 5 minutes and transferred to a data logger. Due to the dilution effect, concentrated draw solution (5 M) for each chemical was added every 0.5 h to maintain a constant draw solution concentration. Two gear pumps (Micropump, Vancouver, WA) were used to circulate the draw solution and feed solution at a flow rate of 1.0 L/min from their respective reservoirs simultaneously. The temperatures of draw solution and feed solution were maintained using temperature regulating units (Thermo Fisher Scientifc, MA) equipped with a stainless steel heat exchanger coil at 25 ± 0.5 ℃ and 45 ± 0.5 ℃, respectively.

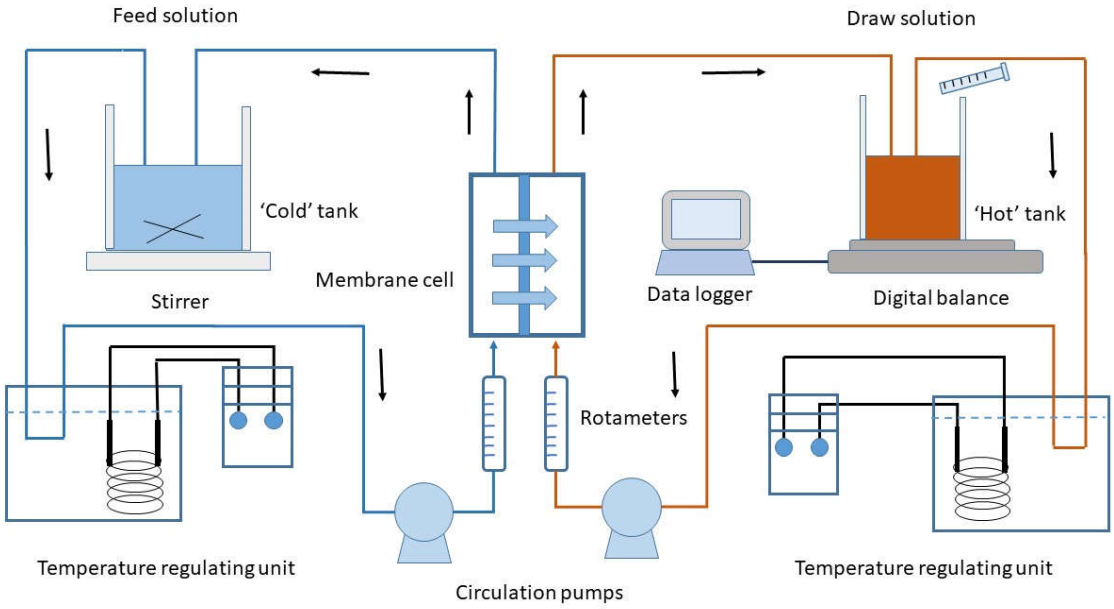

Figure 5-1: A bench-scale forward osmosis system

5.2.6 Experiment protocol

FO experiments were conducted in duplicate for 180 minutes. Glycine (3 M), MEA (1 M), and sodium glycinate (3 M/1.5 M) were used as the draw solution. Treated effluent and seawater were used as the feed solution. The initial volumes of the draw solution and feed solution are 1 and 2 L. The FO process was evaluated in a co-current mode in two membrane orientations, namely, AL-FS and AL-DS configurations. Draw solution temperature was controlled at either 25 or 45 °C to investigate the impact of temperature on water flux. Feed and draw samples of 30 mL were collected at the beginning and end of the experiments for TOC analysis. Water flux, J_w, was calculated as:

$$J_w = \frac{M_t - M_{t-5}}{\Delta t \times A \times \rho_{water}} \quad (5\text{-}1)$$

where M_t and $M_{t\text{-}5}$ are the weights of draw solution at time t min and t-5 min, respectively. A is the effective membrane area; ρ_{water} is the density of water; Δt is the 5 mins.

Given the constant ratio of carbon for three chemicals, it was possible to use TOC analysis to calculate their respective concentrations in the draw solution. The reverse salt flux, J_s, was calculated by a mass balance calculation as:

$$J_s = \frac{(C_t V_{feed,t} - C_0 V_{feed,0})}{A \times t} \quad (5\text{-}2)$$

$$V_{feed,t} = V_{feed,0} - \Delta V_{p,t} \quad (5\text{-}3)$$

where C_0 and C_t are the concentrations of the draw solute in the feed at the beginning and corresponding time t of the experiment, respectively; $V_{feed,0}$ and $V_{feed,t}$ are the volumes of the feed at the beginning and corresponding time t of the experiment; $\Delta V_{p,t}$ is the volume of permeate at time t.

5.3 Results and discussion

5.3.1 Properties of amine-based CO_2 adsorbents

5.3.1.1 Conductivity

Osmotic pressures of the amine-based adsorbents can be further assessed by measuring the electrical conductivity as a function of concentration. Conductivities of sodium glycinate and NaCl solutions at 1 M were 49.3 and 86.6 mS/cm (Figure 5-2a). Thus, despite the non-linear increase in conductivity as a function of concentration, sodium glycinate could still be categorized as a strong electrolyte similar to that of NaCl. On the other hand, unlike sodium glycinate, conductivities of MEA (1 M) and glycine (1 M) were only 0.9 and 0.06 mS/cm (Figure 5-2b-c). Therefore, MEA and glycine could be categorized as weak electrolytes.

As the smallest amino acid, glycine contains a carboxylic group (acidic) and an amine group (basic), thus, it can be characterized as a zwitterion. Glycine exists as a neutral species at pH 6.4, which results in a low conductivity as observed in this study (Supplementary Data Figure S5-1a). MEA is also a neutral species at pH 12 (Supplementary Data Figure S5-1b). It was noteworthy that electrical conductivity of the strong electrolyte sodium glycinate only increased linearly as a function of concentration up to 1.5 M.

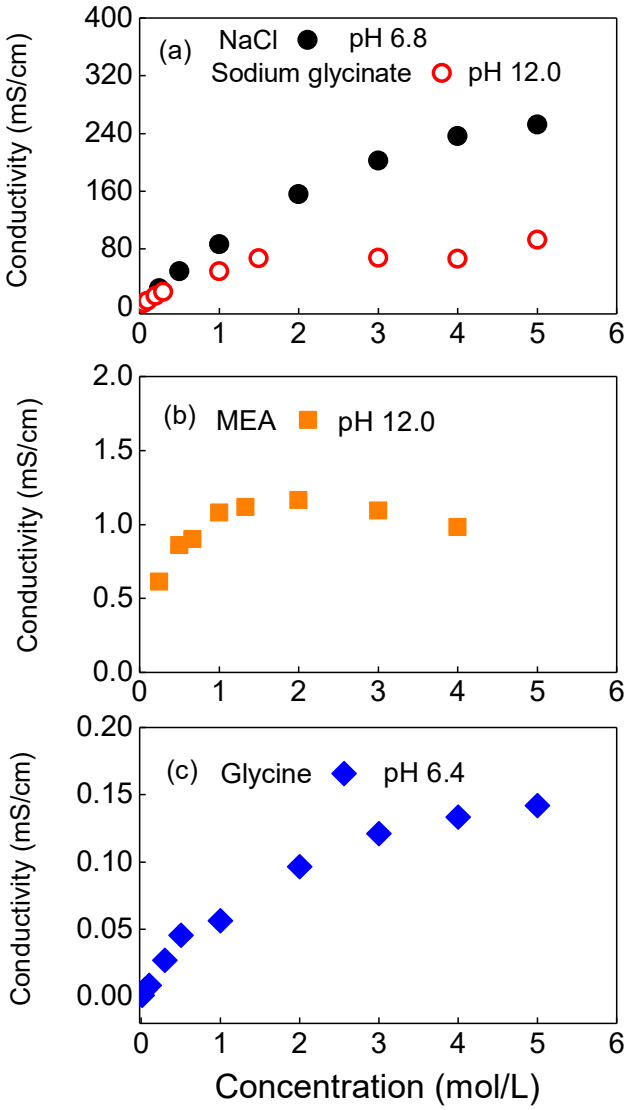

Figure 5-2: Electrical conductivities of the draw solution as a function of concentration at 25 °C at unadjusted pH values: (a) NaCl and sodium glycinate, (b) MEA, (c) glycine.

5.3.1.2 Osmotic pressure

Osmotic pressures of NaCl, MEA and glycine as a function of molarity in Figure 5-3 showed that not all amines-based CO_2 adsorbents behaved like normal inorganic electrolytes. Thus, it is necessary to determine their optimal concentrations as draw solution in the FO process. The calculated osmotic pressures of MEA and glycine solutions were lower than that of NaCl at the same concentration. Of a particular note, the calculated osmotic pressure of the MEA solution increased linearly as a function of concentration similar to that of NaCl (Figure 5-3). In other words, MEA behaved similar to an inorganic electrolyte. On the other hand, the calculated osmotic pressure of glycine

increased linearly as a function of concentration up to 3.3 M. Beyond 3.3 M, further increase in glycine concentration did not result in any further increase in the calculated osmotic pressure (Figure 5-3). Results from Figure 5-3 suggested that amine-based CO_2 adsorbents can only be used as draw solution within a specific concentration range. It was noted that the OLI Stream Analyzer 2.0 software package was not able to simulate the osmotic pressure of sodium glycinate.

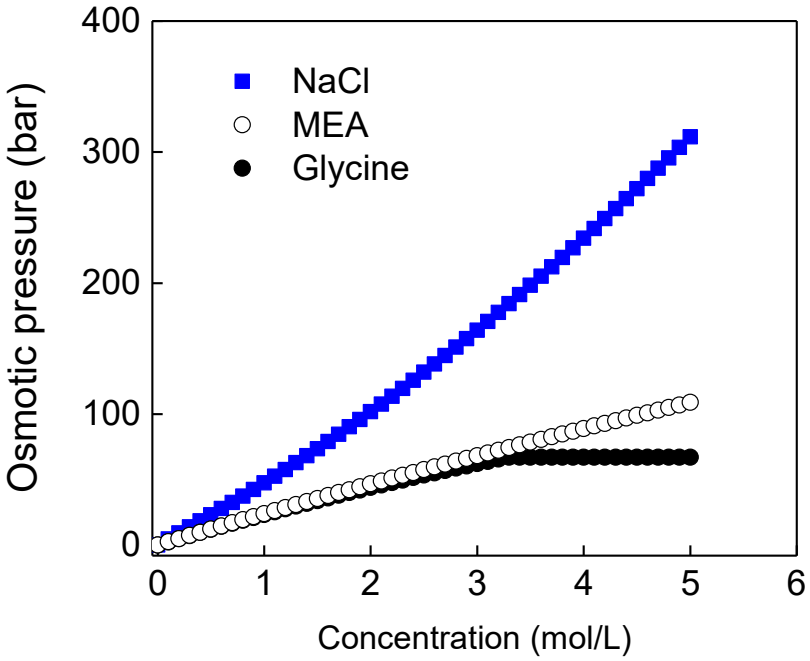

Figure 5-3: Osmotic pressures of NaCl, glycine and MEA solutions as a function of concentration at 25 °C (calculated using the OLI Stream Analyzer 2.0 (OLI System Inc., Morris Plains, NJ) software package).

The non-linear relationship between osmotic pressure/solution conductivity and concentration in Figure 5-2 and 5-3 suggested that there existed a concentration threshold beyond which no further increase in osmotic pressure could be achieved from the CO_2 capture aqueous solution in this study. Based on the data in Figures 5-2 and 5-3, the concentrations for sodium glycinate were chosen to be 1.5 and 3 M to investigate whether they generated similar osmotic pressures at similar conductivities or not. In addition, the maximum concentrations of glycine and MEA in subsequent FO experiments were set at 3 and 1 M, respectively.

5.3.2 Amine-based CO_2 adsorbent as draw solute

Aqueous glycine at 3 M showed the highest water flux among all draw solutes in both membrane orientations (Figure 5-4). External concentration polarization was unlikely the underlying reason for the observed flux decline given the high cross flow velocity (19.8 cm/S) over the membrane surface. The observed lower initial flux in an AL-FS configuration over in an AL-DS one can be attributed to the initial dilution effect in the porous support layer. There is also a trade-off between the dilution and the dilutive ICP in an AL-FS configuration, resulting in a small but discernible flux decline (flux in the range of 18.6-15.5 L/m^{2}h). By contrast, concentrative ICP in the AL-DS configuration amplified this trade-off, leading to a notable flux decline (from 35.4 to 19.2 L/m^{2}h or 45.8% flux decline).

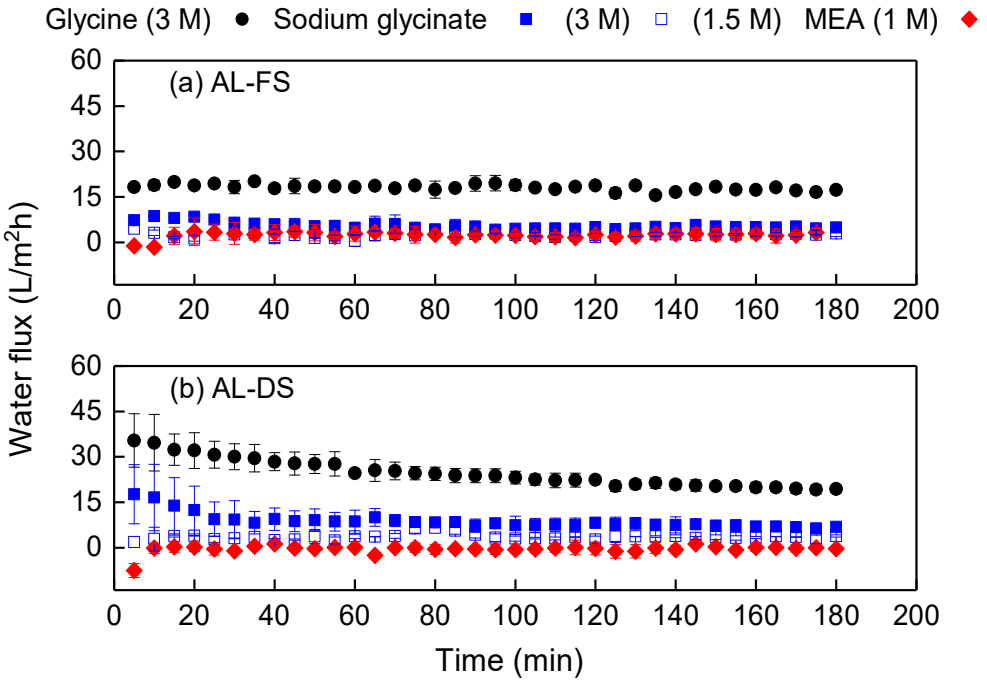

Figure 5-4: Water flux profile as a function of time using different draw solution in both membrane orientations: (a) AL-FS; (b) AL-DS. Treated effluent was used as the FS. Glycine, sodium glycinate, and MEA were used as draw solution. Temperatures of feed solution and draw solution were maintained at 25 and 45 °C. Error bars represent the difference of two replicate measurements.

In agreement with the conductivity results, negligible flux variation was observed between 1.5 M and 3 M sodium glycinate due to their similar osmotic pressures (Figure

5-4). Effective osmotic driving force is affected by the draw solution kinetic characteristics including diffusivity, viscosity, and reverse salt flux [153]. Viscosity of sodium glycinate presented a nonlinear and small rise as a function of concentration [154], resulting in a negligible variation in water flux. Interestingly, for sodium glycinate, a noticeable flux decline was observed in AL-DS configuration than AL-FS configuration at 3 M. The net driving force of forward osmosis is defined as the osmotic pressure gradient between feed solution and draw solution. With a larger reverse salt flux of sodium glycinate in AL-DS configuration (Figure 5-5), a smaller driving force was produced between feed solution and draw solution. Consequently, a more severe flux decline was observed in AL-DS configuration than that for the AL-FS configuration.

As an amino acid salt, sodium glycinate exhibited a noticeably lower water flux than glycine (amino acid) at the same concentration (3 M), which related to the less effective osmotic pressure (Figure 5-4). Although effective osmotic pressure is influenced by the accumulation of back diffusion draw solution in feed as a function of time, the reason for the contrast of initial osmotic pressure between sodium glycinate and glycine is still unclear. Since the osmotic pressure of sodium glycinate is not available in OLI Stream Analyzer 2.0, further research is needed for explaining the difference of osmotic potential for amino acid and amino acid salt in the same concentration.

Negligible water permeations were observed in both membrane orientations when MEA (1 M) was used as the draw solution in Figure 5-4. According to Figure 5-3, the calculated osmotic pressure of MEA at 1 M (24.7 bar) was close to that of NaCl at 0.5 M (23.1 bar). In our previous study [86], 0.5 M NaCl could produce approximately 12-14 L/m^2h water flux when DI water was used as the feed solution. Regarding less organic matters in DI water than that in treated effluent, lower water flux other than no water flux was expected when using 1 M MEA, which was contradictory to the simulation results (Figure 5-3). Results from Figure 5-4 suggest that MEA at 1 M was not able to generate adequate osmotic pressure to extract sufficient water from treated effluent in either membrane orientation. MEA in the range of 20-30 wt. % (corresponding to 4-5 mol/L) aqueous solution is normally employed in the post-combustion CO_2 capture. A sufficient water flux may be expected with a higher concentration of MEA [113].

5.3.3 Reverse diffusion of amine-based CO_2 adsorbent

The reverse salt fluxes of draw solution are shown in Figure 5-5. The reverse salt flux typically increases proportionally with the increasing water flux. However, with the highest water flux (Figure 5-5), glycine showed the lowest reverse salt flux among all draw solutions in both membrane orientations. In the osmotic driven membrane process, reverse salt flux is substantially affected by the diffusivity of draw solution. In other words, a lower reverse salt flux can be achieved for the draw solution with a smaller diffusivity coefficient. For instance, the diffusion coefficient of glycine (1.30×10^{-9} m^2/s at 45 °C) [155] is smallest among all the draw solution, followed by MEA (1.59×10^{-9} m^2/s at 45 °C) [146] and sodium glycinate. The diffusion coefficient of sodium glycinate is estimated to be similar like that of potassium glycinate (1.68×10^{-9} m^2/s at 45 °C) due to the similar physico-chemical property [147]. Thus, the reverse salt fluxes of glycine (3 M) at AL-FS and AL-DS configuration (11.61 g/m^2h; 20.61 g/m^2h) were remarkably lower than those of sodium glycinate at the respective configurations (AL-FS: 65.97 g/m^2h; AL-DS: 77.40 g/m^2h).

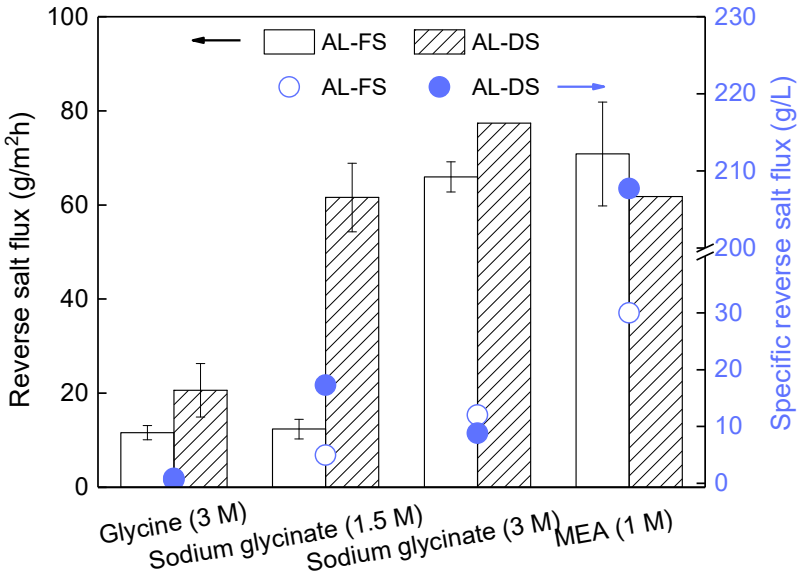

Figure 5-5: Reverse salt fluxes and specific reverse salt fluxes of different draw solution in two membrane orientations. Treated effluent was used as the feed solution. Glycine, sodium glycinate, and MEA were used as draw solution. AL-FS and AL-DS membrane orientations were applied. Error bars represent the difference of two replicate measurements.

The reverse diffusion of glycine was dependent on the back diffusion since glycine existed as neutral species at experimental pH (Supplementary Data Figure S5-1a). Besides the natural back-diffusion phenomenon, electrostatic interaction enhanced the reverse diffusion of MEA and sodium glycinate. For example, the dissociation of MEA resulted in its conjugate acid, ethanolammonium ion, and hydroxyl ion. Transfer of hydroxyl ion led to the corresponding increase from pH 6 to 10.5 in feed solution (Supplementary Data Figure S5-2), which therefore facilitated ethanolammonium ion reversely diffused to reach electroneutrality (Supplementary Data Figure S5-1b). As a result, reverse salt flux of MEA was higher than that of glycine. On the other hand, MEA exhibited a high reverse salt flux in contrast to the low water permeation that it generated. Back diffusion of MEA possibly accounted for the dominant mass transfer process other than water transfer owing to the lack of osmotic driving force.

In general, most amine-based adsorbents displayed the higher reverse salt fluxes in an AL-DS configuration than that in an AL-FS configuration (Figure 5-5), which can be attributed to the higher water flux in the AL-DS configuration (as previously shown in Figure 5-4). Of a particular note, due to the larger difference of reverse salt flux for 1.5 M sodium glycinate, a larger osmotic gradient difference between two configurations was generated than for 3M sodium glycinate (Supplementary Data Table S5-1). There is, however, a notable exception when MEA was used as the draw solution. MEA as the draw solution generated a very small water flux (Figure 5-5). In addition, in the AL-DS configuration, to the diffusion of MEA through the membrane is expected to be lower than in the AL-FS configuration.

In order to choose a suitable draw solution for simultaneous CO_2 capture and cooling, several criteria need to be satisfied. Firstly, it is able to show a good capability of reacting with CO_2. Secondly, it can generate a high osmotic pressure to ascertain the adequate water transfer. Thirdly, it should have a low reverse salt flux to avoid additional cost by adding supplement of draw solution.

Specific reverse salt flux (SRSF) is the ratio of the average reverse salt flux and water flux (J_s/J_w), which indicates the mass loss of draw solution per unit of water transport (Figure 5-5). Glycine showed the lowest SRSF than the other amine-based solvents in both membrane orientations, which were lower than 1 g/L. On the other hand, due to the low water flux and high reverse salt flux, SRSF of sodium glycinate and MEA were

considerably larger than 1 g/L. Of a particular note, sodium glycinate (3 M) showed a larger SRSF in AL-FS than AL-DS configuration, which was due to both the smaller water flux and reverse salt flux in an AL-FS configuration. A draw solution with a low SRSF leads to a small accumulation of draw solution in the feed, resulting in a larger osmotic gradient between draw solution and feed solution. Thus, glycine appears to benefit the FO performance in terms of the trade-off between water flux and reverse salt flux. Further analysis focused on the parameters affecting FO performance when glycine was used the draw solution.

5.3.4 Effects of operating conditions on water flux

5.3.4.1 Temperature gradient

The effect of temperature gradient is depicted in Figure 5-6. As shown in Figure 5-6(a), AL-DS configuration presented a more noticeable flux decline than that in AL-FS configuration. A gradual flux decline from 29 to 15 L/m^{2}h was observed for the AL-DS configuration, in contrast to a stable flux in the range of 20-23 L/m^{2}h for AL-FS configuration. As previously mentioned in section 5.3.2, effect of external concentration polarisation was negligible due to the high cross flow rate over the membrane surface. ICP appeared to be a major factor influencing the water flux [153]. At first, a higher water flux was driven by the larger osmotic pressure between feed solution and draw solution in AL-DS configuration without glycine permeation in the feed solution. However, the AL-DS also resulted in a higher reverse salt flux (Figure 5-6). The back diffusion of glycine into the feed solution as a function of time led to a gradual increase in osmotic pressure in the feed (hence a lower driving force) and exacerbated the concentrative ICP in the porous support layer.

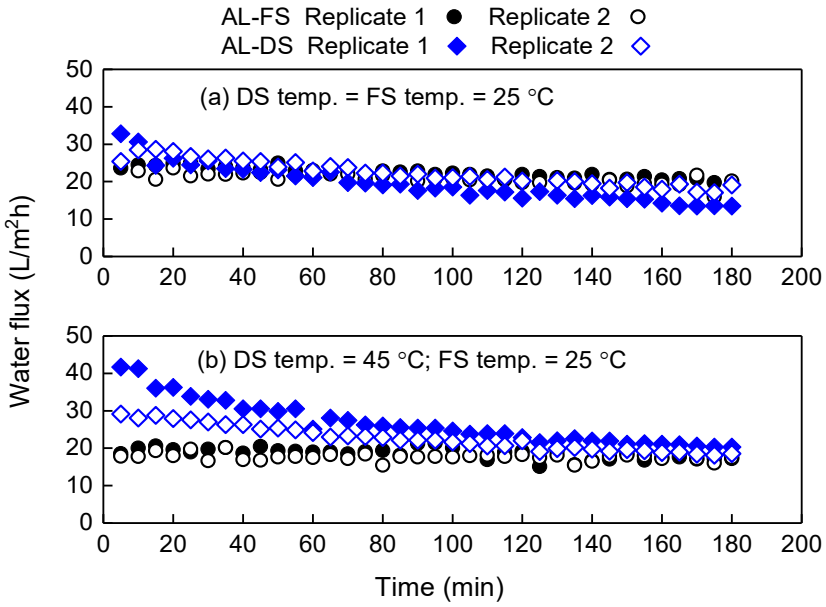

Figure 5-6: FO performance in two membrane orientations. (a) Temperatures of draw solution/feed solution (DS/FS) were maintained at 25 °C/25 °C; (b) Temperatures of DS/FS were maintained at 45 °C/25 °C. Glycine was used as the DS and treated effluent was used as the FS. Two membrane orientations: AL-FS and AL-DS were applied. All the experiments were conducted in duplicate.

Temperature increase in the draw solution enhanced the impact of membrane orientation in terms of water flux (Figure 5-6b). The contrast in terms of flux was more obvious as the draw solution temperature increased. A higher flux (35-19 L/m^{2}h) was observed in AL-DS configuration than that (18-17 L/m^{2}h) in AL-FS configuration. The enhanced flux in AL-DS configuration was likely due to the changing thermodynamic properties of glycine (i.e. osmotic pressure, diffusion coefficient, and viscosity) [156]. On the other hand, a larger diffusion coefficient would lead to the less concentrative ICP and the higher water flux. It was noteworthy that a lower water flux in AL-FS configuration was observed as temperature increased. Temperature enhancement resulted in the increase of reverse diffusion of glycine, and thus a less effective osmotic gradient (Supplementary Data Figure S5-3). The loss of effective osmotic gradient cannot be compensated by the growth of osmotic pressure caused by the temperature increase. This phenomenon contributed to a lower water flux in an AL-FS configuration. In general, these results suggested that more water was able to be transferred from treated effluent at higher temperature, in other words, heated CO_2 lean solution could be directly used as draw

solution. However, increased temperature enhanced the reverse diffusion of glycine in both membrane orientations, leading to the growing supplement of draw solute (Supplementary Data Figure S5-3).

5.3.4.2 Feed solution matrix

Glycine generated higher water fluxes from treated effluent than seawater in both membrane orientations (Figure 5-7). The osmotic pressure of seawater was 28.1 bar similar to the osmotic pressure of 0.6 M NaCl [157]. While, osmotic pressure of treated effluent was close to that of DI water due to the minimal presence of salts. Considering that osmotic gradient is the main driving force in FO, the difference between glycine (3 M) and treated effluent was larger than that between glycine and seawater. Thus, more water was able to be transferred from treated effluent than seawater in both membrane orientations.

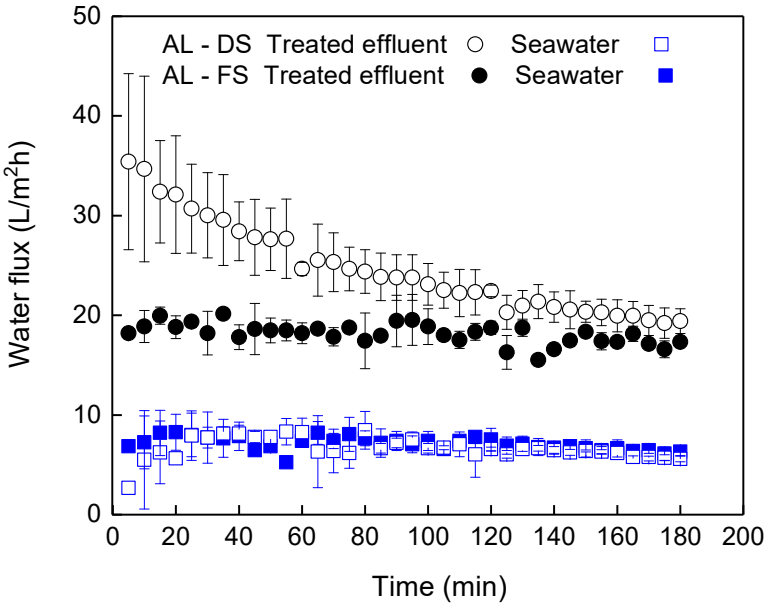

Figure 5-7: Comparison in water flux when using seawater or treated effluent as the FS in two membrane orientations. Glycine (3 M) was used as the DS. Temperatures of FS and DS were maintained at 25 and 45 °C. Two membrane orientations: AL-FS and AL-DS were applied. All experiments were conducted in duplicate and error bars represent the difference of two replicate measurements.

On the other hand, compared to the treated effluent, when seawater was used as the feed solution, the sharp contrast of water flux in the different membrane orientation was not

observed. Because less permeating water from seawater diluted the draw solution to a smaller extent, leading to a smaller ICP. Thus, the water fluxes in both membrane orientations were close due to the similar overall driving force. Despite of the lower water flux, seawater could also be as an alternative cooling source and desalinated simultaneously.

5.4 Conclusions

This chapter lays the groundwork for future research into a potential replacement of trim cooler by FO in post-combustion CO_2 capture. Conductivities of three amine-based draw solution in this study showed a non-linear relationship with concentration, indicating an osmotic pressure threshold in the FO process. Compared to sodium glycinate and MEA, glycine was identified as the most suitable draw solution with the highest water flux, lowest reverse salt flux and SRSF. Of a particular note, glycine showed a higher water flux but with more significant flux decline in the AL-DS configuration compared to the AL-FS configuration. The observed effect of membrane orientation on water flux and flux profile by glycine as the draw solution is possibly due to the higher osmotic pressure in AL-DS configuration and more severe concentrative ICP due to the slow back diffusion of glycine, respectively. In addition, temperature increase (from 25 to 45 °C) enhanced the water flux in AL-DS configuration other than AL-FS configuration due to effects of change in thermodynamic properties of glycine and more severe dilutive ICP. Results in this chapter demonstrated that heated and CO_2 lean amine solution could be directly used as the draw solution. Furthermore, glycine at 3 M could be used for extracting water from seawater and it therefore provided an alternative for simultaneous cooling and provision of make-up water. These results are promising but also highlight the need for more research work to realize a practical application of FO for CO_2 capture from power plant flue gas.

Chapter 6 Low-temperature stripping of CO_2 from aqueous amine-based solvents via integrated direct contact membrane distillation-forward osmosis

This thesis chapter has been submitted for a possible publication as the following journal article.

L. Zheng, K.K. Li, Q.L. Wang, G. Naidu, W.E. Price, X.W. Zhang, and L.D. Nghiem, Low-temperature stripping of CO_2 from aqueous amine-based solvents via integrated direct contact membrane distillation-forward osmosis, Journal of Membrane Science, Submitted.

6.1 Introduction

Results from Chapter 5 demonstrated that a FO system could cool down the heated CO_2-lean solution and produce the make-up water from non-potable water simultaneously. Apart from reducing freshwater consumption in cooling process, how to minimise the energy requirement in regeneration maintains the one of the biggest challenges for CO_2 capture. In addition, solvent regeneration requires 70-80% of the overall operational costs [158, 159]. High regeneration temperature resulted in inevitable thermal degradation and volatile loss of solvents [160].

MEA has been considered as the benchmark in amine-based CO_2 capture due to its several outstanding features: large absorption capacity at low pressure (atmospheric pressure), fast reaction rate and high mass transfer. Apart from MEA, amino acid salts have also gained much attention because of their greater resistance to oxidative degradation and lower toxicity than MEA [161, 162]. They both have an amine group and an acidic carboxylic acid group, which can be protonated, neutral, or deprotonated as a function of pH [102]. Zwitterionic mechanism is therefore considered as the most possible chemical reaction between CO_2 and solvents [100, 163]. In this mechanism, a primary or secondary amino group of amines firstly reacts with CO_2 to form a zwitterion (equation i). The base (i.e. amine, OH^-, or H_2O) immediately neutralize the intermediate to form a carbamate

(equation ii). These carbamates can be thermally driven back to amine and CO_2 due to the exothermic reaction.

$$CO_2 + RNH_2 \leftrightarrow RNH_2^+COO^- \quad \text{(i)}$$

$$\mathrm{RN}H_2^+COO^- + RNH_2 \leftrightarrow RNHCOO^- + RNH_3^+ \quad \text{(ii)}$$

Currently, amines are regenerated by stripping with water vapor at high temperature (100 to 120 ºC), which requires 70-80% of the overall operational costs [17, 158, 159]. In addition, high stripping temperature resulted in the inevitable thermal degradation and volatile loss of solvents [160]. A number of approaches hence focused on the solvent modification with promoters [101, 164], efficient gas-liquid contactors [165, 166], microwave swing regeneration [167, 168] and electrochemically mediated amine regeneration [169, 170]. However, despite of their potentials regarding energy reduction, a long way still toward their full scale employment for CO_2 capture. In addition, the massive freshwater consumption for the trim cooler has also restricted the construction of inland CO_2 capture plant. Consequently, it is aimed to minimise the energy requirement in CO_2 desorption and freshwater consumption during cooling process for further development in CO_2 capture.

Several aspects of these processes are able to resolve the crucial dilemmas in CO_2 desorption process. The first one is that how to reduce CO_2 desorption temperature by utilizing the massive amount of low-grade waste heat. US thermal power plants discharged 18.9 billion GJ_{th} waste heat with weighted average temperature 88.6 °C in 2012 [171]. The proportion of waste heat was approximately 68% of total energy. These abundant waste heat can provide the sufficient energy for CO_2 desorption at low temperature. Novek et al., [172] found that the CO_2 desorption efficiency of ammonium bicarbonate with acetaldehyde could achieve 86.5% at 68 °C. Lai et al., [101] observed that addition of alcohol significantly improved the CO_2 desorption at 75 °C, which was also a promising method to realize exploitation of waste heat.

Furthermore, the second dilemma is to facilitate the CO_2 desorption rate especially at low temperature. It is reported that H_2O reduction in CO_2 capture system can improve CO_2 desorption rate. Either replacing H_2O with solvent or reducing H_2O in amine may therefore enhance CO_2 desorption. Lin et al., [173] lowered the H_2O proportion by adding methanol into the blend amine system. The result showed that the cyclic loading of

diethylenetriamine/piperazine/methanol/water mixed solvent at 80 ºC was 67% higher than that of MEA at 120 ºC. Similarly, the study of Lai et al., [101] also proved that alcohol-amine-water mixed solvent was better than the single amine solvent in terms of CO_2 desorption rate. 40 wt% ethanol addition in 20 wt% MEA solvent significantly enhanced the CO_2 desorption rate from 0.021 to 0.137 mmol/s. By forming the vulnerable functional group $C_2H_5OCO_2^-$ instead of HCO_3^-, ethanol could shrink the dielectric constant of the solvent and be able to release acidic CO_2 at low temperature [174]. Despite of these favourable results from adjustment of H_2O proportion in amine solvent, how to effectively reduce H_2O in amine solvent is still a challenge.

Direct contact membrane distillation (DCMD) appears to simultaneously solve above two dilemmas. First of all, compared to the conventional hydraulic driven membrane process (nanofiltration and reverse osmosis), DCMD is a thermally driven separation process that employs the vapour pressure as the driving force caused by temperature difference between the feed and distillate side [175]. It is not necessary to heat up the solution to its boiling point in DCMD, which possibly realizes either the utilization of low-grade waste heat from power plants for heating solution or direct application of regenerated amine solvent after heat exchanger (temperature 70-80 ºC) as the feed. In addition, for the second dilemma, H_2O in amine solvent keeps decreasing since only vapour molecules (i.e. water vapour and gaseous CO_2) are able to diffuse through the hydrophobic membrane in DCMD. As a result, it is beneficial for accelerating CO_2 desorption rate to achieve environmentally benign and cost-saving amine regeneration. DCMD has been used for ammonia regeneration at the low temperature [172, 176]. Of a particular note, previous studies have proved the feasibility of low-temperature driven CO_2 desorption in amine and amino acid salt by the hollow fibre membrane contactor [168, 177, 178]. However, the feasibility for the low-temperature (especially < 80 ℃) driven DCMD for CO_2 desorption still needs further investigations.

In addition to our previous study [179], which demonstrated that a forward osmosis (FO) system could cool down the regenerated amine solvent and produce the make-up water from non-potable water simultaneously. As another emerging membrane process, FO uses osmotic difference rather than temperature difference as the driving force to produce clean water. Thus, this chapter proposes an integrated DCMD-FO system (Figure 6-1) for two purposes: (1) CO_2 desorption at low temperature; (2) simultaneous cooling and make-

up water production for solvents after desorption. The primary objectives of this study are to extend the previous theoretical framework and to evaluate the effect of membrane material and solvent type on the system performance. This study not only aims to provide a low-temperature desorption method for amine-based solvent, but also highlight the sustainable CO_2 capture process via using wastewater or waste heat.

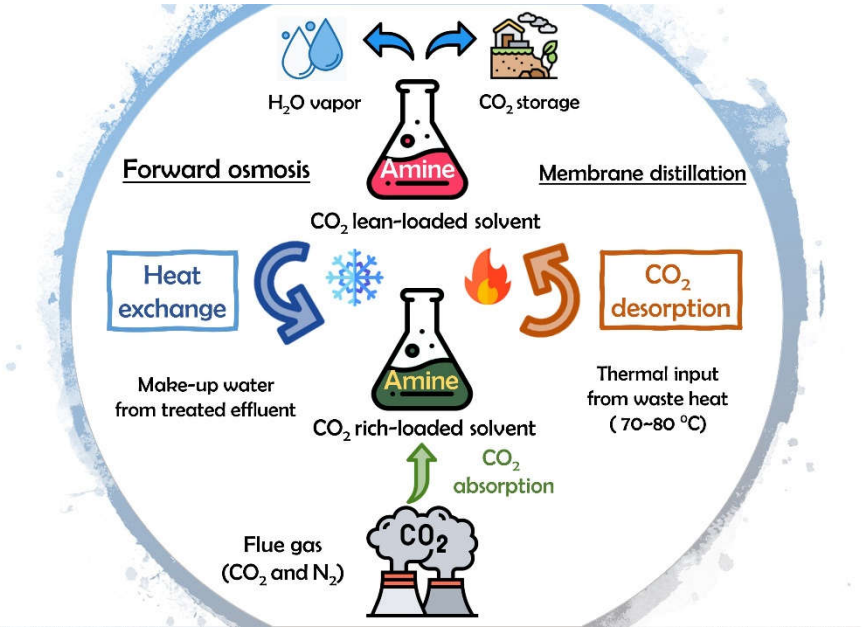

Figure 6-1: Schematic diagram of integrated DCMD-FO system for CO_2 capture.

6.2 Materials and methods

6.2.1 Membranes and chemicals

Two commercially available flat-sheet hydrophobic polytetrafluoroethylene (PTFE) membranes were used for the DCMD process. Their origins and key properties are presented in Table 6-1. A flat-sheet hydrophilic cellulose acetate (CTA) membrane (Fluid Technology, US) was used for FO process. This CTA membrane consists of a cellulose triacetate active layer and an embedded woven support layer. The operational ranges of pH of these membranes are between 3 and 13, which cover the pH range of the amine solution before and after CO_2 adsorption.

Reagent grade MEA, glycine and sodium hydroxide were from Sigma-Aldrich. Sodium glycinate was prepared by mixing glycine with an equal molar ratio between glycine and sodium hydroxide in deionised (DI) water. Instrument grade (>99.8% purity) CO_2 and N_2 gases were from Coregas Australia and stored in pressurised cylinders.

Table 6-1: Specifications of hydrophobic membranes used in this study.

Membrane	Supplier	Thickness (μm)	Porosity (%)	Pore size (μm)
1	General Electric (US)	179	75	0.22
2	Porous Membrane Technology (China)	60	80	0.2

6.2.2 Feed solution for DCMD and FO

CO_2 and N_2 gases were mixed together using Bronkhorst mass flow controllers to obtain a CO_2:N_2 gas of 1:9 in the volume ratio to simulate the composition of flue gas. Simulated flue gas was constantly bubbled into the 5 L of MEA (5 M) or sodium glycinate (3 M) solution in the wetted-wall column at a flow rate of 1.1 L/min at 40 °C controlled by a water bath. Gaseous CO_2 concentration was analysed by a gas analyser (Horiba, VA-3000) with the analytical range of 0-10 vol% every 15 s. The CO_2 rich solution was considered fully loaded when CO_2 concentration in the outlet was the same as in the inlet. These CO_2 rich-loaded solutions were used as the feed solution for DCMD experiment.

CO_2 rich-loaded solutions became CO_2 lean-loaded solution after CO_2 desorption in the DCMD experiment and CO_2 lean-loaded solutions were used as the draw solution in FO process. Treated effluent from a membrane bioreactor [180] was used as the feed solution in FO process. The conductivity and total organic carbon (TOC) of this treated effluent was 5 mS/cm and 7 mg/L. DI water was used as the feed solution in the baseline test with the same draw solution for treated effluent.

6.2.3 DCMD for CO_2 desorption and FO for water supplement

The CO_2 desorption experiments for CO_2 rich-loaded solution were performed using a lab-scale DCMD system described in Figure 6-2a. The membrane module was in the plate-and-frame configuration with the effective membrane area 17.5 cm^2. Feed solution (0.5 L) and distillate (2 L) were circulated counter-currently by two gear pumps (Cole Parmer, model 75211-15, US) at the flow rate of 1.0 L/min (corresponding to 36.2 cm/s). In all experiments, the CO_2 rich-loaded feed solution was placed in a jacketed vessel coupled with a temperature control system (Thermoline, model BL-30, Australia) and maintained at 80 ± 2 °C. The distillate was maintained at the 25 ± 2 °C using another temperature control system (Thermoline, model BL-30, Australia). Temperatures at the inlet and outlet of feed solution and distillate flow channels were recorded by the temperature sensors (Vernier LabQuest 2, US).

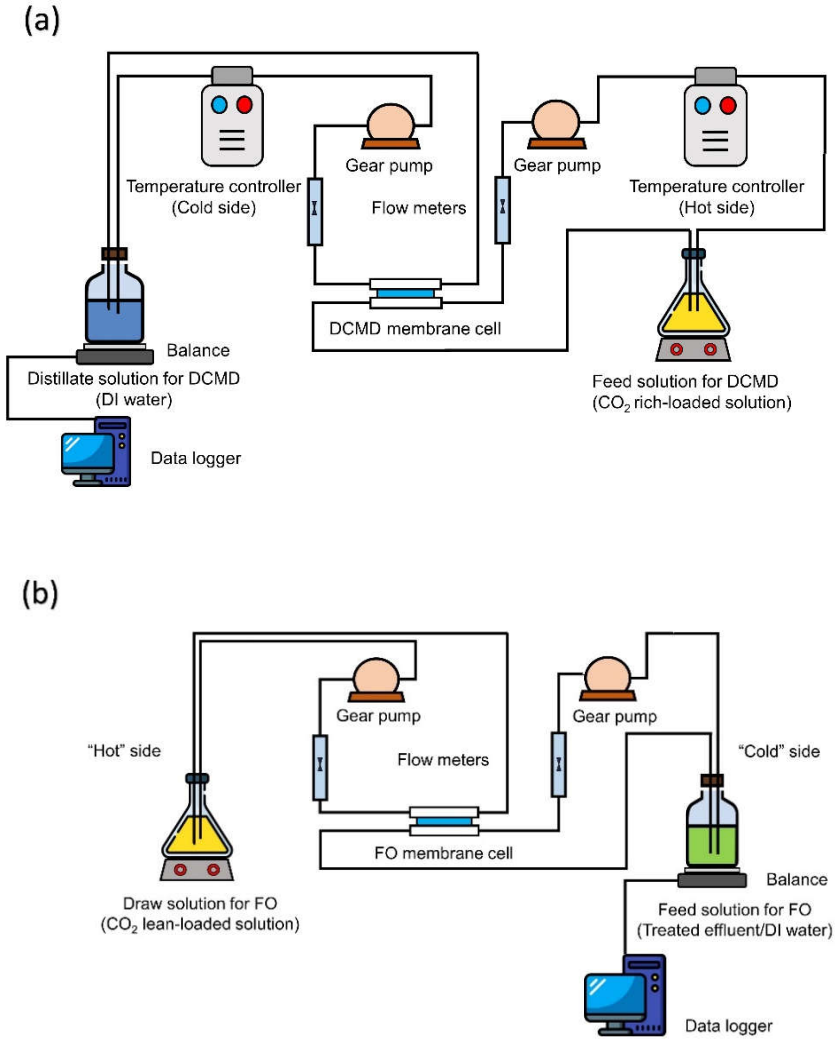

Figure 6-2. Schematic diagram of experimental apparatus for CO_2 desorption and water supplement: (a) a lab-scale DCMD system; (b) a lab-scale FO system.

The distillate reservoir vessel was placed on a digital balance (Adam, model PGL 8001, Australia) and weight change was recorded every 3 min and transferred to a data logger. Preliminary experiments showed that CO_2 desorption stopped at water recovery of 30% or more. Samples (2 mL) from the feed solution were collected at 10, 20, and 30% water recovery to monitor the CO_2 desorption performance as a function of water recovery. Feed and distillate samples (50 mL) were also taken at the beginning and end of each experiment for other analyses. At the conclusion of the CO_2 desorption experiments, the feed solutions of the DCMD process were then used as the draw solution in the subsequent FO experiments. After the CO_2 desorption experiment, the experimental equipment was

rearranged into an FO system. The same membrane cell was used for the FO system to provide make up water and cooling to the CO_2 lean-loaded solution (i.e. the regenerated amine solution) as described in Figure 6-2b. Draw solution (0.35 L) and feed solution (2 L) were circulated counter-currently. The feed solution reservoir was placed on the digital balance for monitoring the water flux. It is assumed that amine loss during CO_2 desorption did not occur. Thus, each experiment was conducted until the amine solution returned to the initial volume of 0.5 L just before CO_2 desorption. In other words, the volume of water permeated through the membrane to the CO_2 lean-loaded solution was the same as the volume of clean water produced by DCMD during CO_2 desorption. Feed solution and draw solution samples (50 mL) were taken at the beginning and end of each experiment for analysis. All DCMD and FO experiments were conducted in duplicate. The results are reported as geometric mean and standard deviation.

6.2.4 Measurement and analysis

6.2.4.1 Contact angle measurement

Membrane surface hydrophobicity was determined by contact angle measurement using a goniometer (model: Theta Lite 100, Biolin Scientific, Sweden) and the standard sessile drop method. Five measurements using DI water (5-8 μL) as the reference liquid were conducted at different locations on the membrane surface. Membrane samples were air-dried before contact angle measurement.

6.2.4.2 Solution chemistry characterization

The chemical property of liquid sample (1 μL) was analysed by a Fourier transform infrared (FTIR) spectroscopy (model: IRAffinity-1, Shimadzu, Japan) equipped with a single reflection attenuated total reflectance (MIRacle 10, Shimadzu, Japan). Absorbance from wavelength 400 to 4000 cm^{-1} of each sample displayed the corresponding spectra at 4 cm^{-1} resolution. TOC analysis was operated by sparging Non-Purgeable Organic Carbon using a TOC analyser (Analytik Jena Multi N/C 3100, Jena, Germany).

6.2.4.3 Water flux and reverse salt flux

Water flux (J_w) is an important performance indicator of membrane process, which can be calculated as follow:

$$J_w = \frac{m_{t1} - m_{t2}}{\Delta t \times \mathrm{A} \times \rho} \qquad (6\text{-}1)$$

where M_{t1} and M_{t2} are the weights of distillate (DCMD)/feed solution (FO) at time t1 and t2, respectively. Δt is 3 min; A is the effective membrane area; and ρ is water density.

Due to the constant ratio of carbon for MEA and sodium glycinate, it was possible to carry out TOC analysis to analyse their respective concentration in the solution sample. Reverse salt flux (J_s) indicates the mass diffusion from draw solution to feed solution, which can be calculated based on the mass balance calculation as follow:

$$J_s = \frac{(C_t \times V_{feed,t} - C_0 \times V_{feed,0})}{A \times t} \quad (6\text{-}2)$$

$$V_{feed,t} = V_{feed,0} - \Delta V_{p,t} \quad (6\text{-}3)$$

where $V_{feed,0}$ and $V_{feed,t}$ are the volumes of the feed at the beginning and corresponding time t of the experiment; C_0 and C_t are the concentrations of draw solution in the feed at the beginning and corresponding time t of the experiment, respectively; $\Delta V_{p,t}$ is the volume of distillate at time t. The solvent rejection by DCMD is calculated based on dilution factor ($DF=V_{draw}/\Delta V_{p,t}$) as follow:

$$R(\%) = \left(1 - \frac{DF \times C_{distillate}}{C_{feed}}\right) \times 100 \quad (6\text{-}4)$$

Water extraction rate, R_w, or the water recovery of MD/FO experiment is calculated as below:

$$R_w = \frac{A\int_0^T J_w d_t}{V_{distillate,0}} \quad (6\text{-}5)$$

6.2.4.4 CO_2 loading ratio analysis

The CO_2 loading ratio (α) values after sorption and desorption were determined by the excessive acid method [181]. By adding an excess amount of strong acid (i.e. 2 mol/L H_2SO_4) to the liquid sample, CO_2 in the liquid sample was released into the gas phase and precisely measured by the variable volume in a burette.

$$\alpha = \frac{V_{CO_2}}{22.4 \times V_L \times m} \times \frac{P}{P_0} \times \frac{273}{t} \quad (6\text{-}6)$$

where V_{CO_2} denotes the measured volume of released CO_2 from the sample, mL; V_L represents sample volume, mL; m denotes the molar concentration of sample, mol/L; P/P_0 stands for the ratio between room atmospheric pressure and standard atmospheric pressure; t is the room temperature, K. In addition, the accuracy of this method was well testified by using different concentration of sodium carbonate (0.5, 1, and 2 mol/L) aqueous solutions.

CO_2 desorption efficiency, ρ, is obtained following below equation:

$$\rho(\%) = (1 - \frac{\alpha_f}{\alpha_i}) \times 100 \quad (6\text{-}7)$$

where α_i and α_f represent initial and final loading of CO_2 rich-loaded and lean-loaded amine solutions. On the other hand, regeneration efficiency, η, is used to compare the loading of regenerated solution (α_r) to that of initial CO_2 rich-loaded solution (α_i).

$$\eta(\%) = \frac{\alpha_r}{\alpha_i} \times 100 \quad (6\text{-}8)$$

6.3 Results and discussions

6.3.1 DCMD performance for CO_2 desorption

6.3.1.1 CO_2 loading

The CO_2 loading ratios for MEA and sodium glycinate were 0.54 and 0.59 mol/mol. These results are consistent with our previous studies and the literatures [182-184]. CO_2 desorption by DCMD was validated by monitoring the CO_2 content of the feed solution. Figure 6-3 shows 32.8 and 32.4% CO_2 desorption efficiencies for MEA using membrane 1 and 2, respectively. The faster desorption rate was observed for MEA until 20% water recovery and the desorption rate became gradually slow even stopped until 30% water recovery. In the current state of the art MEA-based CO_2 capture process, a higher CO_2 desorption efficiency can be achieved but only at much higher temperature (ca. 120 °C) since CO_2 desorption is a thermal process and thus is sensitive to temperature.

Desorption of CO_2 rich-loaded MEA could be divided into two stages (fast and slow) in terms of desorption rate. At the fast desorption stage, namely prior to 20% water recovery with high CO_2 loading, some HCO_3^- or CO_3^{2-} released CO_2 quickly via thermolysis. On the other hand, carbamate was formed via a reaction between other HCO_3^- or CO_3^{2-} and

$MEAH^+$. After the first stage, fresh formed carbamate reacted with abundant H^+ to regenerate MEA and release CO_2 at a slower rate. The temperature used in our study was far lower than in the conventional amine-based CO_2 capture process, thus, the desorption rate was slow. On the other hand, even in the conventional process, some researchers have detected the peak of carbamate in the solution after desorption, which suggested that the regeneration of MEA was incomplete [100].

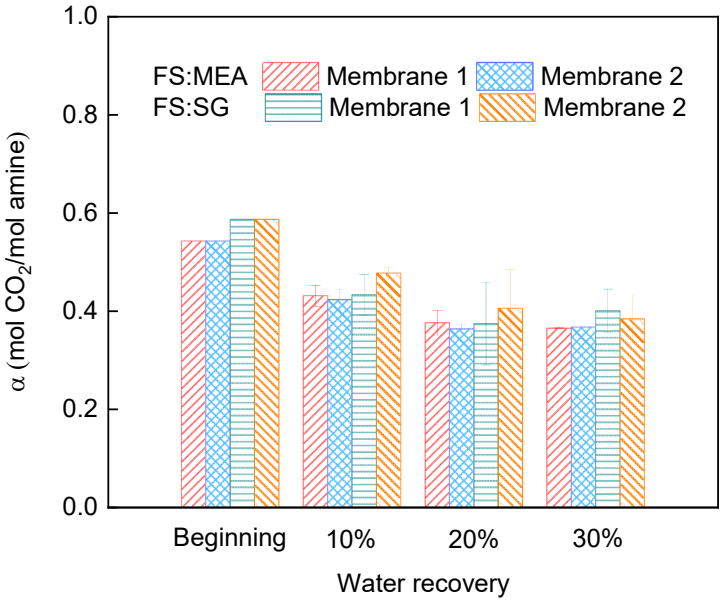

Figure 6-3: CO_2 desorption of CO_2 rich-loaded solvent by using DCMD with two types of membranes. Experimental conditions: DI water was used as the distillate. MEA (5 M) and sodium glycinate (SG, 3 M) were used as the feed. The temperatures for feed solution and distillate were 80 °C and 25 °C, respectively. All experiments were conducted in duplicate and until 30% water recovery (maximum CO_2 desorption). The error bars represent the difference between two replicate experiments.

CO_2 desorption can be also assessed by examining the corresponding pH value of the amine solution. In this study, the pH value of CO_2 rich-loaded MEA was 8.5 and pH increased to 10.7 after desorption (for both membranes). The pH of solution after desorption did not reach the initial value of fresh MEA (12.6), which indicated MEA was not able to be completely regenerated under current experimental condition. Previous works have also reported that CO_2-saturated MEA solution achieved similar desorption

efficiency (32%) at 120 °C or even higher temperature under atmospheric pressure [100, 185].

A small but nevertheless important variations of CO_2 loading for sodium glycinate were observed between two membranes (Figure 6-3). Membrane 1 and 2 showed CO_2 desorption efficiency 31.8% and 34.6%, respectively. Similar to the observation in MEA, the CO_2 loading declined significantly prior to 20% water recovery (stage 1) and reached a stable loading between 20-30% water recovery (stage 2). In addition, membrane 1 showed a slightly faster desorption rate than that of membrane 2 in the first stage. It is postulated that functional groups on membrane 1 might accelerate the decomposition of bicarbonate and carbamate, which released CO_2 quickly. However, as an unhindered primary amine like MEA, sodium glycinate formed a stable intermediate via reaction with CO_2 because of the weaker resisting power from hydrogen atom [186]. Thus, more thermal energy is required for splitting N-C bond to release CO_2 from intermediates, which impeded CO_2 desorption for two membranes after 20% water recovery.

6.3.1.2 Wettability behaviour

The relative wettability of membrane is determined by its hydrophobicity quantified by the contact angle measurement. There was the negligible change of hydrophobicity for membrane 1 after desorption experiment using sodium glycinate as the adsorbent (Figure 6-4). However, MEA resulted in the hydrophobicity decline from 126.5º to 94.7º in membrane 1. Hydrophilic functional groups (i.e. amides) were likely formed by the interaction between the MEA molecules and membrane polymer, thus reducing the membrane hydrophobicity [187]. In addition, these hydrophilic functional groups reduced surface roughness of membrane 1 and also contributed to its rising hydrophilicity. As a result, a partial membrane wetting occurred during the CO_2 desorption using MEA as the adsorbent.

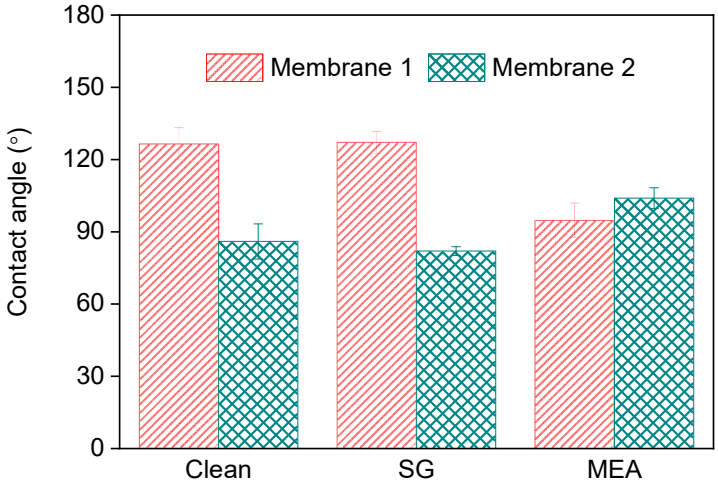

Figure 6-4: Contact angles of membranes before and after DCMD process. Error bars represent the standard deviation of five repetitive measurements

Interestingly, despite of the initially low hydrophobicity, contact angle of membrane 2 increased by 31% after the desorption experiment using MEA as the adsorbent (Figure 6-4). This improvement was possibly due to the membrane swelling caused by the MEA penetration [170]. In addition, membrane swelling resulted in an increasing surface roughness, which was also beneficial for preventing mass transfer of aqueous solution. However, the wettability of membrane 2 should be further validated by other measurements, for example, liquid entry pressure measurement. Sodium glycinate can potentially behave like a surfactant given its molecular structure. Nevertheless, membrane 2 showed a negligible decrease in hydrophobicity after CO_2 desorption when sodium glycinate was used as the adsorbent. Results in Figure 6-4 suggest that both membranes were sustainable for DCMD operation to regenerate amine solution since the membrane surface remained hydrophobic after CO_2 desorption.

6.3.1.3 Water reduction in amine by DCMD

CO_2 desorption rate can be facilitated by the water reduction in amine solvent. Water reduction can be represented by the water production in distillate side in terms of water flux in DCMD. Water fluxes during the CO_2 desorption experiment when MEA was used as the adsorbent are reported in Figure 6-5a. Membrane 1 had an initial flux of 21.2 L/m^{2}h, which was only stable flux for the initial 100 minutes of the desorption experiment. Flux

started to decline since partial wetting occurred and reached 52.3% reduction at the end of process. By contrast, although with a lower initial flux than membrane 1, membrane 2 showed a stable water flux throughout the desorption experiment.

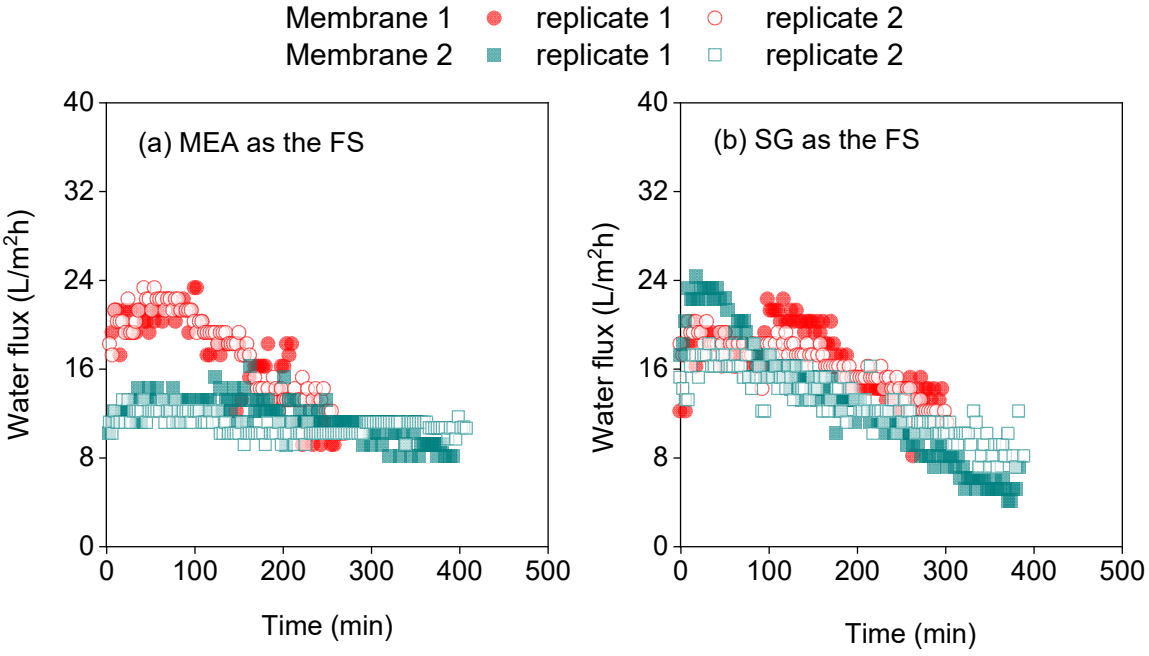

Figure 6-5: Water flux in DCMD during CO_2 desorption using different adsorbent: (a) MEA and (b) SG. Experimental conditions are described in Figure 6-3.

It is well-established that membrane thickness plays a significant role in DCMD due to the inversely proportional relationship between the membrane thickness and water flux. A thicker membrane is assumed to demonstrate a lower water flux because of the increasing heat loss and mass transfer resistance [175]. As reported in the section 2.1.1, membrane 1 was thicker than membrane 2 whereas outperformed a higher water flux before it became partially wetted. This observation was possibly due to the different hydrophobicity between two neat membranes (Figure 6-4). As two membranes displayed opposite changes of hydrophobicity after CO_2 desorption, namely membrane 1 became hydrophilic and membrane 2 converted more hydrophobic, the flux variations between two membranes diminished until the end of process. Hydrophobicity appeared to be a determined factor for water flux in DCMD for MEA regeneration. Despite of the variation in flux decline, both membranes showed the high solvents rejection (over 98%) (Supplementary data Figure. S6-1).

When sodium glycinate was used as the adsorbent, water flux decline was more significant compared to MEA and was observed with both membranes. Both membranes showed the similar initial fluxes in Figure 6-5b. However, their hydrophobicity difference could contribute to the corresponding flux decline of 31.6% for membrane 1 and 63.2 % for membrane 2. As discussed in section 3.1.2, contacting with sodium glycinate had the negligible effect on the hydrophobicity of each membrane. Nevertheless, increasing feed concentration resulted in the growth of sodium glycinate viscosity [188] and decrease of water activity, which led to a lower water vapour pressure and the further flux decline. In addition, the effects of concentration polarisation and temperature polarisation were expected to be enhanced by the increasing feed salinity and feed viscosity simultaneously.

The stable hydrophobicity of both membranes provided an efficient layer between membrane surface and solution. This could prevent the penetration of sodium glycinate through membrane pore into distillate, thus avoiding deteriorated distillate quality. High solute (amine) rejection values (supplementary data Figure S6-1) were observed for both membranes, which indicated the membrane pores were not completely wetted during the process. In general, the high rejections of MEA and sodium glycinate by DCMD were particularly advantageous for avoiding amine loss during the CO_2 desorption.

6.3.1.4 Amine loss in the DCMD distillate

FTIR is a reliable analytical technique to monitor the chemical reaction due to the measurable change of a molecule's dipole moment in the mid-IR region (400 - 4000 cm^{-1}). It is to be noted that peaks appeared between 3000 and 4000 cm^{-1} provided information unrelated with chemical reaction between CO_2 and amine. This is because that hydrogen bonding and O-H stretching of H_2O resulted in some broad peaks between 3200 and 3700 cm^{-1}. In addition, other chemical bonds (i.e. N-H, C-H, and O-H) stretching also resulted in the particular peaks in this wide region. Thus, this region is known as "the hydrogen stretching region", which is not included in our further discussion.

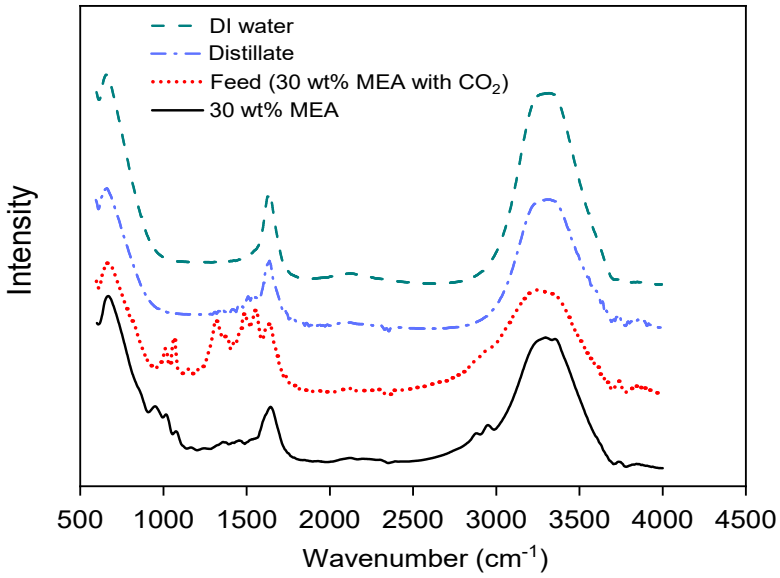

Figure 6-6: Infrared spectra of the aqueous 30 wt % MEA (black line), feed solution: aqueous MEA at 0.59 mol/mol CO_2 loading (red line), distillate from the DCMD process (blue line), DI water as the reference (green line).

The infrared spectra of aqueous MEA prior to/after CO_2 absorption are given in Figure 6-6. Several characteristic vibration modes appeared prior to CO_2 absorption, for example, C-N-H out-of-plane wagging and C-NH_2 twisting at 950 cm^{-1}, C-O stretching at 1016 cm^{-1}, and C-N stretching at 1076 cm^{-1}, and N-H rocking at 1645 cm^{-1} [189]. After molecular CO_2 dissolving into MEA, several peaks shifted due to the protonation of the MEA and formation of carbamate and bicarbonate. Specifically, N-COO^- stretching vibration was observed at 1319 cm^{-1}. COO^- symmetric and asymmetric stretching occurred at 1486 and 1568 cm^{-1}, respectively [189, 190]. As reported by Richner and Puxty [189], the variation in peak intensity was indicated by the difference of CO_2 loading in aqueous MEA. Shifting peaks was therefore not expected to occur after desorption.

6.3.2 Make-up water production in FO performance

Make-up water productions from regenerated MEA and sodium glycinate are compared in the Figure 6-7. DI water was used as the feed solution to provide the baseline test for each solvent. Due to a larger osmotic pressure, the average water flux of MEA (27 L/m^2h) was approximately 50% more than that of sodium glycinate (14 L/m^2h). However, MEA displayed a sharper decline in water flux than that of sodium glycinate. It was due to a larger osmotic gradient reduction caused by the higher reverse salt flux (supplementary

data Figure S6-2). As MEA back-diffusing into DI water, a notable flux decline was observed in Figure 6-7a possibly due to the development of concentrative ICP in the porous support layer [153]. In addition, water permeation from feed solution to draw solution had a considerable dilutive effect on these highly concentrated MEA. It is also noted that the effect of dilutive ECP can be alleviated by a high cross flow velocity or appropriate membrane spacer. The reverse salt flux of sodium glycinate was negligible. Thus, sodium glycinate as the adsorbent and draw solute resulted in a stable water flux throughout the experiment (Figure 6-7b).

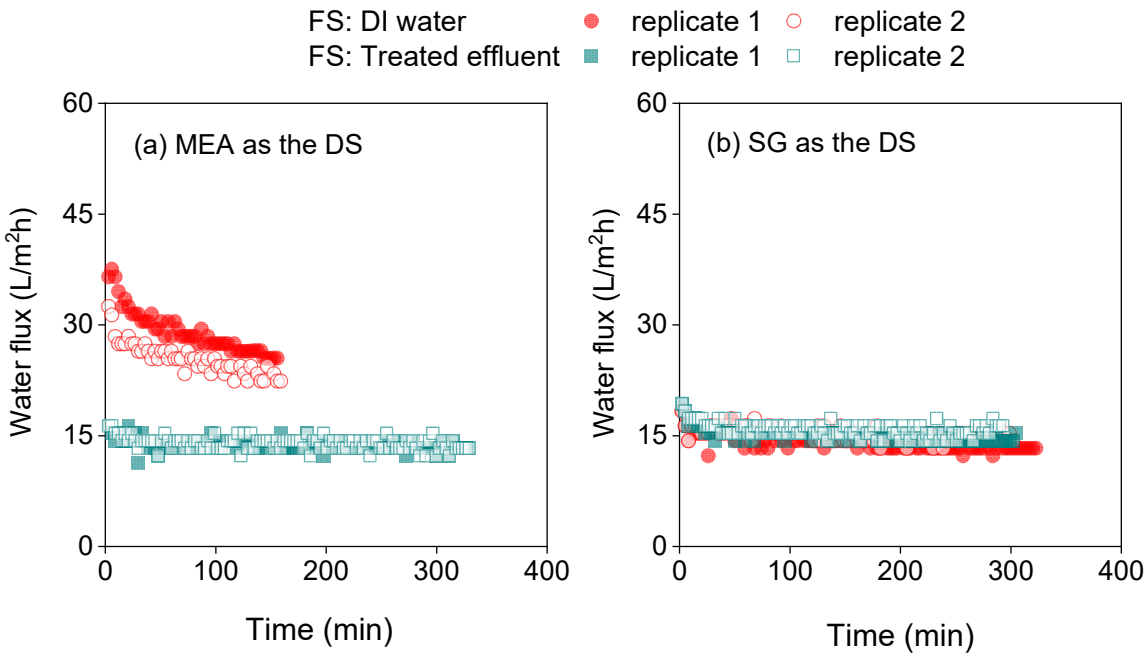

Figure 6-7: Water flux profile for regenerated solvents versus DI water and treated effluent. Feed solution and draw solution were circulated in the counter-current direction. Temperature of feed solution and draw solution were maintained at 25 and 45 °C. Replicate experiments were conducted in AL-DS membrane orientation until 30% water recovery.

Interestingly, despite of the variations in baseline test, both solvents showed similar water fluxes when treated effluent was used as the feed solution. Firstly, it seems understandable that water flux decreased due to the decreasing osmotic gradient across the membrane. Thus, MEA demonstrated a lower flux than that in the baseline test (Figure 6-7a). Nevertheless, sodium glycinate showed a negligible difference in water flux in Figure 6-7b. Of a particular note, sodium glycinate showed a lower reverse salt flux than that in

the baseline test (supplementary data Figure S6-2). A possible reason for this observation was due to the smooth surface of the CTA membrane, and thus, the CTA membrane is more resistant to fouling.

6.3.3 Repetitive CO_2 absorption from regenerated solvents

Repetitive CO_2 absorption and desorption by both MEA and sodium glycinate by the DCMD-FO process is demonstrated in Table 6-2. MEA exhibited an average 85% CO_2 re-absorption capacity and sodium glycinate showed a slightly higher CO_2 re-absorption capacity (89%). Due to the high rejection of FO process, treated effluent could provide adequate "clean" water to cool down the heated solvent for cyclic absorption. Nevertheless, both solvents were not completely regenerated because of solvent degradation in DCMD process and solvent loss in FO process.

Table 6-2: CO_2 loading α from selected solvents in the different stage of experiment. Treated effluent and DI water were used as the cooling sources, unit: mol CO_2/mol amine.

Selected Solution	First CO_2 absorption	First CO_2 desorption	Second CO_2 absorption after FO via different cooling source	
			DI water	Treated effluent
MEA	0.54	0.36	0.45	0.47
SG	0.59	0.39	0.53	0.52

6.4 Future work for practical applications

Overall, the proposed DCMD-FO process has shown some initial and promising result for the repetitive amine-based CO_2 capture from flue gas. Results reported in this chapter also highlight several technical challenges for further research and development. Future research work is recommended to include the screening of other commercially available amine solvents for CO_2 desorption by the DCMD system. Their respective CO_2 desorption and degradation are important parameters to assess their practical applications in the DCMD system. Further FO membrane development is also recommended to limit the reverse salt flux for low or zero solvent loss and stable water flux during the cooling process. A techno-economic analysis of the integrated system that include the overall energy consumption requirement is also necessary to evaluate the potential of our proposed DCMD-FO process for practical applications.

6.5 Conclusion

This chapter demonstrated that the potential of an integrated DCMD-FO system for the repetitive CO_2 capture. Simultaneous low temperature CO_2 desorption and trim cooler replacement conducted by DCMD-FO provide an alternative utilization of waste heat and non-potable water in power plants. The DCMD achieved respective 33.6 and 33.2% of desorption efficiency for MEA and sodium glycinate at 80 °C. MEA and sodium glycinate resulted in the different hydrophobicity changes of each membrane, which therefore led to the partial wetting and corresponding flux decline. Despite of the membrane wetting, TOC and FITR analysis demonstrated that DCMD outperformed a high rejection of solvent. On the other hand, although the regenerated MEA and sodium glycinate exhibited a stable water extraction from treated effluent, they showed a contrast water extraction from DI water due to the osmotic gradient and reverse salt flux. Results of repetitive CO_2 absorption achieved 85% and 89% of CO_2 re-absorption capacity for MEA and sodium glycinate, respectively. In summary, this research could inspire more investigations on efficient CO_2 capture by integrated membrane system.

Chapter 7 Conclusions and recommendations for future work

7.1 Conclusions

Results reported here demonstrated that FO technology could simultaneously produce high quality effluent and harvest energy from wastewater to facilitate the wastewater reclamation for either water purification or post-combustion CO_2 capture. Furthermore, investigation responsible for draw solution chemistry on FO performance provided fundamental perspectives on process optimization including water permeation and TrOCs rejection. On the other hands, this thesis contributed to the existing application of FO by integrating FO-based platform in post-combustion CO_2 capture via wastewater and waste heat. These findings shed a light on the future development and deployment of FO technology.

In Chapter 3, FO membranes and fouling solutions were systematically characterized to elucidate the effects of organic fouling on the rejection of two TrOCs namely sulfamethoxazole and carbamazepine. Municipal wastewater resulted in a more severe flux decline (70%) compared to humic acid and sodium alginate fouling solutions (50%). This result was consistent with the molecular weight distribution of these foulant solutions. Liquid chromatography with organic carbon detection analysis showed that municipal wastewater consists of mostly low molecular weight acids and neutrals, which resulted in a more compact cake layer on the membrane surface. By contrast, humic acid and sodium alginate were consisted of large molecular weight humic substances and biopolymers, respectively.

The results also showed that membrane fouling could significantly alter the membrane surface charge and hydrophobicity as well as the reverse salt flux. In particular, the reverse salt flux of a fouled membrane was significantly higher than that under clean conditions. Although the rejection of sulfamethoxazole and carbamazepine by FO membrane was high (over 96%), a discernible impact of fouling on their rejection can still be observed. The results showed that steric hindrance was the main rejection mechanism of both sulfamethoxazole and carbamazepine. However, they responded to membrane fouling differently. Membrane fouling resulted in an increase in

sulfamethoxazole rejection. By contrast, carbamazepine rejection decreased due to the cake-enhanced concentration polarisation.

Impact of draw solution chemistry (in terms of pH and draw solute species) and membrane fouling on water flux and the rejection of TrOCs by FO was elucidated in Chapter 4. The results showed that draw solution chemistry could induce a notable impact on both water flux and TrOCs rejection. In addition, the impact was further influenced by membrane fouling. The reverse flux of proton (or hydroxyl) could alter the feed solution pH, which governed the separation of ionizable TrOCs. In addition, charged compounds generally exhibited higher rejections than neutral ones by the clean membrane. Electrostatic interaction, rather than steric hindrance, was therefore the dominant rejection mechanism for most compounds. There was also a weak correlation between rejection and molecular sizes of the 43 TrOCs. Compared with Na^+, Li^+ with a larger hydrated radius showed a significant larger reverse salt flux selectivity at the same pH (pH 4.8: NaCl 0.31 L/g, LiCl 2.28 L/g; pH 6.7: NaCl 0.33 L/g, LiCl 3.48 L/g), resulting in a lower ionic strength and therefore a stronger electrostatic interaction. A fouling cake layer consisted of low molecular weight neutral organics could also affect TrOC rejection due to pore blockage and cake-enhanced concentration polarisation.

Chapter 5 evaluated the feasibility of FO as an alternative to a trim cooler for simultaneous post-combustion CO_2 capture and make-up water provision. Three amine-based CO_2 adsorbents (glycine, sodium glycinate, and MEA) were used as the draw solutions. Treated effluent and seawater were used as the sources of make-up water (i.e. feed solution). The non-linear relationship between conductivity and concentration of these three adsorbents indicated an osmotic pressure trend in the FO process. Glycine showed a higher water flux, a lower reverse salt flux and specific reverse salt flux than sodium glycinate and MEA in both membrane orientations, thus was selected for further investigations. A higher water flux but with the considerable flux decline were observed when active layer faced draw solution (AL-FS: from 18.6 to 15.5 L/m^2h; AL-DS: from 35.4 to 19.2 L/m^2h).

In addition, temperature increase in draw solution could alter thermodynamic properties of glycine, thus, resulting in an increase of reverse salt flux. It enhanced water flux due to the diminishing concentrative internal concentration polarisation. On the other hand, changes in water flux were insignificant when active layer faced feed solution even as

temperature increased. It appears that temperature increase was likely to aggravate the severity of dilutive internal concentration polarization and offset the growth of osmotic pressure. Seawater could also be a potential source for simultaneous cooling and providing the make-up water, although the water flux was lower compared to treated effluent.

Chapter 6 proposed an integrated DCMD-FO system via the simultaneous low temperature CO_2 desorption and make-up water production for repetitive CO_2 capture. Since two hydrophobic membranes presented negligible variations in terms of desorption efficiency, DCMD achieved averagely respective 33.6 and 33.2% for MEA and sodium glycinate at 80 °C. Unlike insignificant change caused by sodium glycinate, MEA resulted in either increase or decrease of hydrophobicity for each hydrophobic membrane, thus a partial wetting as well. Wetting was determined to reduce water production in DCMD namely water reduction in aqueous MEA, therefore slowing CO_2 desorption rate.

Apart from unchanged hydrophobicity of membrane, growth of sodium glycinate viscosity and decrease of water activity coherently contributed the constant flux decline for sodium glycinate. Both quantitative and qualitative analyses demonstrated the high solvent rejection, which resulted in the negligible solvent loss. On the other hand, heated regenerated MEA and sodium glycinate resulted in different osmotic pressures and reverse salt fluxes, thus for the corresponding make-up water production as deionised water and treated effluent used as the cooling sources. The results of repetitive CO_2 absorption showed that average 85% and 89% of CO_2 re-absorption capacity for MEA and sodium glycinate, respectively. Therefore, the integrated system not only provided some promising perspectives for energy saving and sustainable non-potable water usage, but also highlighted the need for more research work on cost-effective CO_2 capture based on membrane system.

7.2 Recommendations for future work

Although results from this thesis work have shown the potential of FO as an effective tool to achieve wastewater reclamation for satisfying water purification and post-combustion CO_2 capture, several aspects including draw solution recovery and techno-economic analysis are not included in this thesis. The following research work is recommended to

gain a more comprehensive understanding and a further advancement for full-scale implementation of FO-based system.

1) Draw solution replenishment deserves the attention due to the mass loss in reverse salt flux. Development of draw solution with high reverse solute selectivity and membrane surface modification can help to optimize the trade-off between generated osmotic pressure and reverse diffusion of draw solutes.
2) Concentrated TrOCs in feed solution requires further post-treatment such as advanced oxidation to realize TrOCs removal. A hybrid FO-based system is recommended to achieve energy-efficient TrOCs treatment.
3) Similar to other membrane processes, membrane fouling is an important criterion to assess practical FO operation in the context of wastewater reclamation. Further research may explore cleaning approaches to mitigate membrane fouling effectively.
4) The integration of CO_2 capture with FO-based process can be improved by conducting more comprehensive studies. Life cycle assessment of proposed technology can shed a light on the economic viability of FO assisted post-combustion CO_2 capture.
5) Increasing CO_2 desorption rate in DCMD system may be considered via adding rate promoters. Fast desorption is beneficial for the overall process performance via utilizing waste heat as the energy supply.

Appendix - Supplementary Data

Table S4-1. Key physicochemical properties of the selected trace organic contaminants

Name	CAS number	Molecular structure	pKa	Minimum projection area (Å^2)	Log D at pH 7.4	Log D at pH 6.5	Log D at pH 4.6	Charge at pH 7.4	Charge at pH 6.5	Charge at pH 4.6
Saccharin	81-07-2	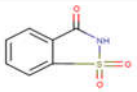	1.94	29.35	-0.49	-0.49	-0.49	-1.00	-1.00	-1.00
Salicyclic acid	69-72-7	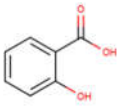	2.79	24.45	-1.52	-1.33	0.17	-1.00	-1.00	-1.00
Cyclamate	100-88-9	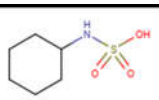	-0.83	30.73	-1.77	-1.77	-1.77	-1.00	-1.00	-1.00
Ketoprofen	22071-15-4	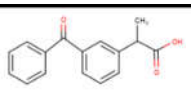	3.88	42.95	0.39	1.05	2.82	-1.00	-1.00	-1.00
Naproxen	22204-53-1	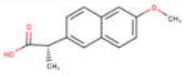	4.19	33.66	-0.05	0.70	2.43	-1.00	-1.00	-1.00
Bisphenol A	80-05-7	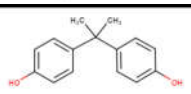	9.78	43.37	4.04	4.04	4.04	-0.01	0.00	0.00
Diclofenac	15307-86-5	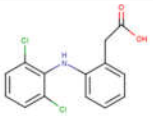	4.00	45.30	1.10	1.79	3.56	-1.00	-1.00	-1.00
Propylparaben	94-13-3	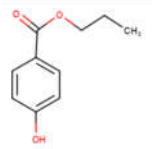	8.50	25.32	2.52	2.55	2.55	-0.07	-0.01	0.00
Diuron	330-54-1	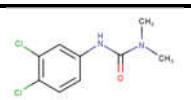	13.18	28.58	2.53	2.53	2.53	0.00	0.00	0.00
Ibuprofen	15687-27-1	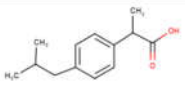	4.85	35.89	1.34	2.19	3.65	-1.00	-0.98	-0.36
Phenylphenol	1322-20-9	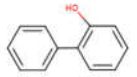	9.69	30.36	3.31	3.32	3.32	-0.01	0.00	0.00
Gemfibrozil	25812-30-0	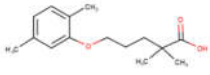	4.42	42.09	1.51	2.32	3.99	-1.00	-0.99	-0.60
Triclocarban	101-20-2	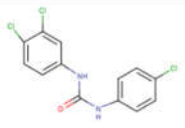	11.42	49.11	4.93	4.93	4.93	0.00	0.00	0.00

Triclosan	3380-34-5	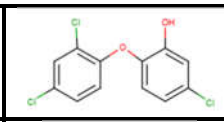	7.68	40.00	4.80	4.95	4.98	-0.34	-0.06	-0.00
Nonylphenol	25154-52-3	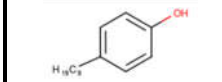	10.30	38.81	5.74	5.74	5.74	-0.01	0.00	0.00
PFOA	335-67-1	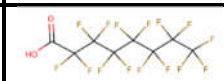	-4.20	36.44	1.58	1.58	1.58	-1.00	-1.00	-1.00
PFOS	45298-90-6		-3.32	40.46	3.05	3.05	3.05	-1.00	-1.00	-1.00
Atenolol	29122-68-7	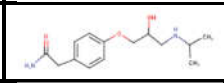	9.67, 14.08	36.85	-1.80	-2.48	-2.81	0.99	1.00	1.00
Paracetamol	103-90-2	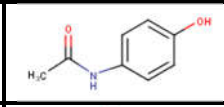	9.46	21.65	0.90	0.91	0.91	-0.01	0.00	0.00
Sulfamethoxazole	723-46-6	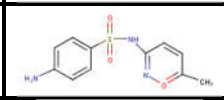	1.97, 6.16	46.79	-0.00	0.38	0.78	-0.95	-0.69	-0.02
Caffeine	58-08-2	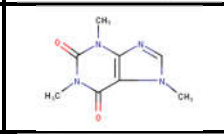	-1.16	30.68	-0.55	-0.55	-0.55	0.00	0.00	0.00
Trimethoprim	738-70-5	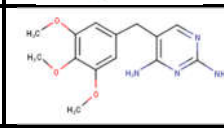	7.16	51.06	1.10	0.60	-0.16	0.85	0.98	1.00
Benzotriazole	95-14-7	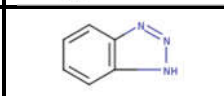	0.22, 9.04	21.46	1.25	1.26	1.26	-0.02	0.00	0.00
Triamterene	396-01-0	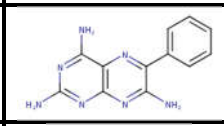	6.2	36.26	1.11	1.11	1.11	0.00	0.00	0.03
Primidone	125-33-7	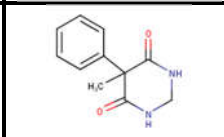	11.50	40.90	1.12	1.12	1.12	0.00	0.00	0.00
Carazolol	57775-29-8	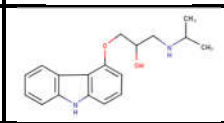	9.67, 14.03	45.59	0.49	-0.19	-0.52	0.98	1.00	1.00
Bisoprolol	66722-44-9	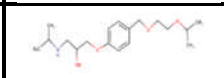	9.67, 14.09	51.96	-0.03	-0.71	-1.04	0.99	1.00	1.00
Meprobamate	57-53-4	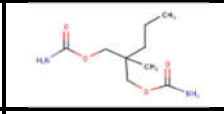	15.17	45.75	0.93	0.93	0.93	0.00	0.00	0.00
TCEP	115-96-8	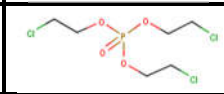	-9.10	49.90	2.11	2.11	2.11	n/a	n/a	n/a
Dilantin	630-93-3	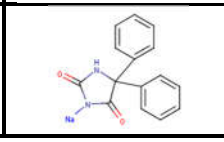	8.49	48.38	2.11	2.14	2.15	-0.08	-0.01	0.00

Simazine	122-34-9	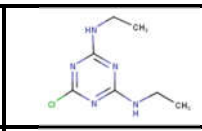	4.23, 14.75	35.92	1.78	1.78	1.63	0.00	0.00	0.22
Carbamazepine	298-46-4	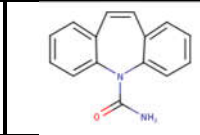	15.96	40.19	2.77	2.77	2.77	0.00	0.00	0.00
Omeprazole	73590-58-6	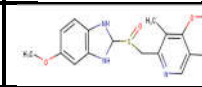	4.77, 9.29	37.09	2.43	2.43	2.06	-0.01	0.02	0.60
Atrazine	1912-24-9	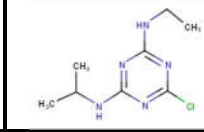	4.20, 14.48	39.04	2.20	2.20	2.05	0.00	0.00	0.20
Verapamil	52-53-9	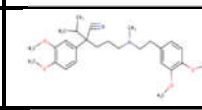	9.68	78.69	2.79	2.03	1.55	0.99	1.00	1.00
Linuron	330-55-2	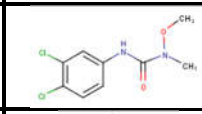	11.94	28.00	2.68	2.68	2.68	0.00	0.00	0.00
Diazepam	439-14-5	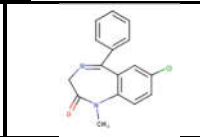	2.92	47.86	3.08	3.08	3.07	0.00	0.00	0.02
Benzophenone	119-61-9	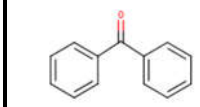	-7.50	22.79	3.43	3.43	3.43	n/a	n/a	n/a
Clozapine	5786-21-0	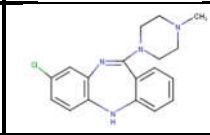	10.08	52.19	1.36	0.63	-1.15	1.54	1.90	2.00
Amitriptyline	50-48-6	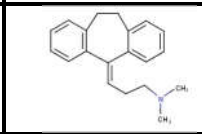	9.76	58.17	2.48	1.75	1.32	1.00	1.00	1.00
Hydroxyzine	68-88-2	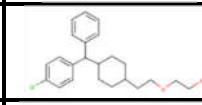	7.45, 15.12	64.72	3.09	2.42	0.65	0.45	0.86	1.00
Oxybenzone	131-57-7	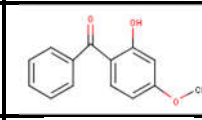	7.07	35.30	3.13	3.52	3.62	-0.68	-0.21	0.00
Diazinon	333-41-5	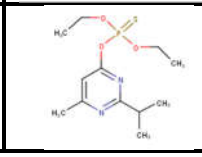	4.19	50.17	4.19	4.19	4.19	0.01	0.05	0.79

Source: SciFinder Scholar (ACS) database and *Chemicalize* online platform.

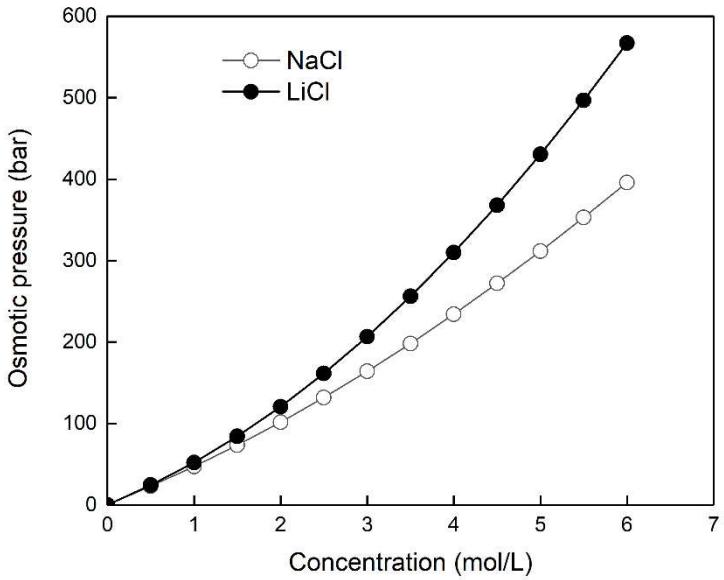

Figure S4-1: Osmotic pressure as a function of draw solutes concentration at 25 ºC. Data were simulated by using OLI Stream Analyzer 2.0.

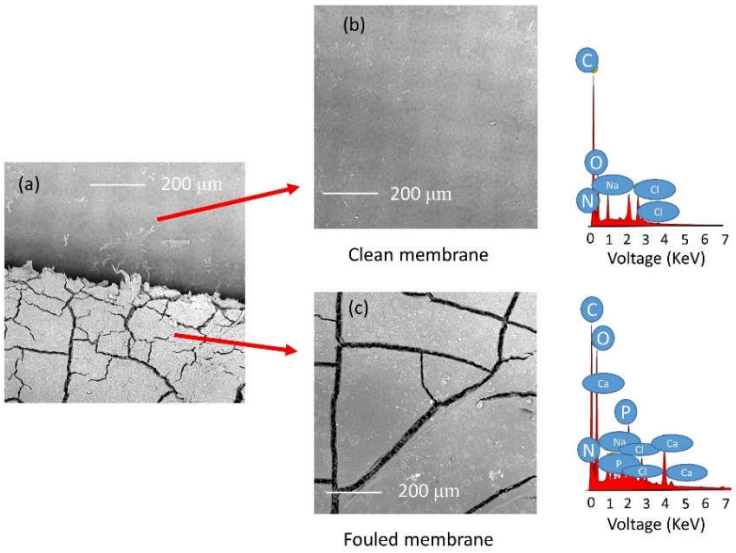

Figure S4-2: SEM – EDX analysis for active layer of clean and fouled membranes (DI water and raw sewage were used as feed solutions; NaCl (0.5 M) at buffered pH 8.0 was used as draw solution).

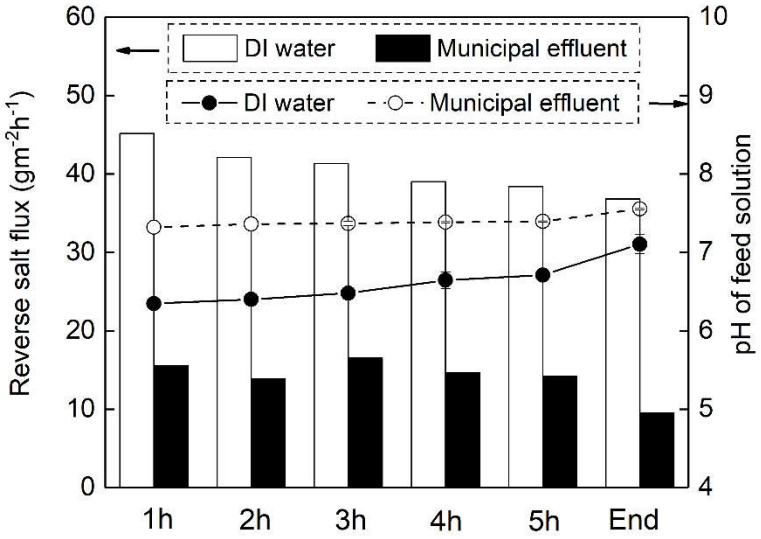

Figure S4-3: Comparison of reverse salt flux affected by the presence of fouling and monitored pH in the feed solution (The data were recorded in the first 5 h and end of experiment). DI water (initial pH 6.4 ± 0.2) or primary treated municipal effluent (initial pH 7.3 ± 0.2) was used as feed solution, respectively; NaCl (0.5 M) with at buffered pH 8.0 was used as draw solution. All experiments were conducted until 50% water recovery.

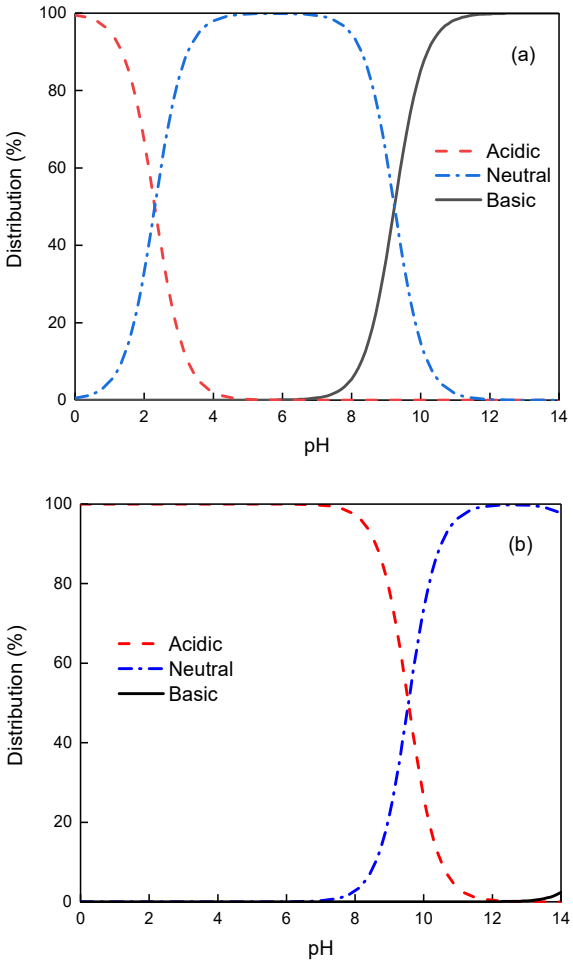

Figure S5-1: Distribution (%) of glycine (a) and MEA (b) between the acid, neutral, and base forms in the pH range of 0 - 14 at 25 °C.

Table S5-1: Osmotic gradients of sodium glycinate (1.5/3 M) in the different membrane orientation

Concentration (mol/L)	Membrane orientation	Π_{FS} (bar)	Π_{DS} (bar)	$\Delta\Pi$ (bar)
1.5	AL-FS	0.08	79.28	79.20
1.5	AL-DS	0.41	79.28	78.86
3	AL-FS	0.44	158.56	158.12
3	AL-DS	0.52	158.56	158.04

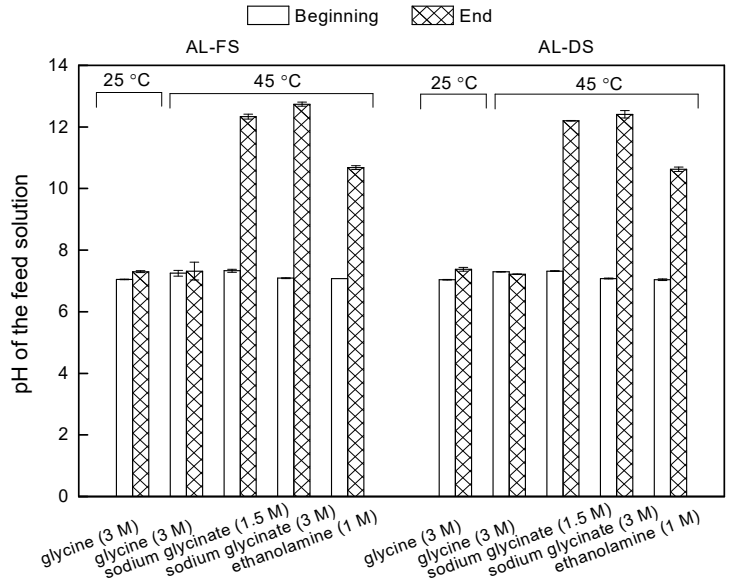

Figure S5-2: pH values of the feed solution at the beginning and end of each experiment in two membrane orientations. Treated effluent was used as the feed solution. The temperature of feed solution was maintained at 25 °C. Two membrane orientations: AL-FS and AL-DS were applied. Error bars represent the difference of two replicate measurements.

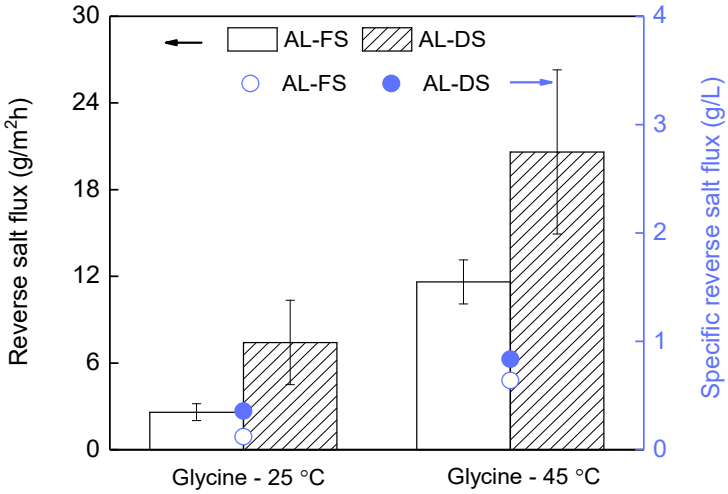

Figure S5-3: Impact of temperature on reverse salt flux and specific reverse salt flux. Treated effluent at 25 °C was used as the feed solution. Glycine (3 M) at 25/45 °C was used as the draw solution. Error bars represent the difference of two replicate measurements.

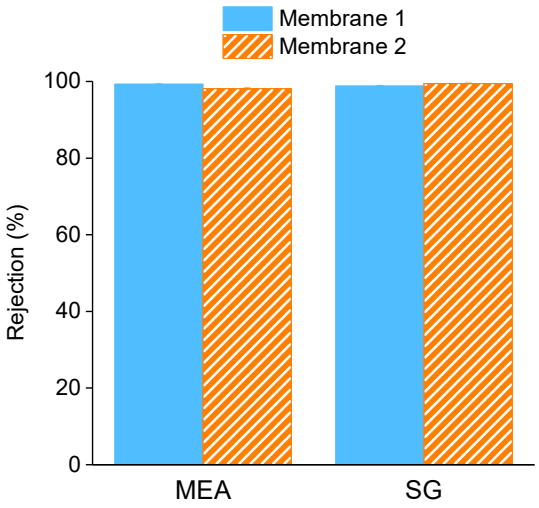

Figure S6-1: Solvent rejection of DCMD for MEA and sodium glycinate (SG) regeneration. Experimental conditions are described as follows: DI water was used as the distillate. MEA (5 M) and SG (3 M) were used as the FS. The temperatures for FS and distillate were 80 °C and 25 °C, respectively. All experiments were conducted in duplicate and until 30% water recovery (maximum CO_2 desorption).

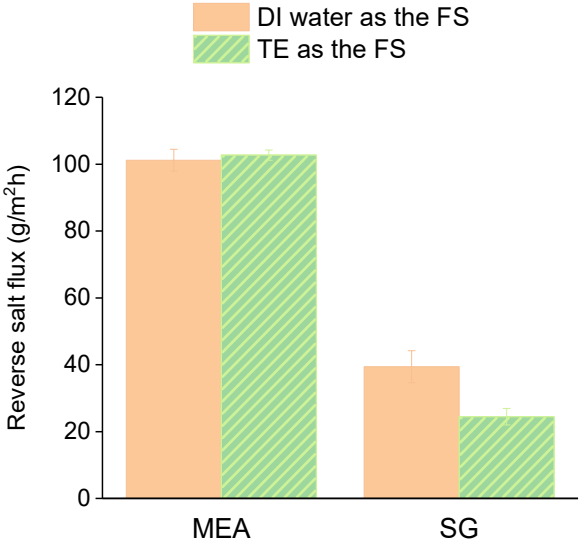

Figure S6-2: Reverse salt fluxes of regenerated MEA and SG in AL-DS membrane orientation. DI water and treated effluent (TE) were used as the FS. Regenerated MEA and SG were used as the draw solutions (DS). The temperatures for FS and DS were 25 °C and 45 °C, respectively. $_2$Error bars represent the difference of two replicate measurements.

Reference

[1] M.A. Shannon, P.W. Bohn, M. Elimelech, J.G. Georgiadis, B.J. Marĩas, A.M. Mayes, Science and technology for water purification in the coming decades, Nature, 452 (2008) 301-310.

[2] M. Young;, C. Esau, Investing in Water for a Green Economy: Services, Infrastructure, Policies and Management, 2009.

[3] Y. Luo, W. Guo, H.H. Ngo, L.D. Nghiem, F.I. Hai, J. Zhang, S. Liang, X.C. Wang, A review on the occurrence of micropollutants in the aquatic environment and their fate and removal during wastewater treatment, Science of The Total Environment, 473-474 (2014) 619-641.

[4] J.C. Carlson, J.C. Anderson, J.E. Low, P. Cardinal, S.D. MacKenzie, S.A. Beattie, J.K. Challis, R.J. Bennett, S.S. Meronek, R.P.A. Wilks, W.M. Buhay, C.S. Wong, M.L. Hanson, Presence and hazards of nutrients and emerging organic micropollutants from sewage lagoon discharges into Dead Horse Creek, Manitoba, Canada, Science of The Total Environment, 445–446 (2013) 64-78.

[5] R.P. Schwarzenbach, B.I. Escher, K. Fenner, T.B. Hofstetter, C.A. Johnson, U. von Gunten, B. Wehrli, The Challenge of Micropollutants in Aquatic Systems, Science, 313 (2006) 1072-1077.

[6] L.D. Nghiem, P.J. Coleman, NF/RO filtration of the hydrophobic ionogenic compound triclosan: Transport mechanisms and the influence of membrane fouling, Separation and Purification Technology, 62 (2008) 709-716.

[7] W. Luo, M. Xie, F.I. Hai, W.E. Price, L.D. Nghiem, Biodegradation of cellulose triacetate and polyamide forward osmosis membranes in an activated sludge bioreactor: Observations and implications, Journal of Membrane Science, 510 (2016) 284-292.

[8] A. Simon, L.D. Nghiem, P. Le-Clech, S.J. Khan, J.E. Drewes, Effects of membrane degradation on the removal of pharmaceutically active compounds (PhACs) by NF/RO filtration processes, Journal of Membrane Science, 340 (2009) 16-25.

[9] S. Yang, F.I. Hai, W.E. Price, J. McDonald, S.J. Khan, L.D. Nghiem, Occurrence of trace organic contaminants in wastewater sludge and their removals by anaerobic digestion, Bioresource Technology, 210 (2016) 153-159.

[10] S. Lee, C. Boo, M. Elimelech, S. Hong, Comparison of fouling behavior in forward osmosis (FO) and reverse osmosis (RO), Journal of Membrane Science, 365 (2010) 34-39.

[11] R.L. McGinnis, M. Elimelech, Energy requirements of ammonia-carbon dioxide forward osmosis desalination, Desalination, 207 (2007) 370-382.

[12] S. Zhao, L. Zou, C.Y. Tang, D. Mulcahy, Recent developments in forward osmosis: Opportunities and challenges, Journal of Membrane Science, 396 (2012) 1-21.

[13] G.P. Peters, R.M. Andrew, J.G. Canadell, P. Friedlingstein, R.B. Jackson, J.I. Korsbakken, C. Le Quéré, A. Peregon, Carbon dioxide emissions continue to grow amidst slowly emerging climate policies, Nature Climate Change, (2019).

[14] D.Y.C. Leung, G. Caramanna, M.M. Maroto-Valer, An overview of current status of carbon dioxide capture and storage technologies, Renewable and Sustainable Energy Reviews, 39 (2014) 426-443.

[15] K. Li, H. Yu, S. Yan, P. Feron, L. Wardhaugh, M. Tade, Technoeconomic Assessment of an Advanced Aqueous Ammonia-Based Postcombustion Capture Process Integrated with a 650-MW Coal-Fired Power Station, Environmental Science & Technology, 50 (2016) 10746-10755.

[16] K. Stéphenne, Start-up of World's First Commercial Post-combustion Coal Fired CCS Project: Contribution of Shell Cansolv to SaskPower Boundary Dam ICCS Project, Energy Procedia, 63 (2014) 6106-6110.

[17] G.T. Rochelle, Amine Scrubbing for CO_2 Capture, Science, 325 (2009) 1652.

[18] P.H.M. Feron, Exploring the potential for improvement of the energy performance of coal fired power plants with post-combustion capture of carbon dioxide, International Journal of Greenhouse Gas Control, 4 (2010) 152-160.

[19] H. Zhai, E.S. Rubin, P.L. Versteeg, Water Use at Pulverized Coal Power Plants with Postcombustion Carbon Capture and Storage, Environmental Science & Technology, 45 (2011) 2479-2485.

[20] A.B. Rao, E.S. Rubin, A Technical, Economic, and Environmental Assessment of Amine-Based CO_2 Capture Technology for Power Plant Greenhouse Gas Control, Environmental Science & Technology, 36 (2002) 4467-4475.

[21] E.S. Rubin, J.E. Davison, H.J. Herzog, The cost of CO_2 capture and storage, International Journal of Greenhouse Gas Control, 40 (2015) 378-400.

[22] S. Lee, C. Boo, M. Elimelech, S. Hong, Comparison of fouling behavior in forward osmosis (FO) and reverse osmosis (RO), Journal of Membrane Science, 365 (2010) 34-39.

[23] D.L. Shaffer, J.R. Werber, H. Jaramillo, S. Lin, M. Elimelech, Forward osmosis: Where are we now?, Desalination, 356 (2015) 271-284.

[24] Y. Yang, H. Song, Z. He, Mitigation of solute buildup by using a biodegradable and reusable polyelectrolyte as a draw solute in an osmotic membrane bioreactor, Environmental Science: Water Research & Technology, 5 (2019) 19-27.

[25] G. Gwak, D.I. Kim, S. Hong, New industrial application of forward osmosis (FO): Precious metal recovery from printed circuit board (PCB) plant wastewater, Journal of Membrane Science, 552 (2018) 234-242.

[26] S. Wu, S. Zou, G. Liang, G. Qian, Z. He, Enhancing recovery of magnesium as struvite from landfill leachate by pretreatment of calcium with simultaneous reduction of liquid volume via forward osmosis, Science of The Total Environment, 610-611 (2018) 137-146.

[27] G. Chen, Z. Wang, L.D. Nghiem, X.-M. Li, M. Xie, B. Zhao, M. Zhang, J. Song, T. He, Treatment of shale gas drilling flowback fluids (SGDFs) by forward osmosis: Membrane fouling and mitigation, Desalination, 366 (2015) 113-120.

[28] B.D. Coday, P. Xu, E.G. Beaudry, J. Herron, K. Lampi, N.T. Hancock, T.Y. Cath, The sweet spot of forward osmosis: Treatment of produced water, drilling wastewater, and other complex and difficult liquid streams, Desalination, 333 (2014) 23-35.

[29] N.C. Nguyen, H.T. Nguyen, S.-T. Ho, S.-S. Chen, H.H. Ngo, W. Guo, S.S. Ray, H.-T. Hsu, Exploring high charge of phosphate as new draw solute in a forward osmosis–membrane distillation hybrid system for concentrating high-nutrient sludge, Science of The Total Environment, 557-558 (2016) 44-50.

[30] S. Liyanaarachchi, V. Jegatheesan, I. Obagbemi, S. Muthukumaran, L. Shu, Effect of feed temperature and membrane orientation on pre-treatment sludge volume reduction through forward osmosis, Desalination and Water Treatment, 54 (2015) 838-844.

[31] P.E. Stackelberg, E.T. Furlong, M.T. Meyer, S.D. Zaugg, A.K. Henderson, D.B. Reissman, Persistence of pharmaceutical compounds and other organic wastewater contaminants in a conventional drinking-water-treatment plant, Science of The Total Environment, 329 (2004) 99-113.

[32] J. Garcia-Ivars, L. Martella, M. Massella, C. Carbonell-Alcaina, M.-I. Alcaina-Miranda, M.-I. Iborra-Clar, Nanofiltration as tertiary treatment method for removing trace pharmaceutically active compounds in wastewater from wastewater treatment plants, Water Research, 125 (2017) 360-373.

[33] T. Fujioka, S.J. Khan, J.A. McDonald, L.D. Nghiem, Rejection of trace organic chemicals by a hollow fibre cellulose triacetate reverse osmosis membrane, Desalination, 368 (2015) 69-75.

[34] K.C. Wijekoon, F.I. Hai, J. Kang, W.E. Price, T.Y. Cath, L.D. Nghiem, Rejection and fate of trace organic compounds (TrOCs) during membrane distillation, Journal of Membrane Science, 453 (2014) 636-642.

[35] X. Wang, J. Zhang, V.W.C. Chang, Q. She, C.Y. Tang, Removal of cytostatic drugs from wastewater by an anaerobic osmotic membrane bioreactor, Chemical Engineering Journal, 339 (2018) 153-161.

[36] M. Xie, W. Luo, H. Guo, L.D. Nghiem, C.Y. Tang, S.R. Gray, Trace organic contaminant rejection by aquaporin forward osmosis membrane: Transport mechanisms and membrane stability, Water Research, 132 (2018) 90-98.

[37] M. Sauchelli, G. Pellegrino, A. D'Haese, I. Rodríguez-Roda, W. Gernjak, Transport of trace organic compounds through novel forward osmosis membranes: Role of membrane properties and the draw solution, Water Research, 141 (2018) 65-73.

[38] J. Xu, T.N. Tran, H. Lin, N. Dai, Removal of disinfection byproducts in forward osmosis for wastewater recycling, Journal of Membrane Science, 564 (2018) 352-360.

[39] R.W. Holloway, A. Achilli, T.Y. Cath, The osmotic membrane bioreactor: a critical review, Environmental Science: Water Research & Technology, 1 (2015) 581-605.

[40] L.D. Nghiem, A.I. Schäfer, M. Elimelech, Role of electrostatic interactions in the retention of pharmaceutically active contaminants by a loose nanofiltration membrane, Journal of Membrane Science, 286 (2006) 52-59.

[41] M. Xie, L.D. Nghiem, W.E. Price, M. Elimelech, Impact of humic acid fouling on membrane performance and transport of pharmaceutically active compounds in forward osmosis, Water research, 47 (2013) 4567-4575.

[42] M. Xie, L.D. Nghiem, W.E. Price, M. Elimelech, Impact of organic and colloidal fouling on trace organic contaminant rejection by forward osmosis: Role of initial permeate flux, Desalination, 336 (2014) 146-152.

[43] T.Y. Cath, A.E. Childress, M. Elimelech, Forward osmosis: Principles, applications, and recent developments, Journal of Membrane Science, 281 (2006) 70-87.

[44] K.L. Lee, R.W. Baker, H.K. Lonsdale, Membrane for power generation by pressure-retarded osmosis, Journal of Membrane Science, 8 (1981) 141-171.

[45] N.T. Hancock, T.Y. Cath, Solute Coupled Diffusion in Osmotically Driven Membrane Processes, Environmental Science & Technology, 43 (2009) 6769-6775.

[46] C.Y. Tang, Q. She, W.C.L. Lay, R. Wang, R. Field, A.G. Fane, Modeling double-skinned FO membranes, Desalination, 283 (2011) 178-186.

[47] Q. She, R. Wang, A.G. Fane, C.Y. Tang, Membrane fouling in osmotically driven membrane processes: A review, Journal of Membrane Science, 499 (2016) 201-233.

[48] J.R. McCutcheon, R.L. McGinnis, M. Elimelech, Desalination by ammonia–carbon dioxide forward osmosis: Influence of draw and feed solution concentrations on process performance, Journal of Membrane Science, 278 (2006) 114-123.

[49] Y. Liu, B. Mi, Combined fouling of forward osmosis membranes: Synergistic foulant interaction and direct observation of fouling layer formation, Journal of Membrane Science, 407–408 (2012) 136-144.

[50] B. Mi, M. Elimelech, Chemical and physical aspects of organic fouling of forward osmosis membranes, Journal of Membrane Science, 320 (2008) 292-302.

[51] B. Mi, M. Elimelech, Organic fouling of forward osmosis membranes: Fouling reversibility and cleaning without chemical reagents, Journal of Membrane Science, 348 (2010) 337-345.

[52] C. Boo, S. Lee, M. Elimelech, Z. Meng, S. Hong, Colloidal fouling in forward osmosis: Role of reverse salt diffusion, Journal of Membrane Science, 390–391 (2012) 277-284.

[53] S. Mikhaylin, L. Bazinet, Fouling on ion-exchange membranes: Classification, characterization and strategies of prevention and control, Advances in Colloid and Interface Science, 229 (2016) 34-56.

[54] C.Y. Tang, Q. She, W.C.L. Lay, R. Wang, A.G. Fane, Coupled effects of internal concentration polarization and fouling on flux behavior of forward osmosis membranes during humic acid filtration, Journal of Membrane Science, 354 (2010) 123-133.

[55] A. Antony, J.H. Low, S. Gray, A.E. Childress, P. Le-Clech, G. Leslie, Scale formation and control in high pressure membrane water treatment systems: A review, Journal of Membrane Science, 383 (2011) 1-16.

[56] X. Liu, S. Qi, Y. Li, L. Yang, B. Cao, C.Y. Tang, Synthesis and characterization of novel antibacterial silver nanocomposite nanofiltration and forward osmosis membranes based on layer-by-layer assembly, Water Research, 47 (2013) 3081-3092.

[57] H. Yoon, Y. Baek, J. Yu, J. Yoon, Biofouling occurrence process and its control in the forward osmosis, Desalination, 325 (2013) 30-36.

[58] V. Parida, H.Y. Ng, Forward osmosis organic fouling: Effects of organic loading, calcium and membrane orientation, Desalination, 312 (2013) 88-98.

[59] J. Cho, G. Amy, J. Pellegrino, Membrane filtration of natural organic matter: factors and mechanisms affecting rejection and flux decline with charged ultrafiltration (UF) membrane, Journal of Membrane Science, 164 (2000) 89-110.

[60] S. Zhao, L. Zou, D. Mulcahy, Effects of membrane orientation on process performance in forward osmosis applications, Journal of Membrane Science, 382 (2011) 308-315.

[61] X. Jin, Q. She, X. Ang, C.Y. Tang, Removal of boron and arsenic by forward osmosis membrane: Influence of membrane orientation and organic fouling, Journal of Membrane Science, 389 (2012) 182-187.

[62] M.M. Motsa, B.B. Mamba, A. D'Haese, E.M.V. Hoek, A.R.D. Verliefde, Organic fouling in forward osmosis membranes: The role of feed solution chemistry and membrane structural properties, Journal of Membrane Science, 460 (2014) 99-109.

[63] Y. Kim, M. Elimelech, H.K. Shon, S. Hong, Combined organic and colloidal fouling in forward osmosis: Fouling reversibility and the role of applied pressure, Journal of Membrane Science, 460 (2014) 206-212.

[64] C.Y. Tang, T.H. Chong, A.G. Fane, Colloidal interactions and fouling of NF and RO membranes: A review, Advances in Colloid and Interface Science, 164 (2011) 126-143.

[65] R.S. Faibish, M. Elimelech, Y. Cohen, Effect of Interparticle Electrostatic Double Layer Interactions on Permeate Flux Decline in Crossflow Membrane Filtration of Colloidal Suspensions: An Experimental Investigation, Journal of Colloid and Interface Science, 204 (1998) 77-86.

[66] T. Koo, Y.J. Lee, R. Sheikholeslami, Silica fouling and cleaning of reverse osmosis membranes, Desalination, 139 (2001) 43-56.

[67] B. Mi, M. Elimelech, Silica scaling and scaling reversibility in forward osmosis, Desalination, 312 (2013) 75-81.

[68] M.M. Motsa, B.B. Mamba, A.R.D. Verliefde, Combined colloidal and organic fouling of FO membranes: The influence of foulant–foulant interactions and ionic strength, Journal of Membrane Science, 493 (2015) 539-548.

[69] B. Mi, M. Elimelech, Gypsum Scaling and Cleaning in Forward Osmosis: Measurements and Mechanisms, Environmental Science & Technology, 44 (2010) 2022-2028.

[70] E. Arkhangelsky, F. Wicaksana, S. Chou, A.A. Al-Rabiah, S.M. Al-Zahrani, R. Wang, Effects of scaling and cleaning on the performance of forward osmosis hollow fiber membranes, Journal of Membrane Science, 415–416 (2012) 101-108.

[71] A.E. Childress, M. Elimelech, Effect of solution chemistry on the surface charge of polymeric reverse osmosis and nanofiltration membranes, Journal of Membrane Science, 119 (1996) 253-268.

[72] R.T. Sanderson, Electronegativity and bond energy, Journal of the American Chemical Society, 105 (1983) 2259-2261.

[73] Y.-N. Wang, E. Järvelä, J. Wei, M. Zhang, H. Kyllönen, R. Wang, C.Y. Tang, Gypsum scaling and membrane integrity of osmotically driven membranes: The effect of membrane materials and operating conditions, Desalination, 377 (2016) 1-10.

[74] M. Zhang, J. Shan, C.Y. Tang, Gypsum scaling during forward osmosis process—a direct microscopic observation study, Desalination and Water Treatment, 57 (2016) 3317-3327.

[75] S.E. Kwan, E. Bar-Zeev, M. Elimelech, Biofouling in forward osmosis and reverse osmosis: Measurements and mechanisms, Journal of Membrane Science, 493 (2015) 703-708.

[76] C.-M. Kim, S.-J. Kim, L.H. Kim, M.S. Shin, H.-W. Yu, I.S. Kim, Effects of phosphate limitation in feed water on biofouling in forward osmosis (FO) process, Desalination, 349 (2014) 51-59.

[77] H.C. Flemming, G. Schaule, T. Griebe, J. Schmitt, A. Tamachkiarowa, Biofouling—the Achilles heel of membrane processes, Desalination, 113 (1997) 215-225.

[78] R. Valladares Linares, S.S. Bucs, Z. Li, M. AbuGhdeeb, G. Amy, J.S. Vrouwenvelder, Impact of spacer thickness on biofouling in forward osmosis, Water Research, 57 (2014) 223-233.

[79] M. Xie, E. Bar-Zeev, S.M. Hashmi, L.D. Nghiem, M. Elimelech, Role of Reverse Divalent Cation Diffusion in Forward Osmosis Biofouling, Environmental Science & Technology, 49 (2015) 13222-13229.

[80] S. Lee, M. Elimelech, Relating Organic Fouling of Reverse Osmosis Membranes to Intermolecular Adhesion Forces, Environmental Science & Technology, 40 (2006) 980-987.

[81] K.A. Kidd, P.J. Blanchfield, K.H. Mills, V.P. Palace, R.E. Evans, J.M. Lazorchak, R.W. Flick, Collapse of a fish population after exposure to a synthetic estrogen, Proceedings of the National Academy of Sciences, 104 (2007) 8897-8901.

[82] C. Baresel, M. Harding, J. Fång, Ultrafiltration/Granulated Active Carbon-Biofilter: Efficient Removal of a Broad Range of Micropollutants, Applied Sciences, 9 (2019) 710.

[83] V. Albergamo, B. Blankert, E.R. Cornelissen, B. Hofs, W.-J. Knibbe, W. van der Meer, P. de Voogt, Removal of polar organic micropollutants by pilot-scale reverse osmosis drinking water treatment, Water Research, 148 (2019) 535-545.

[84] A.F.S. Foureaux, E.O. Reis, Y. Lebron, V. Moreira, L.V. Santos, M.S. Amaral, L.C. Lange, Rejection of pharmaceutical compounds from surface water by nanofiltration and reverse osmosis, Separation and Purification Technology, 212 (2019) 171-179.

[85] H. Lee, S.-J. Im, J.H. Park, A. Jang, Removal and transport behavior of trace organic compounds and degradation byproducts in forward osmosis process: Effects of operation conditions and membrane properties, Chemical Engineering Journal, 375 (2019) 122030.

[86] L. Zheng, W.E. Price, J. McDonald, S.J. Khan, T. Fujioka, L.D. Nghiem, New insights into the relationship between draw solution chemistry and trace organic rejection by forward osmosis, Journal of Membrane Science, 587 (2019) 117184.

[87] H.T. Madsen, N. Bajraktari, C. Hélix-Nielsen, B. Van der Bruggen, E.G. Søgaard, Use of biomimetic forward osmosis membrane for trace organics removal, Journal of Membrane Science, 476 (2015) 469-474.

[88] M. Xie, L.D. Nghiem, W.E. Price, M. Elimelech, Comparison of the removal of hydrophobic trace organic contaminants by forward osmosis and reverse osmosis, Water Research, 46 (2012) 2683-2692.

[89] L.D. Nghiem, D. Vogel, S. Khan, Characterising humic acid fouling of nanofiltration membranes using bisphenol A as a molecular indicator, Water Research, 42 (2008) 4049-4058.

[90] R. Valladares Linares, V. Yangali-Quintanilla, Z. Li, G. Amy, Rejection of micropollutants by clean and fouled forward osmosis membrane, Water Research, 45 (2011) 6737-6744.

[91] A.A. Alturki, J.A. McDonald, S.J. Khan, W.E. Price, L.D. Nghiem, M. Elimelech, Removal of trace organic contaminants by the forward osmosis process, Separation and Purification Technology, 103 (2013) 258-266.

[92] A. D'Haese, P. Le-Clech, S. Van Nevel, K. Verbeken, E.R. Cornelissen, S.J. Khan, A.R.D. Verliefde, Trace organic solutes in closed-loop forward osmosis applications: Influence of membrane fouling and modeling of solute build-up, Water Research, 47 (2013) 5232-5244.

[93] D. Vogel, A. Simon, A.A. Alturki, B. Bilitewski, W.E. Price, L.D. Nghiem, Effects of fouling and scaling on the retention of trace organic contaminants by a nanofiltration membrane: The role of cake-enhanced concentration polarisation, Separation and Purification Technology, 73 (2010) 256-263.

[94] P. Xu, J.E. Drewes, T.-U. Kim, C. Bellona, G. Amy, Effect of membrane fouling on transport of organic contaminants in NF/RO membrane applications, Journal of Membrane Science, 279 (2006) 165-175.

[95] B.D. Coday, B.G.M. Yaffe, P. Xu, T.Y. Cath, Rejection of Trace Organic Compounds by Forward Osmosis Membranes: A Literature Review, Environmental Science & Technology, 48 (2014) 3612-3624.

[96] C. Kim, S. Lee, H.K. Shon, M. Elimelech, S. Hong, Boron transport in forward osmosis: Measurements, mechanisms, and comparison with reverse osmosis, Journal of Membrane Science, 419-420 (2012) 42-48.

[97] Y. Kim, S. Li, L. Chekli, Y.C. Woo, C.-H. Wei, S. Phuntsho, N. Ghaffour, T. Leiknes, H.K. Shon, Assessing the removal of organic micro-pollutants from anaerobic membrane bioreactor effluent by fertilizer-drawn forward osmosis, Journal of Membrane Science, 533 (2017) 84-95.

[98] Y.-N. Wang, W. Li, R. Wang, C.Y. Tang, Enhancing boron rejection in FO using alkaline draw solutions, Water Research, 118 (2017) 20-25.

[99] A.S. Bhown, B.C. Freeman, Analysis and Status of Post-Combustion Carbon Dioxide Capture Technologies, Environmental Science & Technology, 45 (2011) 8624-8632.

[100] B. Lv, B. Guo, Z. Zhou, G. Jing, Mechanisms of CO_2 Capture into Monoethanolamine Solution with Different CO_2 Loading during the Absorption/Desorption Processes, Environmental Science & Technology, 49 (2015) 10728-10735.

[101] Q. Lai, L. Kong, W. Gong, A.G. Russell, M. Fan, Low-energy-consumption and environmentally friendly CO_2 capture via blending alcohols into amine solution, Applied Energy, 254 (2019) 113696.

[102] D. Guo, H. Thee, C.Y. Tan, J. Chen, W. Fei, S. Kentish, G.W. Stevens, G. da Silva, Amino Acids as Carbon Capture Solvents: Chemical Kinetics and Mechanism of the Glycine + CO_2 Reaction, Energy & Fuels, 27 (2013) 3898-3904.

[103] M.G. Plaza, F. Rubiera, Development of carbon-based vacuum, temperature and concentration swing adsorption post-combustion CO_2 capture processes, Chemical Engineering Journal, 375 (2019) 122002.

[104] M. Shan, B. Seoane, E. Andres-Garcia, F. Kapteijn, J. Gascon, Mixed-matrix membranes containing an azine-linked covalent organic framework: Influence of the polymeric matrix on post-combustion CO_2-capture, Journal of Membrane Science, 549 (2018) 377-384.

[105] C. Song, Q. Liu, N. Ji, S. Deng, J. Zhao, Y. Li, Y. Kitamura, Reducing the energy consumption of membrane-cryogenic hybrid CO_2 capture by process optimization, Energy, 124 (2017) 29-39.

[106] M. Campbell, Technology Innovation & Advancements for Shell Cansolv CO_2 capture solvents, Energy Procedia, 63 (2014) 801-807.

[107] P.N.W.A. MIT, Parish Fact Sheet: Carbon Dioxide Capture and Storage Project, Carbon Capture and Sequestration Technologies program at MIT, in, 2016.

[108] S. Evjen, A. Fiksdahl, H.K. Knuutila, High-Capacity Amine-Imidazole Solvent Blends for CO_2 Capture, Industrial & Engineering Chemistry Research, 58 (2019) 10533-10539.

[109] F. Tzirakis, I. Tsivintzelis, A.I. Papadopoulos, P. Seferlis, Experimental measurement and assessment of equilibrium behaviour for phase change solvents used in CO_2 capture, Chemical Engineering Science, 199 (2019) 20-27.

[110] Y. Li, L.a. Wang, Z. Tan, Z. Zhang, X. Hu, Experimental studies on carbon dioxide absorption using potassium carbonate solutions with amino acid salts, Separation and Purification Technology, 219 (2019) 47-54.

[111] D.Y. Kim, H.M. Lee, S.K. Min, Y. Cho, I.-C. Hwang, K. Han, J.Y. Kim, K.S. Kim, CO_2 Capturing Mechanism in Aqueous Ammonia: NH3-Driven Decomposition−Recombination Pathway, The Journal of Physical Chemistry Letters, 2 (2011) 689-694.

[112] G. Magneschi, T. Zhang, R. Munson, The Impact of CO_2 Capture on Water Requirements of Power Plants, Energy Procedia, 114 (2017) 6337-6347.

[113] P. Feron, R. Thiruvenkatachari, A. Cousins, Water production through CO_2 capture in coal-fired power plants, Energy Science & Engineering, 5 (2017) 244-256.

[114] A.J. Ansari, F.I. Hai, T. He, W.E. Price, L.D. Nghiem, Physical cleaning techniques to control fouling during the pre-concentration of high suspended-solid content solutions for resource recovery by forward osmosis, Desalination, 429 (2018) 134-141.

[115] X. An, Y. Hu, N. Wang, Z. Zhou, Z. Liu, Continuous juice concentration by integrating forward osmosis with membrane distillation using potassium sorbate preservative as a draw solute, Journal of Membrane Science, 573 (2019) 192-199.

[116] G. Gwak, D.I. Kim, J. Kim, M. Zhan, S. Hong, An integrated system for CO_2 capture and water treatment by forward osmosis driven by an amine-based draw solution, Journal of Membrane Science, 581 (2019) 9-17.

[117] T.Y. Cath, M. Elimelech, J.R. McCutcheon, R.L. McGinnis, A. Achilli, D. Anastasio, A.R. Brady, A.E. Childress, I.V. Farr, N.T. Hancock, J. Lampi, L.D. Nghiem, M. Xie, N.Y. Yip, Standard Methodology for Evaluating Membrane Performance in Osmotically Driven Membrane Processes, Desalination, 312 (2013) 31-38.

[118] I. Sutzkover, D. Hasson, R. Semiat, Simple technique for measuring the concentration polarization level in a reverse osmosis system, Desalination, 131 (2000) 117-127.

[119] L.D. Nghiem, A.I. Schäfer, M. Elimelech, Removal of Natural Hormones by Nanofiltration Membranes: Measurement, Modeling, and Mechanisms, Environmental Science & Technology, 38 (2004) 1888-1896.

[120] P.M. Bungay, H. Brenner, The motion of a closely-fitting sphere in a fluid-filled tube, International Journal of Multiphase Flow, 1 (1973) 25-56.

[121] M. Elimelech, W.H. Chen, J.J. Waypa, Measuring the zeta (electrokinetic) potential of reverse osmosis membranes by a streaming potential analyzer, Desalination, 95 (1994) 269-286.

[122] S.A. Huber, A. Balz, M. Abert, W. Pronk, Characterisation of aquatic humic and non-humic matter with size-exclusion chromatography – organic carbon detection – organic nitrogen detection (LC-OCD-OND), Water Research, 45 (2011) 879-885.

[123] M. Xie, L.D. Nghiem, W.E. Price, M. Elimelech, Relating rejection of trace organic contaminants to membrane properties in forward osmosis: Measurements, modelling and implications, Water Research, 49 (2014) 265-274.

[124] H.-Q. Liang, W.-S. Hung, H.-H. Yu, C.-C. Hu, K.-R. Lee, J.-Y. Lai, Z.-K. Xu, Forward osmosis membranes with unprecedented water flux, Journal of Membrane Science, 529 (2017) 47-54.

[125] G. Han, T.-S. Chung, M. Toriida, S. Tamai, Thin-film composite forward osmosis membranes with novel hydrophilic supports for desalination, Journal of Membrane Science, 423 (2012) 543-555.

[126] H.-C. Flemming, T.R. Neu, D.J. Wozniak, The EPS Matrix: The “House of Biofilm Cells”, Journal of Bacteriology, 189 (2007) 7945-7947.

[127] X. Jin, X. Huang, E.M.V. Hoek, Role of Specific Ion Interactions in Seawater RO Membrane Fouling by Alginic Acid, Environmental Science & Technology, 43 (2009) 3580-3587.

[128] J.R. McCutcheon, M. Elimelech, Influence of concentrative and dilutive internal concentration polarization on flux behavior in forward osmosis, Journal of Membrane Science, 284 (2006) 237-247.

[129] C. Boo, M. Elimelech, S. Hong, Fouling control in a forward osmosis process integrating seawater desalination and wastewater reclamation, Journal of Membrane Science, 444 (2013) 148-156.

[130] W.A. Phillip, J.S. Yong, M. Elimelech, Reverse Draw Solute Permeation in Forward Osmosis: Modeling and Experiments, Environmental Science & Technology, 44 (2010) 5170-5176.

[131] L.D. Nghiem, S. Hawkes, Effects of membrane fouling on the nanofiltration of pharmaceutically active compounds (PhACs): Mechanisms and role of membrane pore size, Separation and Purification Technology, 57 (2007) 176-184.

[132] L.D. Nghiem, P.J. Coleman, C. Espendiller, Mechanisms underlying the effects of membrane fouling on the nanofiltration of trace organic contaminants, Desalination, 250 (2010) 682-687.

[133] M. Xie, W.E. Price, L.D. Nghiem, Rejection of pharmaceutically active compounds by forward osmosis: Role of solution pH and membrane orientation, Separation and Purification Technology, 93 (2012) 107-114.

[134] S. Zhu, M. Li, M. Gamal El-Din, The roles of pH and draw solute on forward osmosis process treating aqueous naphthenic acids, Journal of Membrane Science, 549 (2018) 456-465.

[135] D.A. Eaton, S.L. Clesceri, E.A. Greenberg, Standard Methods for Examination of Water & Wastewater 23rd ed, American Public Health Association 2005.

[136] N. Tadkaew, F.I. Hai, J.A. McDonald, S.J. Khan, L.D. Nghiem, Removal of trace organics by MBR treatment: The role of molecular properties, Water Research, 45 (2011) 2439-2451.

[137] J.A. McDonald, N.B. Harden, L.D. Nghiem, S.J. Khan, Analysis of N-nitrosamines in water by isotope dilution gas chromatography-electron ionisation tandem mass spectrometry, Talanta, 99 (2012) 146-154.

[138] J.-J. Qin, S. Chen, M.H. Oo, K.A. Kekre, E.R. Cornelissen, C.J. Ruiken, Experimental studies and modeling on concentration polarization in forward osmosis, Water Science and Technology, 61 (2010) 2897-2904.

[139] M. Ersöz, Diffusion and Selective Transport of Alkali Cations on Cation-Exchange Membrane, Separation Science and Technology, 30 (1995) 3523-3533.

[140] E.R. Nightingale, Phenomenological Theory of Ion Solvation. Effective Radii of Hydrated Ions, The Journal of Physical Chemistry, 63 (1959) 1381-1387.

[141] T. Fujioka, S.J. Khan, J.A. McDonald, L.D. Nghiem, Rejection of trace organic chemicals by a nanofiltration membrane: the role of molecular properties and effects of caustic cleaning, Environmental Science: Water Research & Technology, 1 (2015) 846-854.

[142] Hyperchem, Release 7.0 for Windows, Molecular Modeling System, Hypercube Inc., Gainesville, FL, (2002).

[143] B. Van der Bruggen, J. Schaep, D. Wilms, C. Vandecasteele, Influence of molecular size, polarity and charge on the retention of organic molecules by nanofiltration, Journal of Membrane Science, 156 (1999) 29-41.

[144] S. Darvishmanesh, J. Vanneste, E. Tocci, J.C. Jansen, F. Tasselli, J. Degrève, E. Drioli, B. Van der Bruggen, Physicochemical Characterization of Solute Retention in Solvent Resistant Nanofiltration: the Effect of Solute Size, Polarity, Dipole Moment, and Solubility Parameter, The Journal of Physical Chemistry B, 115 (2011) 14507-14517.

[145] L. Zheng, W.E. Price, L.D. Nghiem, Effects of fouling on separation performance by forward osmosis: the role of specific organic foulants, Environmental Science and Pollution Research, (2018).

[146] E.D. Snijder, M.J.M. te Riele, G.F. Versteeg, W.P.M. van Swaaij, Diffusion coefficients of several aqueous alkanolamine solutions, Journal of Chemical & Engineering Data, 38 (1993) 475-480.

[147] E.S. Hamborg, W.P.M. van Swaaij, G.F. Versteeg, Diffusivities in Aqueous Solutions of the Potassium Salt of Amino Acids, Journal of Chemical & Engineering Data, 53 (2008) 1141-1145.

[148] Y. Liu, S. Lin, H. Lu, C. Liu, K. Wu, W. Jiang, B. Liang, Studies on viscosity and conductivity of 1,8-diazabicyclo[5.4.0]undec-7-ene (DBU)-glycerol and CO_2-DBU-glycerol solutions at temperatures from 288.1 K to 328.1 K, The Journal of Chemical Thermodynamics, 136 (2019) 16-27.

[149] S. Phuntsho, S. Vigneswaran, J. Kandasamy, S. Hong, S. Lee, H.K. Shon, Influence of temperature and temperature difference in the performance of forward osmosis desalination process, Journal of Membrane Science, 415-416 (2012) 734-744.

[150] C.Y. Tang, Q. She, W.C.L. Lay, R. Wang, A.G. Fane, Coupled effects of internal concentration polarization and fouling on flux behavior of forward osmosis membranes during humic acid filtration, Journal of Membrane Science, 354 (2010) 123-133.

[151] G.T. Gray, J.R. McCutcheon, M. Elimelech, Internal concentration polarization in forward osmosis: role of membrane orientation, Desalination, 197 (2006) 1-8.

[152] M.R. Chowdhury, J.R. McCutcheon, Elucidating the impact of temperature gradients across membranes during forward osmosis: Coupling heat and mass transfer models for better prediction of real osmotic systems, Journal of Membrane Science, 553 (2018) 189-199.

[153] J.R. McCutcheon, M. Elimelech, Influence of concentrative and dilutive internal concentration polarization on flux behavior in forward osmosis, Journal of Membrane Science, 284 (2006) 237-247.

[154] S. Lee, S.I. Choi, S. Maken, H.J. Song, H.C. Shin, J.W. Park, K.R. Jang, J.H. Kim, Physical properties of aqueous sodium glycinate solution as an absorbent for carbon dioxide removal, Journal of Chemical and Engineering Data, 50 (2005) 1773-1776.

[155] Y.C. Chang, A.S. Myerson, Diffusivity of glycine in concentrated saturated and supersaturated aqueous solutions, AIChE Journal, 32 (1986) 1567-1569.

[156] S. Banerjee, H. Briesen, Molecular dynamics simulations of glycine crystal-solution interface, The Journal of Chemical Physics, 131 (2009) 184705.

[157] M.T. Vu, A.J. Ansari, F.I. Hai, L.D. Nghiem, Performance of a seawater-driven forward osmosis process for pre-concentrating digested sludge centrate: organic enrichment and membrane fouling, Environmental Science: Water Research & Technology, 4 (2018) 1047-1056.

[158] P. Singh, G.F. Versteeg, Structure and activity relationships for CO_2 regeneration from aqueous amine-based absorbents, Process Safety and Environmental Protection, 86 (2008) 347-359.

[159] R. Idem, M. Wilson, P. Tontiwachwuthikul, A. Chakma, A. Veawab, A. Aroonwilas, D. Gelowitz, Pilot Plant Studies of the CO_2 Capture Performance of Aqueous MEA and Mixed MEA/MDEA Solvents at the University of Regina CO_2 Capture

Technology Development Plant and the Boundary Dam CO_2 Capture Demonstration Plant, Industrial & Engineering Chemistry Research, 45 (2006) 2414-2420.

[160] S.J. Vevelstad, I. Eide-Haugmo, E.F. da Silva, H.F. Svendsen, Degradation of MEA; a theoretical study, Energy Procedia, 4 (2011) 1608-1615.

[161] Z. Zhang, Y. Li, W. Zhang, J. Wang, M.R. Soltanian, A.G. Olabi, Effectiveness of amino acid salt solutions in capturing CO_2: A review, Renewable and Sustainable Energy Reviews, 98 (2018) 179-188.

[162] S. Moioli, L.A. Pellegrini, M.T. Ho, D.E. Wiley, A comparison between amino acid based solvent and traditional amine solvent processes for CO_2 removal, Chemical Engineering Research and Design, 146 (2019) 509-517.

[163] M. Caplow, Kinetics of carbamate formation and breakdown, Journal of the American Chemical Society, 90 (1968) 6795-6803.

[164] B. Yu, H. Yu, K. Li, L. Ji, Q. Yang, X. Wang, Z. Chen, M. Megharaj, A Diamine-Based Integrated Absorption–Mineralization Process for Carbon Capture and Sequestration: Energy Savings, Fast Kinetics, and High Stability, Environmental Science & Technology, 52 (2018) 13629-13637.

[165] Z. Chen, Q. Shen, H. Gong, M. Du, Preparation of a novel dual-layer polyvinylidene fluoride hollow fiber composite membrane with hydrophobic inner layer for carbon dioxide absorption in a membrane contactor, Separation and Purification Technology, 248 (2020) 117045.

[166] Q. He, G. Yu, S. Yan, L.F. Dumée, Y. Zhang, V. Strezov, S. Zhao, Renewable CO_2 absorbent for carbon capture and biogas upgrading by membrane contactor, Separation and Purification Technology, 194 (2018) 207-215.

[167] F. Bougie, X. Fan, Microwave regeneration of monoethanolamine aqueous solutions used for CO_2 capture, International Journal of Greenhouse Gas Control, 79 (2018) 165-172.

[168] S.J. McGurk, C.F. Martín, S. Brandani, M.B. Sweatman, X. Fan, Microwave swing regeneration of aqueous monoethanolamine for post-combustion CO_2 capture, Applied Energy, 192 (2017) 126-133.

[169] K. Li, P.H.M. Feron, T.W. Jones, K. Jiang, R.D. Bennett, A.F. Hollenkamp, Energy harvesting from amine-based CO_2 capture: proof-of-concept based on mono-ethanolamine, Fuel, 263 (2020) 116661.

[170] N.A. Ahmad, C.P. Leo, A.L. Ahmad, Amine wetting evaluation on hydrophobic silane modified polyvinylidene fluoride/silicoaluminophosphate zeolite membrane for membrane gas absorption, Journal of Natural Gas Science and Engineering, 58 (2018) 115-125.

[171] D.B. Gingerich, M.S. Mauter, Quantity, Quality, and Availability of Waste Heat from United States Thermal Power Generation, Environmental Science & Technology, 49 (2015) 8297-8306.

[172] E.J. Novek, E. Shaulsky, Z.S. Fishman, L.D. Pfefferle, M. Elimelech, Low-Temperature Carbon Capture Using Aqueous Ammonia and Organic Solvents, Environmental Science & Technology Letters, 3 (2016) 291-296.

[173] P.-H. Lin, D.S.H. Wong, Carbon dioxide capture and regeneration with amine/alcohol/water blends, International Journal of Greenhouse Gas Control, 26 (2014) 69-75.

[174] E.S. Hamborg, C. van Aken, G.F. Versteeg, The effect of aqueous organic solvents on the dissociation constants and thermodynamic properties of alkanolamines, Fluid Phase Equilibria, 291 (2010) 32-39.

[175] A. Alkhudhiri, N. Darwish, N. Hilal, Membrane distillation: A comprehensive review, Desalination, 287 (2012) 2-18.

[176] M. Fang, Q. Ma, Z. Wang, Q. Xiang, W. Jiang, Z. Xia, A novel method to recover ammonia loss in ammonia-based CO_2 capture system: ammonia regeneration by vacuum membrane distillation, Greenhouse Gases: Science and Technology, 5 (2015) 487-498.

[177] N.A. Rahim, N. Ghasem, M. Al-Marzouqi, Absorption of CO_2 from natural gas using different amino acid salt solutions and regeneration using hollow fiber membrane contactors, Journal of Natural Gas Science and Engineering, 26 (2015) 108-117.

[178] Z. Wang, M. Fang, Y. Pan, S. Yan, Z. Luo, Amine-based absorbents selection for CO_2 membrane vacuum regeneration technology by combined absorption–desorption analysis, Chemical Engineering Science, 93 (2013) 238-249.

[179] L. Zheng, W.E. Price, T. He, L.D. Nghiem, Simultaneous cooling and provision of make-up water by forward osmosis for post-combustion CO_2 capture, Desalination, 476 (2020) 114215.

[180] M.T. Vu, H.P. Vu, L.N. Nguyen, G.U. Semblante, M.A.H. Johir, L.D. Nghiem, A hybrid anaerobic and microalgal membrane reactor for energy and microalgal biomass production from wastewater, Environmental Technology & Innovation, 19 (2020) 100834.

[181] A. Aroonwilas, P. Tontiwachwuthikul, Mass Transfer Coefficients and Correlation for CO_2 Absorption into 2-Amino-2-methyl-1-propanol (AMP) Using Structured Packing, Industrial & Engineering Chemistry Research, 37 (1998) 569-575.

[182] K. Li, A. Cousins, H. Yu, P. Feron, M. Tade, W. Luo, J. Chen, Systematic study of aqueous monoethanolamine-based CO_2 capture process: model development and process improvement, 4 (2016) 23-39.

[183] X. Zhang, X. Zhang, H. Liu, W. Li, M. Xiao, H. Gao, Z. Liang, Reduction of energy requirement of CO_2 desorption from a rich CO_2-loaded MEA solution by using solid acid catalysts, Applied Energy, 202 (2017) 673-684.

[184] M. Rabensteiner, G. Kinger, M. Koller, G. Gronald, S. Unterberger, C. Hochenauer, Investigation of the suitability of aqueous sodium glycinate as a solvent for post combustion carbon dioxide capture on the basis of pilot plant studies and screening methods, International Journal of Greenhouse Gas Control, 29 (2014) 1-15.

[185] Y. Zhao, Y. Bian, H. Li, H. Guo, S. Shen, J. Han, D. Guo, A Comparative Study of Aqueous Potassium Lysinate and Aqueous Monoethanolamine for Postcombustion CO_2 Capture, Energy & Fuels, 31 (2017) 14033-14044.

[186] H.-J. Song, S. Park, H. Kim, A. Gaur, J.-W. Park, S.-J. Lee, Carbon dioxide absorption characteristics of aqueous amino acid salt solutions, International Journal of Greenhouse Gas Control, 11 (2012) 64-72.

[187] Z. Rezaiyan, P. Keshavarz, M. Khorram, Experimental investigation of the effects of different chemical absorbents on wetting and morphology of poly(vinylidene fluoride) membrane, Journal of Applied Polymer Science, 134 (2017) 45543.

[188] M.S. Shaikh;, A.M. Shariff;, M.A. Bustam;, G. Murshid, Analysis of Physicochemical Properties of Aqueous Sodium Glycinate (SG) Solutions at Low Concentrations from 0.1-2.0 M, Journal of Applied Sciences, 14 (2014) 1055-1060.

[189] G. Richner, G. Puxty, Assessing the Chemical Speciation during CO_2 Absorption by Aqueous Amines Using in Situ FTIR, Industrial & Engineering Chemistry Research, 51 (2012) 14317-14324.

[190] K. Robinson, A. McCluskey, M.I. Attalla, An FTIR Spectroscopic Study on the Effect of Molecular Structural Variations on the CO_2 Absorption Characteristics of Heterocyclic Amines, ChemPhysChem, 12 (2011) 1088-1099.